“Roles of Bassoon in assembling the presynaptic active zone for neurotransmitter release”

Dissertation
zur Erlangung des akademischen Grades

doctor rerum naturalium
(Dr. rer. nat.)

genehmigt durch die Fakultät für Naturwissenschaften
der Otto-von-Guericke-Universität Magdeburg

von

Diplom Biologin Daria Davydova

geb.am
21.10.1982 in Leningrad, Russian Federation

Gutachter: **Prof. Dr. Eckart D. Gundelfinger**
Prof. Dr. Thomas Kuner

eingericht am: 20.10.2009
verteidigt am: 22.04.2010

Acknowledgements

To: Dr. Anna Fejtova, Dr. Wilko D. Altrock, Dr. Stefano Romorini, Claudia Marini, Ferdinand Bischof, and Prof. Eckart D. Gundelfinger,
Thank you very much.

This thesis was supported by the DFG graduate program GRK 1167. I am very grateful to the members of the GRK, in particular to the two chairs, Prof. Michael Naumann and Prof. Eckart D. Gundelfinger.

Summary
Chemical synapses are highly specialized cellular junctions between neurons and their target cells, composed of a presynaptic bouton, which harbors synaptic vesicles (SVs), a postsynaptic terminal, which contains receptors for neurotransmitters and a synaptic cleft, which separates the pre- and postsynaptic compartments. In presynaptic terminals, SVs form clusters around a specialized region of the plasma membrane, known as the active zone. At the active zone a complex protein network forms the cytomatrix at the active zone (CAZ). It is thought to be involved in tethering SVs and in the spatial and temporal organization of the exocytosis machinery. Bassoon and Piccolo, two related proteins, are core components of this CAZ.
Bassoon and Piccolo are transported on membranous organelles, called Piccolo-Bassoon transport vesicles (PTVs). They are transported from the neuronal soma to distal axonal locations, where they participate in assembling new presynaptic terminals. Despite their net anterograde transport, PTVs move in both directions within the axon. How PTVs are linked to retrograde motors is unclear. In this study, a direct interaction of Bassoon with dynein light chains (DLCs) DLC1 and DLC2 is reported. This interaction potentially links PTVs to retrograde dynein motor complexes. Three independently functional DLC-binding sites were identified on Bassoon, all resembling but not exactly matching the DLC-binding consensus sequence (K/R)XTQT. Both DLCs interact with Bassoon in yeast and mammalian cells. A newly developed mito-targeting system confirmed the functionality of the heterologous expression in COS-7 cells. Quantitative binding assays revealed a significantly higher affinity of Bassoon for DLC2 than for DLC1. These data suggest that, via its interaction with DLCs, Bassoon might function as a cargo adapter for the retrograde motor dynein.
In a mouse mutant for Bassoon the lack of functional protein leads to impaired fast exocytosis and reduced Ca^{2+} current in cochlea inner hair cells, suggesting insufficient recruitment and/or stabilization of voltage-dependent calcium channels (VDCCs) in the presynaptic active zone. The molecular mechanism for these findings is unclear. In this study an interaction between the CAZ proteins Bassoon and Piccolo with Rim-binding proteins (RBPs), binding partners for the Rab3-effector Rim as well as VDCCs – $Ca_V2.1$ and $Ca_V2.2$, is reported. RBP1 and RBP2 interact with specific PXXP motifs in Bassoon and Piccolo preferentially via their first SH3 domain. The interaction between RBPs and Bassoon can be inhibited by phosphorylation of the Ser-2893 residue in the RBP-interacting PSPP motif of Bassoon, while Piccolo's interaction with RBPs is phosphorylation-independent. The existence of three SH3 domains in RBPs and several described binding partners – Rim1, $Ca_V2.2$, Bassoon and Piccolo – raised the question whether RBPs might serve as physical modules linking VDCCs with SVs and components of the CAZ. Indeed, quantitative *in vitro* assays disclosed clear differences in binding affinities of distinct RBP-SH3 domains to Rim1, $Ca_V2.2$, Bassoon and Piccolo. This suggests that RBPs might interact with these proteins simultaneously in a RBP-based protein complex. In immunofluorescence analysis the amount of presynaptic $Ca_V2.1$ was significantly reduced in Bassoon knockout compared with wild-type synapses. To assess whether Bassoon effects on VDCC localization require RBPs as linkers connecting these two proteins, the distribution of $Ca_V2.1$ in rat hippocampal neurons transfected either with EGFP-tagged wild-type Bassoon or RBP-binding deficient Bassoon mutant was compared. Bassoon clustering in the cell body was observed in both cases, while endogenous RBP2 and $Ca_V2.1$ were co-recruited only to clusters formed by wild-type Bassoon. At synapses formed by axons of neurons transfected with EGFP-tagged wild-type Bassoon the intensities of immunofluorescence of both RBP2 and $Ca_V2.1$ showed strong positive correlation with the intensity of EGFP fluorescence. On the contrary, a negative correlation was observed for the RBP2 and $Ca_V2.1$ immunofluorescence intensities and EGFP fluorescence intensity at synapses containing RBP binding-deficient Bassoon mutant. Overall, the data suggest that Bassoon is involved in recruitment and exact localization of VDCCs in the presynaptic terminal active zones. This mechanism requires RBPs, which interact simultaneously with Bassoon and VDCCs and therefore can serve as physical linkers for this protein complex assembly.
These findings provide a new insight in the mechanism contributing to the organization of the exocytosis machinery and regulation of synaptic transmission.

Zusammenfassung
Chemische Synapsen sind hoch spezialisierte Zell-Zell-Kontakte zwischen Neuronen und ihren Zielzellen. Sie bestehen aus einem präsynaptischen Bouton, der mit synaptischen Vesikeln angefüllt ist, einem postsynaptischen Kompartiment, welches die Neurotransmitterrezeptoren und dem damit verknüpften Apparat zur Signaltransduktion enthält, und einem synaptischen Spalt, der Prä- und Postsynapse voneinander trennt. In der präsynaptischen Endigung bilden die synaptischen Vesikel eine Traube an der aktive Zonen – jener spezialisierten Region der Plasmamembran an der die Neurotransmitterfreisetzung erfolgt. An der aktiven Zone befindet sich ein hoch komplexes Proteinnetzwerk, welches als Cytomatrix an der aktiven Zone (CAZ) oder präsynaptisches Gitter bekannt ist. Es wird vermutet, dass Komponenten dieser CAZ an der Rekrutierung von synaptischen Vesikeln und der Organisation der Exocytosemaschinerie beteiligt sind. Bassoon und Piccolo, zwei nahe miteinander verwandte Proteine, sind integrale Komponenten dieser CAZ.
Diese beiden ungewöhnlich großen Proteine werden auf membranären Organellen, den so genannten Piccolo-Bassoon-Transportvesikeln (PTVs), aus dem Soma ins Axon bis hin zu deren distalen Enden transportiert. Sie sind entlang des Axons am Aufbau neuer synaptischer Verbindungen beteiligt sind. Trotz ihres in der Summe anterograden Transports werden die PTVs innerhalb des Axons in beide Richtungen transportiert. Bislang war unklar, wie PTVs an einen dafür notwendigen retrograden Motor gekoppelt sein könnten. In dieser Studie wird eine Interaktion von Bassoon mit den leichten Ketten von Dynein, der *dynein light chain* 1 (DLC1) sowie der *dynein light chain* 2 (DLC2) untersucht. Hierdurch könnten PTVs mit Dyneinkomplexen, die als retrograde Motoren an axonalen Microtubuli fungieren, verknüpft sein. Es zeigte sich, dass Bassoon drei voneinander unabhängig funktionierende DLC-Bindungsstellen besitzt, die zwar alle der Konsensussequenz (K/R)XTQT ähneln, aber nicht exakt mit ihr übereinstimmen. Diese Bindungsstellen sind in der homologen Region von Piccolo nicht zu finden. Die beiden DLC-Isoformen interagieren mit Bassoon im Hefe-Zwei-Hybrid-System und in Säugetierzellen. Quantitative Bindungstests ergaben weiterhin, dass DLC2 eine signifikant höhere Affinität zu Bassoon besitzt als DLC1. Interaktionsstudien in einem im Rahmen der Arbeit neu etablierten heterologen Expressionsystem in COS7-Zellen, dem *Mito-targeting*-Ssytem, bestätigte die Funktionalität der Bassoon-DLC-Interaktion. Werden Mitochondrien in COS7-Zellen durch die Expression von Bassoon-Fusionsproteinen mit *Mito-targeting*-Signalen auf der Oberfläche dekoriert so können diese über DLC an Microtubili-Motoren binden und retrograd transportiert werden. Sie reichern sich dann nachweislich am Microtubuli-Organisationszentrum (MTOC) an. Diese Daten lassen vermuten, dass Bassoon durch die Interaktion mit DLCs als Cargo-Adaptor der PTVs für den retrograden Motor Dynein fungiert.
In einer Mausmutanten für Bassoon kommt es in Abwesenheit von funktionellem Bassoon-Protein in den inneren Haarzellen der Cochlea zu einer behinderten Exocytose und reduzierten Ca^{2+}-Strömen, was auf eine unvollständige Rekrutierung und/oder Stabilisierung von spannungsabhängigen Calciumkanälen (*voltage-dependent calcium channels*: VDCCs) in der aktiven Zone hindeutet [Khimich et al. (2005) Nature 434:889-894]. Der genaue molekulare Mechanismus hierfür ist jedoch bisher unklar. In dieser Studie wird eine Bindung von Bassoon und Piccolo an RIM-bindende Proteine (RBPs), gezeigt. RBPs binden neben dem CAZ-Protein RIM (Rab3-interacting molecule) auch VDCCs und könnten somit als Bindeglieder zwischen CAZ-Netzwerk, Exocytose-Maschinerie und Calciumkanälen der präsynaptischen Membran von großem Interesse sein.
RBP1 und RBP2 interagieren vorrangig über die erste SH3-Domäne mit spezifischen PXXP-Motiven in Bassoon und Piccolo. Bemerkenswerterweise kann die Interaktion von RBPs und Bassoon durch Phosphorylierung des Ser-2893-Restes im mit RBP interagierenden P<u>S</u>PP-Motiv von Bassoon inhibiert werden. Die Interaktion mit Piccolo ist dagegen phosphorylierungsunabhängig. Die Existenz von drei SH3-Domänen in RBPs und mehreren verschiedenen Bindungspartnern – Rim1, $Ca_v2.1$, Bassoon und Piccolo – stellte die Frage auf, ob RBPs wirklich als Bindungsmodule fungieren, die VDCCs mit SVs und Komponenten der CAZ verknüpfen, oder ob die Interaktionspartner um Bindung an RBPs konkurrieren. Tatsächlich deckten *in vitro*-Experimente deutliche Unterschiede in den Bindungsaffinitäten verschiedener RBP-SH3-Domänen zu Rim1, $Ca_v2.1$, Bassoon und Piccolo auf. Dies lässt

darauf schließen, dass RBPs tatsächlich mit allen diesen Proteinen gleichzeitig in einem RBP-basierten Proteinkomplex interagieren könnten. Um herauszufinden, ob der Einfluss von Bassoon auf die Lokalisation von VDCCs von RBPs als Verknüpfungselemente beider Proteine abhängt, wurde die Verteilung von $Ca_v2.1$ in hippocampalen Primärkultur-Neuronen aus der Ratte verglichen, die entweder mit EGFP-markiertem wildtypischen Bassoon oder einer entprechend markierten RBP-Bindungsmutanten von Bassoon transfiziert wurden. In beiden Fällen wurden Ansammlungen von Bassoon im Zellkörper beobachtet, wobei endogene RBP2 und $Ca_v2.1$ jedoch nur zu Ansammlungen von wildtypischen Bassoon, nicht aber zu Bassoon, das nicht zur Interaktion mit RBP in der Lage war, rekrutiert wurden. An Synpasen von Axonen, die von mit EGFP-markierten wildtypischen Bassoon transfizierten Neuronen stammen, wurde eine starke positive Korrelation zwischen den Immunfluoreszenz-Intensitäten von RBP2 und $Ca_v2.1$ mit der EGFP-Intensität gemessen. Im Gegensatz dazu war eine negative Korrelation zwischen der RBP2- und $Ca_v2.1$-Intensität mit der EGFP-Intensität an Synapsen vorhanden, die die RBP-Bindungsmutante von Bassoon enthielten. In dieser Studie konnte weiter gezeigt werden, dass die Menge an präsynaptischem Calciumkanal $Ca_v2.1$ in Synapsen der Bassoon-mutanten Maus im Vergleich zu wildtypischen Synapsen signifikant kleiner ist.
Zusammenfassend lassen die Daten darauf schließen, dass Bassoon an der Retention und/oder der exakten Lokalisation von VDCCs in den präsynaptischen Nervenendigungen beteiligt ist. Der Retentionsmechanismus benötigt RBPs, die gleichzeitig mit Bassoon und VDCCs interagieren können und demnach als Integrationsglied für die Bildung dieses Proteinkomplexes dienen kann. Diese Resultate ermöglichen einen neuen Einblick in die Mechanismen, die zur Organisation der Exocytosemaschinerie und der Regulation von synaptischer Transmission beitragen.

Contents

CONTENTS 6

FIGURES AND TABLES.....8

1. INTRODUCTION 10

1.1 CHEMICAL SYNAPSES. PRESYNAPTIC BOUTONS: ORGANIZATION AND FUNCTION 10
1.2 PRESYNAPTIC VOLTAGE DEPENDENT CALCIUM CHANNELS: STRUCTURE AND FUNCTION AND REGULATION 13
1.3 PRESYNAPTIC VOLTAGE DEPENDENT CALCIUM CHANNELS: PRECISE LOCALIZATION IS ESSENTIAL 15
1.4 RIM BINDING PROTEINS (RBPS): POSSIBLE LINKERS OF VDCCS AND SYNAPTIC VESICLE FUSION MACHINERY 17
1.5 BASSOON AND PICCOLO: TWO MAJOR COMPONENTS OF THE CYTOMATRIX AT THE ACTIVE ZONE 20
1.6 AXONAL TRANSPORT OF PRESYNAPTIC COMPONENTS: A ROLE FOR DYNEIN MOTORS? 23
1.7 AIMS OF THIS WORK.....24

2. MATERIALS AND METHODS 26

2.1 MATERIALS 26
2.1.1 Chemicals.....26
2.1.2 Kits, enzymes and molecular biology reagents 26
2.1.3 Molecular weight markers 26
2.1.4 Bacteria and yeast cells 26
2.1.5 Mammalian cells 27
2.1.6 Cell culture media and reagents for mammalian cells 27
2.1.7 Culture media and additives for yeast and bacteria cells.....27
2.1.8 Buffers used in biochemical or molecular biology work 28
2.1.9 Yeast assay buffers 28
2.1.10 Antibodies: Primary antibodies for Western blot and immunocitochemistry 28
2.1.11 Antibodies: Secondary antibodies for Western blot and immunocitochemistry ...29
2.1.12 Animals.....29
2.2 METHODS 30
2.2.1 Molecular biological methods.....30
2.2.1.1 Genotyping of mutant mice.....30
2.2.1.1a DNA extraction for genotyping of mutant mice 30
2.2.1.1b Polymerase chain reaction (PCR) for genotyping 30
2.2.1.2 PCR for amplification 31
2.2.1.3 Introduction of point mutations by PCR 31
2.2.1.4 DNA agarose gel electrophoresis 31
2.2.1.5 cDNA cloning into expression vectors 32
2.2.1.6 Heat shock transformation of competent *E.coli* XL 10 Gold bacteria cells 32
2.2.1.7 Plasmid isolation (Mini DNA preparation).....32
2.2.1.8 DNA restriction enzyme digestion 33
2.2.2 Yeast experiments 33
2.2.3 Biochemical methods.....34
2.2.3.1 Protein concentration determination: Micro amidoblack protein assay 34
2.2.3.2 SDS-PAGE using Laemmli system 34
2.2.3.3 Coommassie staining of SDS-PAGE 35
2.2.3.4 Western blotting.....35
2.2.3.5 Immunoblot detection.....35
2.2.3.6 Purification of fusion proteins 36
2.2.3.6.1 Induction of fusion protein synthesis (GST and His-Trx) 36
2.2.3.6.2 Bacterial extract preparation.....36
2.2.3.6.3 Affinity purification.....36

2.2.3.7 EGFP-fusion proteins precipitation from transfected HEK293-T cells 37
2.2.4 Cell culture techniques 37
2.2.4.1 Splitting of cells into culture plates 38
2.2.4.2 Preparation of glass coverslips 38
2.2.4.3 Glial cells 38
2.2.4.4 Mouse hippocampal neurons 39
2.2.4.5 Rat hippocampal neurons 39
2.2.4.6 Transfections 40
2.2.4.6.1 Transfection of HEK293-T cells with Ca phosphate method 40
2.2.4.6.2 Transfection of COS-7 cells on 24 well plates 40
2.2.4.6.3 Transfection of rat hippocampal neurons with EGFP-Bsn and EGFP-BsnRBM ... 40
2.2.5 Immunocytochemistry, microscopy and image analysis 41
2.2.5.1 Immunostaining of cell cultures 41
2.2.5.2 Microscopy and image analysis 41
2.2.5.3 Analysis of synaptic immunofluorescence (IF) 41
2.2.6 Biosensor analysis 42
2.2.6.1 Biosensor analysis of RBPs interaction with Bassoon, Piccolo, Rim1 and $Ca_V2.2$ (direct amine coupling) 42
2.2.6.2 Biosensor analysis of Bassoon interactions with DLCs (GST capturing) 42
2.2.7 Statistical data analysis 43

3. RESULTS 44

3.1 CHARACTERIZATION OF BASSOON INTERACTION WITH DYNEIN LIGHT CHAIN 44
3.1.1 Development of a new mito-targeting system 44
3.1.2 Interaction of Bassoon with Dynein Light Chain (DLC) in living cells tested by mito-targeting assay 46
3.1.3 DLC1 and DLC2 bind Bassoon with different strength 46
3.1.4 Bassoon can function as a cargo adaptor in COS-7 cells 48
3.2 CHARACTERIZATION OF BASSOON AND PICCOLO INTERACTIONS WITH RIM BINDING PROTEINS 51
3.2.1 Bassoon can interact with Rim binding proteins 51
3.2.2 Mapping of functional Bassoon and Piccolo binding motifs on RBP1 and RBP2 .. 53
3.2.3 Identification of functional RBP-binding motifs on Bassoon and Piccolo 54
3.2.4 Distinct SH3 domains of RBPs bind Bassoon and Piccolo with relatively different strength 55
3.2.5 Bassoon's but not Piccolo's interaction with RBPs might be regulated by phosphorylation 56
3.3 DISTINCT SH3 DOMAINS OF RBPS HAVE DIFFERENT BINDING AFFINITIES TO RIM1, $CA_V2.2$, BASSOON, AND PICCOLO 59
3.4 POTENTIAL PHYSIOLOGICAL FUNCTIONS OF BASSOON INTERACTION WITH RIM BINDING PROTEINS 63
3.4.1 The lack of functional Bassoon reduces the amount of $Ca_V2.1$ at synapses 63
3.4.2 Bassoon recruits calcium channels through the interaction with Rim binding proteins 64

4. DISCUSSION 67

4.1 BASSOON – DLC INTERACTION: THREE FUNCTIONAL DLC-BINDING SITES IN BASSOON, ROLE OF BASSOON AS A CARGO ADAPTOR PROTEIN FOR DYNEIN MOTORS 67
4.2 PICCOLO AND NONPHOSPHORYLATED BASSOON BIND PREFERENTIALLY TO THE FIRST SH3 DOMAIN OF RBPS 69
4.3 RBPS CAN PLAY AN INTEGRATIVE ROLE INTERACTING SIMULTANEOUSLY WITH RIM1, VDCCS AND BASSOON OR PICCOLO 70
4.4 BASSOON MIGHT BE INVOLVED IN RETENTION OF VDCCS AT SYNAPSES 72
4.5 PERSPECTIVES 74

5. REFERENCES 75

6. APPENDIX **86**
6.1 RBP1 AND RBP2 SEQUENCE ALIGNMENT 86
6.2 CONSTRUCTS USED IN THIS PROJECT 88
6.3 ABBREVIATIONS 89

Figures and tables

Figure 1. Molecular organization of the CAZ (from Fejtova and Gundelfinger, 2006). 11
Figure 2. Subunit Structure of VDCCs (from Catterall and Few, 2008). 14
Figure 3. Model for the organization of neurotransmitter release site (from Stanley, 1993). 16
Figure 4. Structure of the RBP protein family (from Mittelstaedt and Schoch, 2007). 18
Figure 5. RBPs can serve as linkers between VDCCs and synaptic vesicle fusion machinery (from Hibino et al., 2002). 20
Figure 6. Bassoon and Piccolo are two major components of the CAZ. 21
Table 1: Molecular biology reagents 26
Table 2: Molecular weight markers for DNA and proteins 26
Table 3: Bacteria and yeast cells 27
Table 4: Yeast cell strains 27
Table 5: Mammalian cell lines 27
Table 6: Media and reagents for mammalian cell culture 27
Table 7: Media and reagents for yeast and bacteria cell culture 28
Table 8: Bufferes used in biochemical and molecular biological assays 28
Table 9: Buffers used in yeast assays 28
Table 10: Primary antibodies for WB and ICC 29
Table 11: Secondary antibodies used for WB and ICC 29
Table 12: Animal lines 29
Table 13: Primer sequences used for genotyping of BGT and wild-type alleles as well as size of expected PCR products 30
Table 14: PCR programmes used for genotyping of BGT mouse pups 31
Table 15: PCR programmes used for generation of cDNA fragments 31
Table 16: Buffers for DNA preparation (mini scale) 32
Table 17: Solutions for micro amidoblack protein assay 34
Table 18: Buffers for Tris-glycine SDS-PAGE 34
Table 19: Solutions for Coommassie staining of SDS-PAGE 35
Table 20: Buffers for affinity purification of fusion proteins from bacteria 36
Table 21: Media and reagents for eukaryotic cell cultures 37
Table 22: Solutions for transfection of HEK293-T cells with Ca phosphate method 40
Figure 7. Development of a new mito-targeting system. 45
Figure 8. Bassoon interacts with DLC1 and DLC2 in mito-targeting assay. 47
Figure 9. DLC1 and DLC2 bind Bassoon with different affinity in surface plasmon resonance assay. 48
Figure 10. Mapping of three independently functional DLC-binding sites in Bassoon. 49
Figure 11. Bassoon can serve as a cargo adapter for retrograde transport in COS-7 cells. 50
Figure 12. Mapping of RBP interaction regions on Bassoon and Piccolo. 51
Figure 13. Bassoon interacts with Rim binding proteins in mammalian cells. 53
Figure 14. Rim binding proteins can interact with Bassoon and Piccolo through their three SH3 domains. 54
Figure 15. Bassoon and Piccolo can interact with RBPs through PXXP motifs. 57
Figure 16. The interaction of Bassoon, but not of Piccolo, with RBPs can be modulated by phosphorylation. 58
Figure 17. Rim binding proteins can interact simultaneously with Bassoon or Piccolo, RIM1 and $Ca_V2.2$. 60
Figure 18. Bassoon co-localizes with RBP2 and $Ca_V2.1$ at synapses. 62
Figure 19. The lack of functional Bassoon reduces the amount of $Ca_V2.1$ at synapses. 64
Figure 20. Bassoon but not Bassoon deficient for RBP binding recruits $Ca_V2.1$. 65
Figure 21. Bassoon via its interaction with DLCs functions as a cargo adaptor for the retrograde motor dynein in COS-7 cells. 68

Figure 22. Via their multiple SH3 domains, RBPs interacting with Bassoon and Piccolo may act as linkers between Rims and voltage-dependent calcium channels, thus organizing individual steps of the SV cycle and localizing the priming and fusion apparatus in the vicinity of the VDCC. 72
Figure 23. Primary structure of Rim binding proteins: comparison of RBP1 and RBP2..... 87

1. Introduction

1.1 Chemical synapses. Presynaptic boutons: organization and function

Chemical synapses are highly specialized cellular junctions between neurons and their target cells, designed for the rapid and efficient transmission of signals between these cells. They are asymmetric structures, composed of a presynaptic bouton, which harbors neurotransmitter filled synaptic vesicles (SVs), and a postsynaptic compartment, which contains receptors for the neurotransmitters. The two synaptic compartments are separated from each other by an approximately 20 nm wide synaptic cleft.

At these synapses signals are transduced by temporally and spatially tightly regulated release of neurotransmitters from the presynaptic terminal. In response to the action potential calcium ions pass through voltage-dependent calcium channels (VDCCs) and enter the presynaptic terminal. The rise in intracellular calcium concentration causes SVs to fuse with the presynaptic membrane and thereby release neurotransmitters into the synaptic cleft, where they diffuse towards the postsynaptic membrane and bind to specific receptors.

Presynaptic boutons of conventional central nervous system synapses are composed of distinct structural and functional compartments. These include the large reservoir of synaptic vesicles and the active zone (AZ) where SVs dock and fuse. The AZ is characterized by a distinctive electron-dense meshwork of proteins facing the synaptic cleft (Landis, 1988). This protein network is thought to represent the molecular machinery that mediates and regulates transmitter release. Using electron microscope tomography, Harlow et al. (2001) provided the first three-dimensional view of the cytoskeletal matrix of the active zone (CAZ) at the frog neuromascular junction. It consists of three identifiable structures: beams, ribs and pegs. The presynaptic membrane underneath the CAZ is curved outwards forming a ridge and the beams run parallel to the ridge's long axis, whereas the pegs connect the CAZ and the presynaptic membrane. The ribs extend orthogonally to the ridge's long axis and form 7-12 connections to docked vesicles located on each flank of the ridge. At conventional synapses SVs were also shown to be interconnected and connected to the presynaptic membrane via a dense meshwork of filaments (Siksou et al., 2007). Although the full molecular composition of the CAZ is still not defined, several CAZ-specific proteins including Rim1, Munc13-1, Bassoon, Piccolo/Aczonin, CAST and liprin-α were identified (Fig. 1). These proteins act in spatial and functional regulation of SV cycle including vesicle tethering to their release sites, docking and priming, fusion with the presynaptic membrane and compensatory endocytosis.

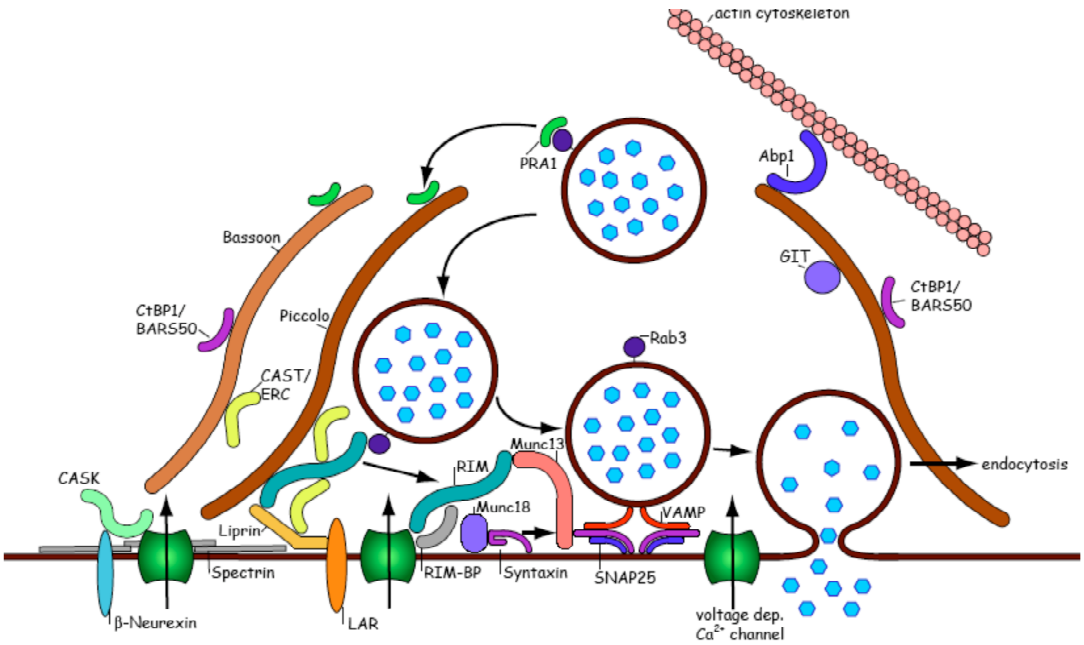

FIGURE 1. MOLECULAR ORGANIZATION OF THE CAZ (FROM FEJTOVA AND GUNDELFINGER, 2006).
The CAZ-specific proteins RIMs, Munc13s, Bassoon, Piccolo and CAST/ERC are thought to localize and organize membrane trafficking events of the synaptic vesicle cycle and connect it to the active zone membrane proteins including VDCCs and cell adhesion molecules such as the neurexins. Further components that are not exclusive CAZ components include Ca^{2+}/calmodulin kinase domain-containing membrane-associated guanylate kinase CASK, the transcriptional co-repressor CtBP1/BARS50, the RIM-binding proteins (RBP), the prenylated Rab3 acceptor protein PRA1, the ARF-GTPase-activating protein GIT, the receptor tyrosine phosphatase LAR and its interacting protein Liprin, components of the SNARE complex and its control elements (e.g. Munc18). The interaction between Piccolo and the actin-binding protein Abp1 is thought to link the active zone to the neighboring endocytic zone.

Each SV can be assigned to one of three pools, which are called as readily releasable pool (RRP), the recycling pool and the reserve pool (reviewed in Rizzoli and Betz, 2005). The RRP comprises all SVs that are available to be exocytosed immediately upon stimulation. These vesicles are generally thought to be docked and primed for release at the AZ. The recycling pool is defined as the pool of vesicles that maintain neurotransmitter release upon physiological stimulation. This pool is thought to contain about 5-20% of all SVs (reviewed in Südhof, 2004). Physiological frequencies of stimulation cause a continuous recycling of the cycling pool, so that it is constantly refilled by newly endocytosed and refilled vesicles. The reserve pool is defined as a depot of SVs from which release is only triggered during intense stimulation. These vesicles constitute the majority (typically 80-90%) of SVs in most presynaptic terminals. Notably, the recycling and reserve vesicle pools are spatially intermingled and can not be distinguished by their location relative to the active zone (Rizzoli and Betz, 2005). In resting terminals most SVs are immobile (Henkel et al., 1996; Kraszewski et al., 1996). It is believed that the best candidates to hold them together are the synapsins. Several studies using synapsin knockout mice (Li et al., 1995; Takei et al., 1995) and acute anti-synapsin antibody injection (Pieribone et al., 1995) showed that lack of functional

synapsins leads to the specific loss of SVs distant from the presynaptic membrane. These observations led to the suggestion that synapsin holds SVs together specifically in the reserve pool (Rizzoli and Betz, 2005). However, other observations show that synapsin molecules do not always discriminate between reserve and non-reserve vesicles (reviewed in Rizzoli and Betz, 2005).

In order to release neurotransmitter into the synaptic cleft, SVs undergo a series of trafficking events including tethering, docking, priming and, finally, fusion of SV membrane with the presynaptic membrane at the AZ.

Tethering and docking of SVs to the presynaptic membrane is most likely mediated by members of Rab family of small GTPases, which interact with various effectors on the plasma membrane side (reviewed in Zerial and McBridge, 2001). In presynaptic terminals of conventional synapses tethering is thought to be achieved through the interaction of CAZ specific protein Rim1 (Rab3 interacting molecule 1) and the vesicular Rab3 (Rosenmund et al., 2003). Two proteins have been firmly implicated in docking, Munc18-1 (Voets, 2001) and syntaxin-1 (de Wit et al., 2006). Currently a new model for the docking step was proposed by de Wit and co-workers (2009): first, Munc18-1 binds the closed conformation of syntaxin-1. Second, SNAP-25 binds the syntaxin-1/Munc18-1 heterodimer. Third, secretory vesicles reach the target membrane area and associate via synaptotagmin-1 to this trimeric syntaxin-1/Munc18-1/SNAP-25 complex, which effectuates docking.

Synaptic vesicles then have to undergo the priming procedure, which is initiated by the CAZ protein of Munc13 family (Rosenmund et al., 2002; reviewed in Rosenmund et al., 2003). In the absence of Munc13 proteins, no fusion-competent vesicles are available and transmitter release is completely blocked (Varoqueaux et al., 2002). Munc13 proteins are regulated by multiple proteins, e.g. Rims, and second messengers, e.g. diacylglycerol, making SV priming a highly dynamic regulated process (reviewed in Rosenmund et al., 2003).

In the presynaptic AZ, after arrival of the action potential calcium influx into the cells occurs through VDCCs. Synaptotagmin 1, located on the SV membrane (Tucker et al., 2004), functions as a Ca^{2+} sensor and triggers the fusion of primed synaptic vesicles with presynaptic plasma membrane, in turn releasing neurotransmitter into the cleft. Functional studies established that fast-regulated exocytosis requires the interaction of small cytoplasmically exposed membrane proteins called SNAREs (soluble N-ethyl-maleimide-sensitive fusion protein attachment protein receptors). For regulated-exocytosis, the relevant SNAREs are synaptobrevin/VAMP (located on vesicle membrane), syntaxin-1 and SNAP-25 (synaptosome-associated protein 25 kDa) (both located on the plasma membrane), which form a complex and represent the minimal machinery for fusion (Jahn and Südhof, 1999; Chen and Scheller, 2001). Fusion is driven by the progressive zippering of vesicle and plasma membrane SNAREs to form a four-helix bundle, referred in literature as the SNARE

complex (Hayashi et al., 1994; Fasshauer et al., 1998; Poirier et al., 1998). Fully primed vesicles require additional interactions with complexins to increase vesicle release probability and to speed up the release time course (reviewed in Rosenmund et al., 2003).

Two structurally related CAZ components, Bassoon and Piccolo/Aczonin, are known to be involved in the assembly of the active zone (Zhai et al., 2001; Shapira et al., 2003). Analysis of Bassoon mutant mice has revealed that Bassoon is essential for the attachment of the retinal (Altrock et al., 2003; Dick et al., 2003) and inner hear cell (IHC) (Khimich et al., 2005) synaptic ribbons to the active zone. Synaptic ribbons are thought to correspond to the CAZ of conventional synapses (Zhai and Bellen, 2004; tom Dieck et al. 2005). CAST (CAZ-associated structural protein) can directly bind Rim1, Bassoon and Piccolo and is believed to be involved in neurotransmitter release through these interactions (Takao-Rikitsu et al., 2004). Several studies have defined crucial functions for liprin-α in the regulation of the active zone assembly (reviewed in Stryker and Johnson, 2007). Moreover, a number of studies on the invertebrate neuromuscular junction support a model, in which liprin-α and its binding partner the receptor protein tyrosine phosphatase LAR cooperate to maintain presynaptic proteins (such as ERC2, Rim, the MALS/Veli-Cask-Mint1 complex) in a dense molecular scaffold at the AZ. In their absence, the tight association of active zone components that is crucial for optimal synaptic vesicle release is severely disrupted (reviewed in Stryker and Johnson, 2007).

1.2 Presynaptic voltage dependent calcium channels: structure and function and regulation

Entry of Ca^{2+} ions through presynaptic VDCCs can be measured electrophysiologically as calcium currents. These currents have diverse physiological roles and pharmacological properties in different cell types, and a systematic nomenclature has evolved for the distinct classes of calcium currents (Tsien et al., 1988). N-type, P/Q-type, and R-type calcium currents require strong depolarization for activation (Tsien et al., 1991) and are blocked by specific polypeptide toxins from snail and spider venoms (Miljanich and Ramachandran, 1995). N-type and P/Q-type calcium currents are observed primarily in neurons, where they initiate neurotransmission at most fast conventional synapses (Catterall, 2000; Dunlap et al., 1995; Olivera et al., 1994). The calcium channels are composed of four or five distinct subunits (Fig. 2A) (Catterall, 2000; Takahashi et al., 1987). The α1 subunit of 190–250 kDa is the largest subunit, and it harbors the conduction pore, the voltage sensors and gating apparatus, and most of the known sites of channel regulation by second messengers, drugs, and toxins. The ~2000 amino acid residues of the α1 subunit are organized in four homologous domains (I–IV). Each domain of the α1 subunit consists of six transmembrane α

helices (S1 through S6) and a membrane-associated P loop between S5 and S6. The S1 through S4 segments serve as the voltage sensor module (Fig. 2B, yellow), whereas transmembrane segments S5 and S6 in each domain and the P loop between them form the pore module (Fig. 2B, green). The α1 subunits are associated with four distinct auxiliary protein subunits (Catterall, 2000) (Fig. 2A and 2B). The intracellular β subunit is a hydrophilic protein of 50–65 kDa. The transmembrane, disulfide-linked α2δ subunit complex is encoded by a single gene, but the resulting pre-polypeptide is cleaved posttranslationally and linked via disulfide-bonds to yield the mature α2 and δ subunits. A γ-subunit having four transmembrane segments is a component of skeletal muscle calcium channels, and related subunits are expressed in heart and brain.

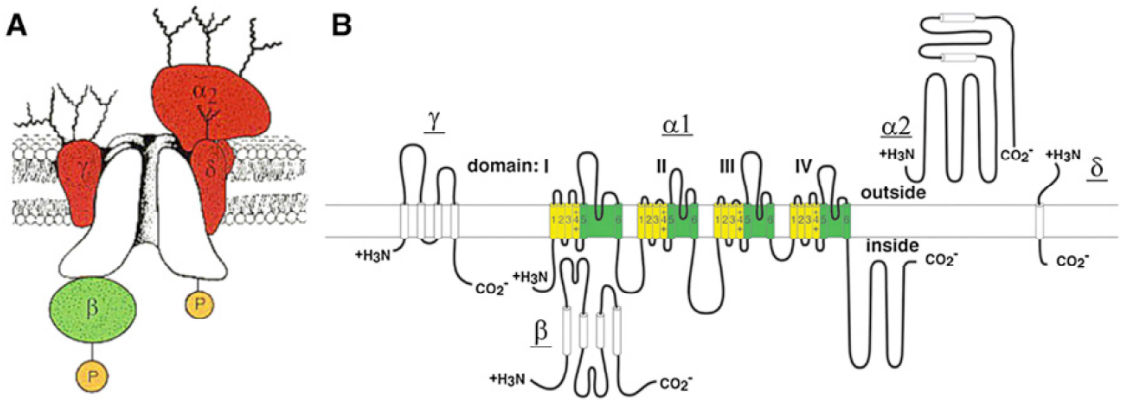

FIGURE 2. SUBUNIT STRUCTURE OF VDCCS (FROM CATTERALL AND FEW, 2008).
(A and B) The subunit composition and structure of VDCCs are illustrated. **(B)** Predicted helices are depicted as cylinders. The lengths of lines correspond approximately to the lengths of the polypeptide segments represented. The voltage-sensing module is illustrated in yellow and the pore-forming module in green.

The auxiliary subunits of VDCCs have an important influence on their function (Dolphin, 2003; Hofmann et al., 1999). $Ca_V\beta$ subunits greatly enhance the cell surface expression of the α1 subunits and shift their kinetics and voltage dependence of activation and inactivation. The α2δ subunits also enhance cell surface expression of α1 subunits, but have smaller and less consistent effects on the kinetics and voltage dependence of gating (Davies et al., 2007). The γ–subunits do not increase cell surface expression of VDCCs and, in some cases, even reduce it substantially. The functional role of the γ subunits of VDCCs is the least well defined. Although these four auxiliary subunits modulate the functional properties of the calcium channel complex, the pharmacological and physiological diversity of VDCCs arises primarily from the existence of multiple α1 subunits. $Ca_V\alpha1$ subunits are encoded by ten distinct genes in mammals, which are divided into three subfamilies by sequence similarity (Catterall, 2000; Ertel et al., 2000; Snutch and Reiner, 1992). The Ca_V2 subfamily members ($Ca_V2.1$, $Ca_V2.2$, and $Ca_V2.3$) conduct P/Q-type, N-type, and R-type Ca^{2+} currents, respectively (Catterall, 2000; Ertel et al., 2000; Olivera et al., 1994; Snutch and Reiner,

1992). Ca^{2+} entering neurons through $Ca_V2.1$ and $Ca_V2.2$ channels is primarily responsible for initiating synaptic transmission at fast conventional synapses (Dunlap et al., 1995; Olivera et al., 1994). $Ca_V2.2$ channels, which conduct N-type Ca^{2+} current, are most important at synapses formed by neurons of the peripheral nervous system. In contrast, $Ca_V2.1$ channels, which conduct P/Q-type Ca^{2+} currents, play the major role at most synapses formed by neurons of the adult mammalian central nervous system. However, in some central synapses, including a subset of inhibitory interneurons of the hippocampus (Poncer et al., 1997), $Ca_V2.2$ channels are predominant in neurotransmitter release. N-type currents also seem to play an important role during development. $Ca_V2.2$ start to function on DIV3-4. At this developmental stage preceding synaptogenesis, $Ca_V2.2$ are involved in controlling synaptic vesicle recycling. It is only at later developmental stages (10–12 DIV), when the neurons have established a clear axodendritic polarity and form synaptic contacts, that these channels are progressively excluded from the axon (Pravettoni et al., 2000) and substituted with $Ca_V2.1$.

1.3 Presynaptic voltage dependent calcium channels: precise localization is essential

Ca^{2+} entry through a single calcium channel can trigger vesicular release (Fig. 3) (Stanley, 1993), and Ca^{2+}-triggered synaptic vesicle exocytosis depends on the assembly of the SNARE complex. Neurotransmitter release is proportional to the third or fourth power of Ca^{2+} entry (Augustine et al., 1987; Regehr, 2002). Thus, regulation of presynaptic Ca^{2+} channels provides a sensitive and efficient tool to regulate neurotransmitter release, as a 2-fold change in the presynaptic Ca^{2+} current results in an 8- to 16-fold change in exocytosis.

The precise co-localization of VDCCs and the fusion machinery can be maintained through a direct interaction of Ca^{2+} channels with SNARE proteins. Both $Ca_V2.1$ and $Ca_V2.2$ channels co-localize tightly with syntaxin-1 in presynaptic nerve terminals (Cohen et al., 1991; Westenbroek et al., 1992, 1995). These channels can be isolated as a complex with SNARE proteins (Bennett et al., 1992; Leveque et al., 1994; Yoshida et al., 1992). The plasma membrane SNARE proteins syntaxin-1A and SNAP-25, but not the synaptic vesicle SNARE synaptobrevin, specifically interact with the $Ca_V2.2$ channel by binding to the intracellular loop between domains II and III (LII-III) of the α1 subunit (Sheng et al., 1994) at the synaptic protein interaction (*synprint*) site. This interaction is Ca^{2+} dependent, with maximal binding at 20 µM Ca^{2+} and reduced binding at lower or higher Ca^{2+} concentrations (Sheng et al., 1996). $Ca_V2.1$ channels have an analogous *synprint* site, and different channel isoforms have distinct interactions with syntaxin and SNAP-25 (Kim and Catterall, 1997; Rettig et al., 1996), what may confer specialized regulatory pathways that contribute to synaptic modulation. The

molecular interaction between syntaxin and presynaptic $Ca_V2.2$ channels has been confirmed in intact nerve terminals by molecular imaging and correlation analysis (Li et al., 2004). The interaction between presynaptic calcium channels and the *synprint* is a regulated process, which might be influenced by phosphorylation of specific amino acids of *synprint* by PKC or CaMKII (Yokoyama et al., 1997, 2005). These studies suggest that phosphorylation of the synprint site may serve as a biochemical switch controlling the SNARE-synprint interaction. Despite the clear evidence of *synprint* involvement in VDCCs co-localization with SV fusion apparatus, two $Ca_V2.2$ splice variants lack large parts of the cytoplasmic II-III loop (Δ1 R756-L1139, Δ2 K737-A1001) including the synprint protein–protein interaction domain were targeted into the axons (Szabo et al., 2006). Nevertheless, their ability to form presynaptic clusters was almost abolished for $Ca_V2.2$-Δ1 and significantly reduced for $Ca_V2.2$-Δ2. Thus, the synprint site is important for normal synaptic targeting of $Ca_V2.2$ but not essential. Based on their observations, the authors of the original paper suggested that protein–protein interactions with the *synprint* site must cooperate with other targeting mechanisms in the incorporation of $Ca_V2.2$ into presynaptic specializations of hippocampal neurons but are neither necessary nor sufficient for axonal targeting.

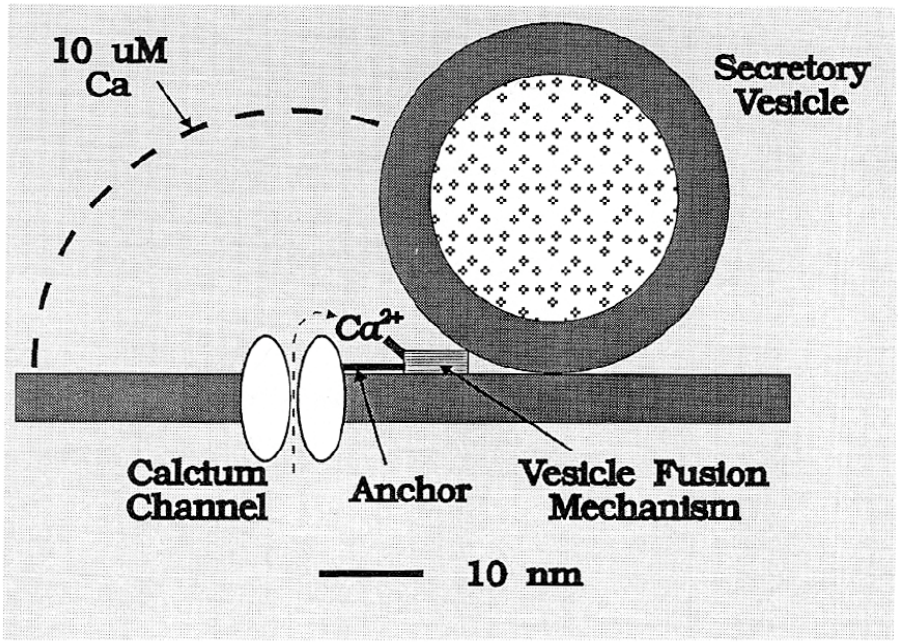

FIGURE 3. MODEL FOR THE ORGANIZATION OF NEUROTRANSMITTER RELEASE SITE (FROM STANLEY, 1993). Single calcium domain model of fast neurotransmitter secretion with inter-element distances approximately to scale. The 10 µM iso-concentration line of the calcium domain is shown.

Three lines of evidence indicate that the interactions with *synprint* are unlikely to be the primary mechanism for targeting presynaptic VDCCs to nerve terminals. First, inhibition of *synprint* interaction or deletion of the *synprint* site on both $Ca_V2.1$ and $Ca_V2.2$ channels reduces the efficiency of exocytosis but does not completely abolish synaptic transmission or hormone secretion (Harkins et al., 2004; Mochida et al., 1996, 2003; Rettig et al., 1997).

Second, although invertebrate Ca_V2 channels effectively initiate synaptic transmission, they lack a *synprint* site (Spafford et al., 2003). Third, SNARE proteins are not selectively localized at nerve terminals themselves, making it unlikely that SNARE proteins provide the primary targeting information. Evidently, interactions with other proteins are also involved in targeting and trafficking of presynaptic Ca^{2+} channels.

Consistent with this idea, the specific association of $Ca_V2.2$ alpha carboxyl termini with the first PDZ domain of Mint1 and SH3 domain of CASK has been reported (Maximov et al., 1999; Maximov and Bezprozvanny, 2002). Furthermore, for *Lymnaea* Ca_V2 channels, lacking the *synprint* region, the interaction with Mint1 and CASK has been shown to be required for proper targeting of channels to the synapse (Spafford et al., 2003). The other line of evidence speaking for involvement of scaffolding proteins in calcium channel targeting comes from studies on *Drosophila* protein Bruchpilot (BRP). BRP is a large coiled-coil domain structural protein, which shows homologies to mammalian scaffolding protein CAST. BRP was visualized as donut-form structures at active zones of *Drosophila* neuromuscular junctions (Kittel et al., 2006). BRP mutant active zones were lacking electron dense projections (T-bars). Ca^{2+} channel density was reduced and their active zone localization was altered as well as evoked vesicle release and short-term plasticity. Authors of the original paper suggested that BRP is not part of the T-bar structure itself but rather tightly surrounds it establishing a matrix, required for both a T-bar assembly as well as the appropriate localization of its components, including VDCCs. Similar mechanisms might be involved in the formation of the mammalian AZ. The presynaptic plasma membrane glycoprotein neurexin is similarly required for development of functional synapses containing presynaptic VDCCs in mice (Missler et al., 2003). Mice deficient for α-neurexins showed a severe reduction in neurotransmitter release due to impairment in VDCCs function. This is presumably mediated by neurexins interaction with synaptotagmin, Mint1 or CASK - direct VDCCs binding molecules. The regulation of VDCCs by α-neurexins predominantly affects calcium currents evoked by $Ca_v2.2$ and $Ca_v2.1$ (Zhang et al., 2005).

1.4 Rim Binding Proteins (RBPs): possible linkers of VDCCs and synaptic vesicle fusion machinery

Vesicle release is modulated by the GTP binding protein Rab3 and the associated proteins rabphilin (Shirataki et al., 1993), Noc2 (Haynes et al., 2001) and Rim1 (Wang et al., 1997). Rab3 is a negative regulator of exocytosis (reviewed in Geppert and Südhof, 1998). In its GTP-bound form, Rab3 is associated with synaptic vesicles as well as with rabphilin, Noc2, and Rim1. Because Rim1 is specifically associated with the synaptic plasma membrane at the AZ, it may act as a regulator of SV fusion by including the formation of a GTP-dependent

complex between SVs and the plasma membrane (Wang et al., 1997; Schoch and Gundelfinger, 2006). Two homologous Rim-binding partners named RBP1 and RBP2 were identified (Wang et al., 2000). A sequence related to rat RBP1 was isolated from human brain cDNA library and published as that of PRAX-1, a protein interacting with mitochondrial peripheral benzodiazepine receptor (Galiegue et al., 1999). Sequence analyses revealed that RBPs contain three dispersed SH3 domains and three contiguous fibronectin type III repeats (Fig. 4; Wang et al., 2000). These domains are the most closely related sequences in RBPs and are flanked by highly charged sequences that are less well conserved. The sequences outside of the SH3 domains and fibronectin type III repeats are rich in charged amino acid residues.

Comparative and phylogenetic analyses with RBPs and related genes in different organism performed by Mittelstaedt and Schoch (2007) revealed that while invertebrate genomes contain only one, vertebrates include at least two RBP genes. They also identified an additional gene, RBP3, which is exclusively expressed in mammals (Fig. 4A). Quantitative real-time PCR analyses of mouse tissue showed that RBP1 and RBP2 were synthesized at high levels exclusively in brain. RBP3 mRNA in contrast was detected ubiquitously, with the highest level of expression in testis (Mittelstaedt and Schoch, 2007).

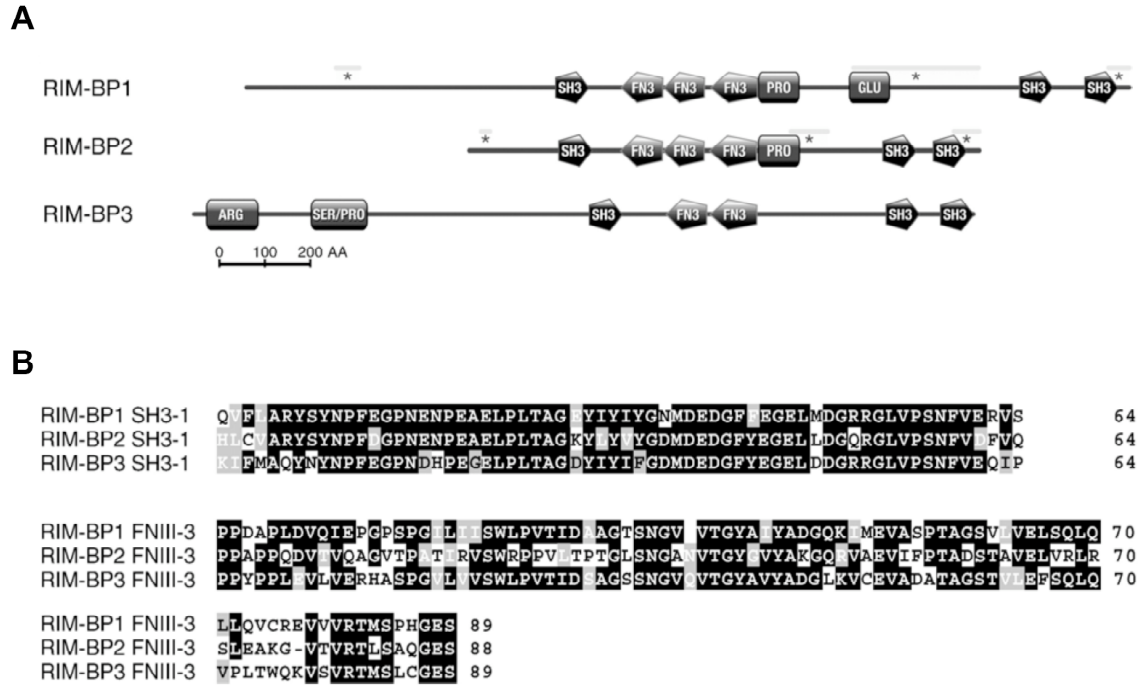

FIGURE 4. STRUCTURE OF THE RBP PROTEIN FAMILY (FROM MITTELSTAEDT AND SCHOCH, 2007).
(A) Diagram of the domain composition of RBPs. RBPs share a similar domain organization with an SH3-domain and a cluster of fibronectin type III (FNIII) repeats in the center of the protein and a doublet of SH3-domain in the C-terminus. Asterisks mark the three sites of alternative splicing in RBP1 and -2. **(B)** The RBP SH3- and FNIII domains are highly homologous, as shown here for SH3-1 and FNIII-3. Filled black boxes mark amino acids identical in all three human RBP proteins and grey boxes indicate conserved residues.

In brain both RBP1 and RBP2 showed neuron-specific expression (Mittelstaedt and Schoch,

2007). RBP1 mRNA is present throughout the brain with highest levels in the cerebellum, cortex, hippocampus and olfactory bulb. Striatum, thalamus and the pontine nuclei also show strong RBP1 expression (Mittelstaedt and Schoch, 2007; Chardenot et al., 2002). RBP2 mRNA is highly concentrated in the telencephalon, consisting of hippocampus, olfactory bulb, and cortex, while it is expressed at lower levels in all other brain regions (Mittelstaedt and Schoch, 2007).

The second SH3 domain of RBP1 and RBP2 bind to PXXP-motifs present in Rim1 and Rim2 (RQLPQL/VP) (Wang et al., 2000; Hibino et al., 2002). This sequence is present in the short region between the two alternatively spliced sequences in the C terminus of the Rims and is the only conserved sequence in this short region. RBPs were also identified as direct interaction partners for $Ca_V\alpha1D$ subunit of L-type VDCCs ($Ca_V1.3$) in afferent synapses of inner ear hair cells (Hibino et al., 2002), where these channels initiate neurotransmitter release (Zidanic and Fuchs, 1995). In yeast-two hybrid system the C-terminal part of $Ca_V1.3$ interacted with each of the three SH3 domains of RBP2, but not with the fibronectin III repeats (Hibino et al., 2002). The RBP-interaction site of $Ca_V1.3$ was narrowed down to a specific PXXP motif – RLLPPTP.

Two major classes of ligands for SH3 domains have been identified (Mayer et al., 2001). Class I ligands have the general consensus +XφPXφP whereas class II ligands display the consensus sequence φPXφPX+, in which + is a basic residue, usually arginine, X is any amino acid, and φ is a hydrophobic residue. The $Ca_V1.3$ motif, RLLPPTP, fits the consensus sequence for class I ligands, differing only by a non-hydrophobic threonine residue in the sixth position. Screening of protein databases for the presence of other $Ca_V\alpha$ subunits that contain a motif similar to SH3-binding motif of $Ca_V1.3$ revealed that it is conserved in α1A ($Ca_V2.1$), B ($Ca_V2.2$) and F ($Ca_V1.4$) subunits. The α1E ($Ca_V2.3$) subunit lacks the threonine residue in the sixth position but otherwise fits to the α1D sequence. Therefore $Ca_V2.2$ was examined for its ability to interact with RBP2 (Hibino et al., 2002). A fusion protein containing the last two SH3 domains of RBP2 quantitatively precipitated a full-length α1B subunit expressed in tsA201 cells. Furthermore, native RBPs were precipitated from brain extracts by a GST fusion protein containing the RQLPQTP motif of α1B and its flanking sequences. Taken together, these results suggest that RBPs can interact with α1B and perhaps with other α1 subunits in the brain. Finally, based on their observations, Hibino and collegues suggested that by virtue of their multiple SH3 domains RBPs could serve as bifunctional linkers between Rims and VDCCs (Fig.5) (Hibino et al., 2002).

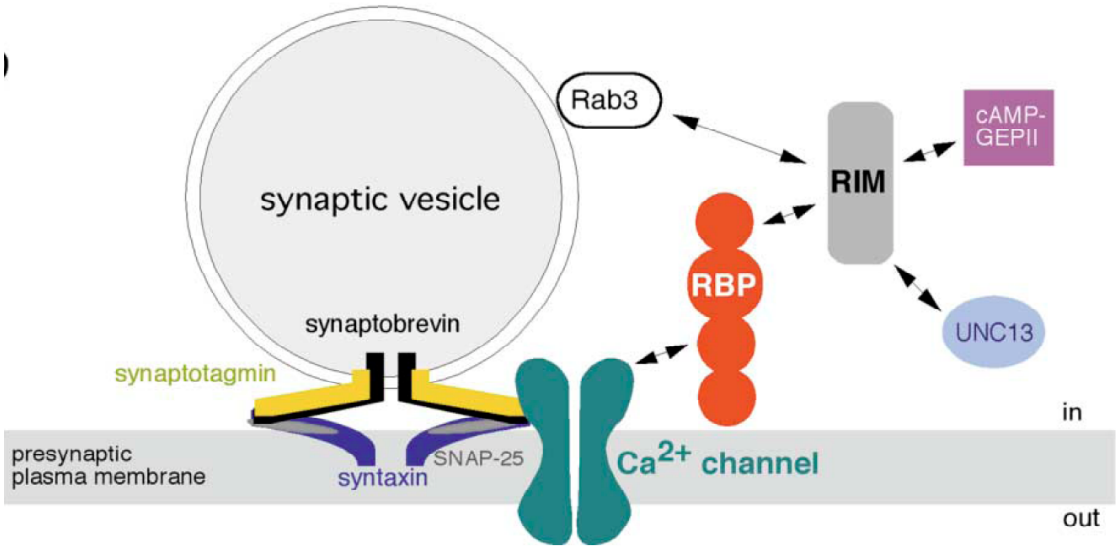

FIGURE 5. RBPS CAN SERVE AS LINKERS BETWEEN VDCCS AND SYNAPTIC VESICLE FUSION MACHINERY (FROM HIBINO ET AL., 2002).
By virtue of their multiple SH3 domains, RBPs may act as linkers between Rims and VDCCs, thus forming a physical connection between the priming and fusion apparatus constituted by the SNARE complex and the vesicles tethered by Rim and Rab3 at the presynaptic active zone. The proteins cAMP-GEPII and UNC-13 also interact with Rim.

1.5 Bassoon and Piccolo: two major components of the cytomatrix at the active zone

Bassoon and Piccolo are two key components of CAZ network. They are present in this CAZ at both excitatory and inhibitory synapses (tom Dieck et al., 1998; Richter et al., 1999) and appear very early during synaptogenesis at nascent synapse (Zhai et al., 2001), suggesting a role in the assembly of functional AZs. Ten regions of high homology (50%-80% identity) referred to as Piccolo-Bassoon homology (PBH) regions were identified (Fenster et al., 2000) in Bassoon and Piccolo (Fig. 6).

To date, among all CAZ proteins only liprin-α and Bassoon are known to be involved in aspects of AZ formation and structure. At retina photoreceptor synapses the physical interaction of Bassoon with the ribbon-specific polypeptide Ribeye has been shown to be essential for the assembly of ribbon complex and in turn for a proper neurotransmitter release. It has also been shown that Bassoon-mutant mice lack AZ-anchored ribbons in retinal photoreceptors and display impaired vision (Dick et al., 2005; tom Dieck et al., 2005). Similar abnormalities were demonstrated in inner hair cells of knockout mice (Khimich et al., 2005). Here, calcium currents were reduced and fast exocytosis was strongly decreased in mutant IHC. The authors suggested that the proper localization and/or plasma membrane anchoring of $Ca_V1.3$ in the active zone is impaired in the absence of Bassoon, which implicates Bassoon in clustering of VDCCs. While Ribeye is specific for ribbon synapses its close homologue CtBP1 is present at conventional synapses as well, where it also can

interact with Bassoon (tom Dieck et al., 2005).

At hippocampal neurons lack of functional Bassoon causes a reduction in normal synaptic transmission (Altrock et al., 2003). A significant fraction of glutamatergic synapses at hippocampal neurons of knockout mice was inactivated. At these synapses, vesicles were clustered and docked in normal numbers but were unable to fuse. According to these data Bassoon is not essential for the formation of conventional synapses but plays a crucial role in the regulated neurotransmitter release. Another line of evidence for Bassoon's involvement in neurotransmitter release comes from discovery of a CAST-dependent large molecular complex at CAZ. The C-terminal region of CAST can interact with Rim1 and Bassoon and Piccolo, thus leading to a formation of a triple complex between these proteins. Furthermore, a link to another genuine CAZ component, Munc-13, can be provided via its direct interaction with Rim1 (Brose et al., 2000). A dominant-negative approach used to interfere with this complex formation leads to impaired synaptic transmission in cultured superior cervical ganglion neurons (Takao-Rikitsu et al., 2004).

In our recent paper we showed that Bassoon but not Piccolo interacts with dynein light chains (Fejtova et al., 2009). Through these interactions Bassoon is involved in trafficking and synaptic delivery of AZ components.

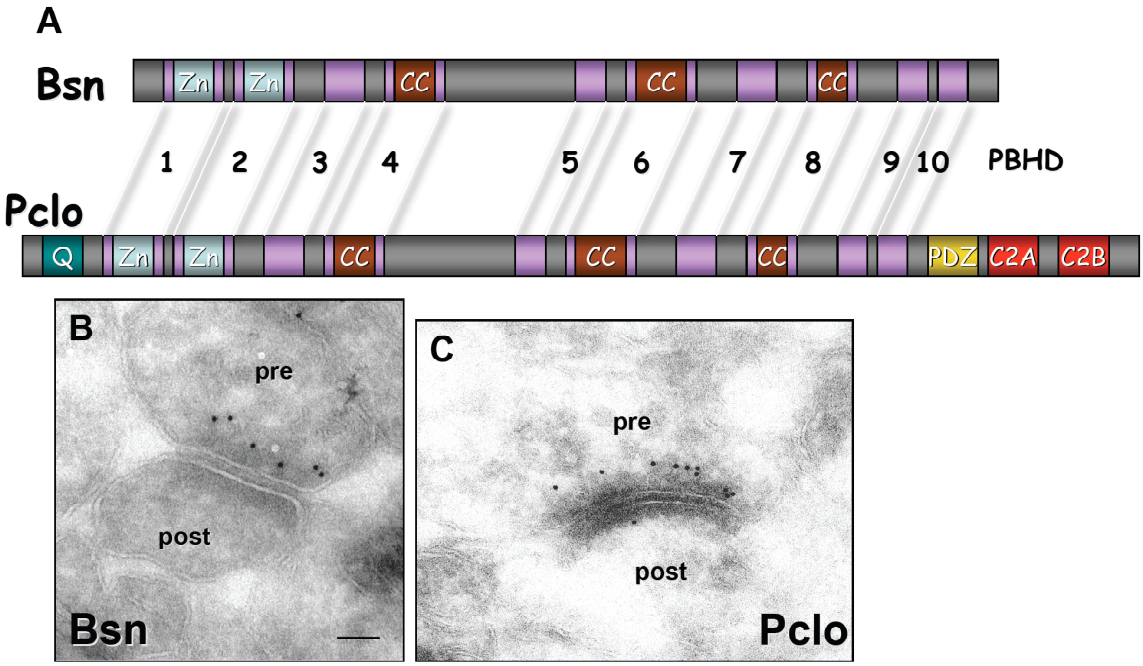

FIGURE 6. BASSOON AND PICCOLO ARE TWO MAJOR COMPONENTS OF THE CAZ.
(A) Schematic representation of Bassoon and Piccolo domain composition. Zn1/2, zink fingers; CC1-3, coiled-coil regions; PDZ, PSD-95/Dlg/zonula occludens-1 homology domain; C2A/B, C2 domains; PBHD1-10, regions of the Piccolo - Bassoon homology. **(B and C)** Electron micrographs showing Bsn (B) and (Pclo) exclusive presynaptic localization (kindly provided by K. Richter, Otto-von-Guericke University Magdeburg).

Piccolo is a multidomain zinc finger protein structurally related to Bassoon. At the C terminus, Piccolo/Aczonin contains a single PDZ and one or two C2 domains which are absent in

Bassoon (Wang et al., 2000; Fenster et al., 2000). The Piccolo-Bassoon zinc fingers are most similar to those found in rabphilin-3A and Rim (40% and 39% similarity, respectively) (Fenster et al., 2000). The second zinc finger domain of Piccolo interacts with rab3-VAMP2/SynaptobrevinII-interacting protein PRA1. Through this interaction Piccolo might be involved in the recycling of synaptic vesicles in nerve terminals. The C2 domain of Piccolo is able to bind Ca^{2+}, suggesting that calcium influx through VDCCs at the AZ may regulate the biological activity of Piccolo (Fenster et al., 2000). Furthermore, Fujimoto et al. (2002) showed that Piccolo can form homodimers through its first C2 domain in a Ca^{2+}-dependent manner. The PDZ domain of Piccolo, absent in Bassoon, interacts with cAMP-GEFII (cAMP-guanidine nucleotide exchange factor II) in pancreatic beta-cells (Fujimoto et al., 2002). Treatment of pancreatic islets with antisense oligodeoxynucleotides against Piccolo inhibited insulin secretion induced by cAMP analogue 8-bromo-cyclic AMP plus high glucose stimulation, suggesting that Piccolo serves as a Ca^{2+} sensor in exocytosis in pancreatic beta-cells and that the formation of a cAMP-GEFII - Rim2 - Piccolo complex is important in cAMP-induced insulin secretion. In addition Piccolo directly binds $Ca_V1.2$ in pancreatic beta-cells (Shibasaki et al., 2004). Recently, Piccolo has been shown to act as a negative regulator of SV exocytosis in neurons (Leal-Ortiz et al., 2008). Using interference RNAs to disrupt expression of Piccolo in developing neurons, Leal-Ortiz and colleagues showed that Piccolo negatively regulates SV exocytosis by modulating synapsin dynamics, thus potentially coupling the mobilization of SVs in the reserve pool to events at the AZ.

Piccolo but not Bassoon directly interacts with GIT1 (Kim et al., 2003) – a member of GIT family, known to regulate endocytosis of various membrane proteins (Premont et al., 1998) and the assembly of focal adhesion complexes (reviewed in Zhao et al., 2000). In brain, Piccolo forms a complex with GIT1 and various GIT-associated proteins. Although the specific function for GIT1 in neurons remains unclear, it may be involved in receptor trafficking, actin cytoskeleton rearrangement, and neurotransmitter release at the AZ (Kim et al., 2003), where it is recruited *via* interaction with Piccolo. The actin-binding protein Abp1 is also recruited to the AZ in a Piccolo-dependent manner. A direct interaction between these two proteins has been reported by Fenster et al. (2003). Abp1 binds to both F-actin and the GTPase dynamin and has been implicated in linking the actin cytoskeleton to clathrin-mediated endocytosis. The authors suggested that Piccolo, as a structural protein of the CAZ, might serve to localize Abp1 at AZs where it can actively participate in creating a functional connection between the dynamic actin cytoskeleton and SV recycling.

The high structural similarity of Bassoon and Piccolo and the overlap of many binding partners suggest that they may share functions in synaptic boutons. In line with this assumption, while neither lack of Bassoon (Altrock et al., 2003) nor Piccolo has lethal effect, the Bsn/Pclo double knockout mice are not viable (Anna Fejtova, personal communication).

1.6 Axonal transport of presynaptic components: a role for dynein motors?

When a developing axon meets an appropriate target, a functioning synapse can form within minutes. This speed can only be achieved because axonal transport has already brought the key components of the synapse into the growing axon. In neurons, the transport of membranous organelles along axons is based on molecular motors that propel organelles along microtubules, which in axons are oriented uniformly, with their plus ends pointing toward the growing tips (Burton and Paige, 1981). Anterograde transport is driven by members of the kinesin family of molecular motors, whereas retrograde transport relies mainly on the cytoplasmic dynein 1 motor complex (Vale, 2003). The role of anterograde transport in trafficking of axonal proteins is well documented and molecular motors carrying axonal cargos were identified (Hirokawa and Takemura, 2005).

In a developing neuron, the components needed for synaptogenesis travel in armadas composed of multiple vesicular organelles that contain at least two classes of transport vesicles. The first component, SV precursors (SVPs), contains markers of SV (Jin and Garner, 2008). The second vesicle class, the Piccolo-Bassoon transport vesicles (PTVs), are dense-core 80 nm vesicles with a coat of electron-dense material that contain AZ proteins. Though PTVs and SVPs cluster together while moving and are recruited together to new synaptic sites, they may in fact use distinct kinesins (reviewed in Goldstein et al., 2008). The transport of SVPs is dependent on kinesin-3 heavy chain KIF1A (Okada et al., 1995). Liprin-α has been suggested either to act as a cargo adaptor protein linking SVPs to KIF1A (Miller et al., 2005) or to be a molecule that signals the motor to unload its vesicles at the synapse (Patel et al., 2006).

PTVs were originally characterized as vesicles carrying Bassoon and Piccolo (Zhai et al., 2001). Furthermore, PTVs were found to contain additional AZ proteins but not SV proteins or periactive zonal proteins (Zhai et al., 2001; Shapira et al., 2003). These studies indicate that PTVs may serve as preassembled AZ precursor vesicles, which can be directly inserted into the presynaptic plasma membrane to constitute a functional AZ (Shapira et al., 2003). Whereas kinesin-3 family members predominate in transport of SVPs, the transport of PTVs is more complex. In hippocampal neurons, a protein called syntabulin is implicated in transport of PTVs (Cai et al., 2007; reviewed in Goldstein et al., 2008). This protein has been shown to act as a cargo adaptor for PTV transport via its binding to the kinesin-1 motor KIF5b. Reduced syntabulin levels also decreased activity-dependent formation of new synapses, therefore confirming the crucial role of PTV transport for this form of plasticity (Cai et al., 2007).

Imaging of most anterogradely transported axonal cargos reveals that they move bidirectionally (Miller et al., 2005; Schroer et al., 1985; Shapira et al., 2003) suggesting that most cargos are able to associate with both anterograde and retrograde motors. The retrograde transport of vesicles might be necessary for even distribution of material over the axon before synaptogenesis. However, little attention has been paid to the understanding of the molecular mechanisms and physiological meaning of retrograde transport of material predestined for delivery to distal axonal locations.

In a yeast-two hybrid screen dynein light chain LC8 (DLC or DYNLL) has been discovered as a novel interaction partner for Bassoon by our laboratory. DLC represents one of 3 dimeric light chains of the cytoplasmic dynein motor complex (Pfister et al., 2005; Vallee et al., 2004). In mammals, two DLC isoforms DLC1 and DLC2, were reported to link cargos to the dynein motor (Lee et al., 2006; Navarro et al., 2004; Schnorrer et al., 2000), to associate with the actin-dependent motor myosinV (Espindola et al., 2000), where it might also function as a cargo adaptor (Puthalakath et al., 2001), and to have additional, motor-independent cellular functions (Jaffrey and Snyder, 1996; Vadlamudi et al., 2004).

1.7 Aims of this work

Several interaction partners of Bassoon, including dynein light chain-1 (DLC1) and Rim-binding protein-1 (RBP1) had been identified in a yeast-two hybrid screen by Dr. Wilko Altrock. In order to confirm these interactions and to investigate their physiological significance it was necessary to study them in independent heterologous and homologous expression systems.

To this end a new expression system was established to test the interactions in living mammalian cells. The assay is based on the idea of targeting one binding partner artificially to the surface of mitochondria and to study the co-recruitment of co-expressed potential binding partners – the mito-targeting system.

A second assay to be established for my work was designed to study direct protein-protein interactions in a quantitative manner based on the surface plasmon resonance technology using Biacore device.

Based on these techniques and applying further technologies established in the laboratory it was the aim of my thesis to study the role of Bassoon in assembling the active zone of neurotransmitter release. In this context I have studied the interactions (1) between Bassoon and DLCs and (2) between Bassoon and RBPs in more details. As Piccolo, a closely related protein to Bassoon, is present in the same compartment, it was further of interest to study potential interactions also with this CAZ protein.

1) As described above, the interaction of Bassoon with DLCs may serve to link Bassoon and subsequently entire PTV to the retrograde microtubular motor dynein. This in turn may have implication for the appropriate distribution of active zone material along axons and between synapses. Therefore it is of high importance to study the nature of this interaction in more detail. In frame of this project following aspects were addressed:
    - Bassoon binding to DLC1 and DLC2, previously shown only in yeast cells, were further characterized in living mammalian cells using newly developed mito-targeting assay.
    - Since both DLC1 and DLC2 were shown to interact with three independent sites in Bassoon molecule, the other goal in this study was to characterize those interactions in terms of preferences of distinct DLC-binding motifs of Bassoon to DLCs. To tackle this question surface plasmon resonance technique was applied to measure relative binding affinities for distinct DLC-binding motifs of Bassoon to DLC1 and DLC2.

2) Reduced Ca^{2+} currents and impaired exocytosis in ribbon synapses of Bassoon mutant mice indicated the possible mislocalization and/or instability of VDCCs in the presynaptic active zone in the absence of functional Bassoon. RBPs had been shown to interact with both Rims and VDCCs, thus forming a physical connection between Ca^{2+} channels and synaptic vesicles tethered by Rim and Rab3 at the presynaptic active zone. Given this and taking into account the newly discovered interaction of RBPs and Bassoon, my working hypothesis was that the interaction of Bassoon and/ or Piccolo with RBPs might contribute to VDCCs retention and accurate localization in the active zone of the presynaptic plasma membrane. More specifically three aspects were addressed:
    - First, Bassoon and Piccolo bindings to RBP1 and RBP2 were characterized: the interaction motifs in these proteins were pinpointed and a possible regulation of these interactions by phosphorylation was investigated.
    - The other goal was to characterize RBPs as organizers of the presynaptic active zone in terms of linker molecules connecting CAZ proteins with VDCCs: the linking abilities of RBPs were assessed by investigating whether binding to different proteins is simultaneous or competitive.

Finally, the role of Bassoon in synaptic targeting of VDCCs was assessed: the effect of Bassoon loss on amount of VDCCs at synapses as well as the ability of Bassoon to recruit VDCCs through RBPs were investigated.

2. Materials and methods

2.1 Materials

2.1.1 Chemicals

The kits and chemicals that were used in this work were purchased from the described companies. The quality of the reagents was of analytical grade. If special reagents were used for experiments, it is described at the beginning of each section.

2.1.2 Kits, enzymes and molecular biology reagents

Item	**Company**
Endonucleases (Restriction enzymes)	New England Biolabs; Fermentas
Taq DNA polymerase	Qiagen
Phusion® DNA Polymerase	Finnzymes
Alkaline Phosphatase from calf intestine (CIAP)	Fermentas
Deoxynucleoside Triphosphate Set (dNTPs)	Fermentas
T4 DNA ligase	Fermentas
T4 Polynucleotide Kinase (PNK)	Fermentas
Oligonucleotides (Primer)	Invitrogen
Nucleospin PCR cleanup gel extraction Kit	Macherey-Nagel

TABLE 1: MOLECULAR BIOLOGY REAGENTS

2.1.3 Molecular weight markers

DNA molecular weight markers	**Company**
Smart Ladder DNA	Eurogentec
GeneRuler™ 1 kb DNA Ladder, ready-to-use	Fermentas
GeneRuler™ 100 bp Plus DNA Ladder, ready-to-use	Fermentas
Protein molecular weight markers	**Company**
Precision Plus Protein™ Standarts	BIO-RAD

TABLE 2: MOLECULAR WEIGHT MARKERS FOR DNA AND PROTEINS

2.1.4 Bacteria and yeast cells

Bacterial Cells	**Company**

E.coli BL21-CodonPlus®(DE3)-RIPL	Stratagene
E.coli XL10 Gold Bacteria	Stratagene

TABLE 3: BACTERIA AND YEAST CELLS

Yeast strains	Genotype	Transformation marker	Reporter gene	Company
S. cerevisiae AH 109	MAT a, trp 1-901, leu2-3, 112, ura-3-52, his3-200, gal4Δ, gal80Δ, LYS2::GAL1$_{uas}$-GAL1$_{TATA}$-HIS3, GAL2$_{UAS}$-GAL2$_{TATA}$-ADE2, URA3::MEL1$_{UAS}$-MEL1$_{TATA}$-*lacZ*	trp1, leu2	*LacZ*, HIS3	Clontech

TABLE 4: YEAST CELL STRAINS

2.1.5 Mammalian cells

Mammalian cell line	Company
Kidney Fibroblast Cells from African green monkey (COS-7 cells)	Clontech
Human Embrionic Kidney Cells (HEK293-T)	ATCC

TABLE 5: MAMMALIAN CELL LINES

2.1.6 Cell culture media and reagents for mammalian cells

Item	Composition
COS-7 and HEK293-T cell culture medium	DMEM (Invitrogen), 10% fetal calf serum, 2 mM L-glutamine, 100 U/ml penicillin, 100 µg/ml streptomycin
Trypsin	0.5% Stock solution, diluted 1:10 in HBSS (Invitrogen)
Poly-D-lysin	100 mg/l poly-D-lysin in 100 mM boric acid, pH 8.5, sterile filtered.
HBSS	Hank's balanced salt solution, $Ca^{2+}$and Mg^{2+} free (Invitrogen)

TABLE 6: MEDIA AND REAGENTS FOR MAMMALIAN CELL CULTURE

2.1.7 Culture media and additives for yeast and bacteria cells

Culture medium	
Bacterial-culture medium	**Composition**
LB-medium	20 g LB Broth Base (Invitrogen) / 1000 ml H_2O
SOC-medium	20 g/l peptone 140 (Gibco); 5 g/l yeast extract (Gibco); 10 mM NaCl; 2.5mM KCl; 10 mM $MgSO_4$; 20 mM Glucose
LB-Agar	15 g Select Agar (Invitrogen) / 1000 ml LB-medium
Yeast medium	**Composition**
YPDA-medium	50 Broth (Gibco) / 1000 ml H_2O; plus 10 ml 0.3%

	Adeninehemisulfate
Minimal-SD-medium	20 g Glucose; 1.7 g Yeast-Nitrogen Base (Gibco), 5 g $(NH_4)_2SO_4$/ l000 ml H_2O; pH 7.0.
-LW-medium	0.64g -Leu/-Trp DO Supplement (Clontech) pro 1l Minimal SD-Medium
-ALWH-medium	0.60g -Ade/-Leu/-Trp/-His DO Supplement (Clontech) pro 1l Minimal-SD-medium; 1 mM 3-amino-1,2,4-triazole

TABLE 7: MEDIA AND REAGENTS FOR YEAST AND BACTERIA CELL CULTURE

All media were autoclavated at 121°C for 15 minutes. The additives were filtered with a 0.2 µm filter-unit (Schleicher & Schuell) and stored at –20°C.

2.1.8 Buffers used in biochemical or molecular biology work

Buffer	Composition
PBS	2.7 mM KCl, 1.5 mM KH2PO4, 137 mM NaCl, 8 mM Na2HPO4, pH 7.4
PBST	2.7 mM KCl, 1.5 mM KH2PO4, 137 mM NaCl, 8 mM Na2HPO4, pH 7.4, 0.1% Tween 20
6× DNA sample buffer	30% (v/v) Glycerine, 50 mM EDTA, 0.25% Bromophenol-blue, 0.25% Xylene Cyanol
Cell lysis buffer	10 mM Hepes (pH 7.5), 100 mM NaCl, 0.5% Triton-X100, protease inhibitors Complete mini (Roche) 1 Tbl per 10 ml

TABLE 8: BUFFERES USED IN BIOCHEMICAL AND MOLECULAR BIOLOGICAL ASSAYS

2.1.9 Yeast assay buffers

Solution	Composition
10× LiAc	1 M LiAc in H_2O, pH 7.5
10× TE	0.1 M Tris-HCl, 10 mM EDTA, pH 7.5
PEG	50 % (v/v) polyethylenteglycol 4000 (PEG) in H_2O
PEG/TE/LiAc	8 ml PE; 1 ml 10x TE; 1 ml 10x LiAc

TABLE 9: BUFFERS USED IN YEAST ASSAYS

2.1.10 Antibodies: Primary antibodies for Western blot and immunocitochemistry

Antibodies	Antigen	WB dilution	ICC dilution	Company/ Origin
rb[1] Sap7f	Bassoon		1:2000	tom Dieck, 1998
gp[2] Synapsin 1,2	Synapsin 1,2		1:1000	SySy

[1] rb - rabbit
[2] gp – guinea pig

rb Synapsin 1,2	Synapsin 1,2		1:2000	SySy
m[3] Synapsin 1,2	Synapsin 1,2		1:2000	SySy
rb $Ca_V2.1$	$Ca_V2.1$		1:1000	Alamone labs
gp RBP2	RBP2		1:1000	provided by A. Fejtova
m α-tubulin	α-tubulin		1:1000	Sigma Aldrich
phalloidin– Alexa Fluor 568	actin		1:500	Invitrogen
rb GFP	GFP	1:10000		Abcam
m c-myc 9C10	c-myc	1:1000		Santa Cruz Biotechnology, Inc.

TABLE 10: PRIMARY ANTIBODIES FOR WB AND ICC

2.1.11 Antibodies: Secondary antibodies for Western blot and immunocitochemistry

Antibodies	Antigen	WB dilution	ICC dilution	Company
donkey or goat Alexa Fluor™488	rb or m or gp IgG		1:2000	Invitrogen
donkey or goat Cy3	rb or m or gp IgG		1:2000	Jackson ImmunoResearch
donkey or goat Cy5	rb or m or gp IgG		1:1000	Jackson ImmunoResearch
goat IgG, peroxidase-conjugated	rb or m IgG	1:20000		Jackson ImmunoResearch

TABLE 11: SECONDARY ANTIBODIES USED FOR WB AND ICC

2.1.12 Animals

Rodent lines used for organ harvesting are listed in Table 2. They were bred in the animal facilities of the Leibniz Institute for Neurobiology, Magdeburg and of the ZENIT, Magdeburg. Homozygot mutant mice were obtained from heterozygot breedings.

Animal line	Notes	Origin
C57Bl6|J cre	*Mus musculus* (wild type)	Charles River
SV129EMSJ	*Mus musculus* (wild type)	Jackson Laboratories
BGT KO	Omnibank clone 486029; Gene trapping vector VICTR 48; mixed genetic background	Lexicon pharmaceutics
Wistar rats	*Rattus norvegicus familiaris*	Leibniz Institute for Neurobiology

TABLE 12: ANIMAL LINES

[3] m - mouse

2.2 Methods

2.2.1 Molecular biological methods

All molecular biological work was carried out corresponding to standard protocols. All methods are described in the literature in detail: *Current Protocols in Molecular Biology* (Ausubel *et al.*, 1990) and *Molecular Cloning* (Sambrook *et al.*, 1989). Therefore, only a brief description will be given and the modifications will be described in more detail if this applies.

2.2.1.1 Genotyping of mutant mice

2.2.1.1a DNA extraction for genotyping of mutant mice

Newborn pups were labeled and tailcut samples were taken for DNA extraction. The tailcut samples were incubated together with 500 µl lysis buffer including freshly added Proteinase K at 55°C for 20 min under shaking. Inactivation of the enzyme followed by incubation for 10 minutes at 98°C. The samples were now ready for PCR. One tube without tailcut sample was used as a negative control.

2.2.1.1b Polymerase chain reaction (PCR) for genotyping

PCR was performed using 21 µl of master mix for WT and KO PCR with freshly added Taq Polymerase and 4 µl of DNA extract for genotyping. The final concentrations of the PCR reagents were: 1 pM forward primer, 1 pM reverse primer (see Table 13 for sequences), 2.5 mM $MgCl_2$, 0.1 units/µl Taq-polymerase, 0.2 mM dNTPs in Q-solution (Qiagen, 5x) and PCR buffer (Qiagen, 10x). For reagents used see Table 1. The temperature profile of the PCR is highlighted in Table 14.

Genotype	Forward primer	Reverse primer	Product size
BGT WT	5'-ctaagctattgcttcctcctcac-3'	5'-ctgaggctcttgagttcctacga-3'	600 bp
BGT KO	5'-ctaagctattgcttcctcctcac-3'	5'-ataaaccctcttgcagttgcatc-3'	400 bp

TABLE 13: PRIMER SEQUENCES USED FOR GENOTYPING OF BGT AND WILD-TYPE ALLELES AS WELL AS SIZE OF EXPECTED PCR PRODUCTS

Process	Time and temperature	Cycles
Initial denaturation	5 minutes at 95°C	1
Denaturation Annealing Extension	45 seconds at 95°C 45 seconds at 65°C 60 seconds at 72°C	34

Final extension	30 seconds at 72°C	1

TABLE 14: PCR PROGRAMMES USED FOR GENOTYPING OF BGT MOUSE PUPS

2.2.1.2 PCR for amplification

If cDNA constructs were generated by PCR, specific primers were resuspended at a concentration of 100 pmol/µl and used in the amplification reaction at a final concentration of 10 pmol/µl. The concentration of the dNTPs was 0.2 mM plus 2 U of Phusion® DNA Polymerase in PCR buffer HF (Finnzymes). For reagents used see Table 1. The temperature profile used for PCR is highlighted in Table 15 (Annealing temperature is primer depending and was for this reason specific for the pair of primers; the amount of cycles varied between experiments).

Process	Time and temperature	Cycles
Initial denaturation	1 minute at 98°C	1
Denaturation Annealing Extension	30 seconds at 98°C 30 seconds at 50-70°C 60 seconds at 72°C	30-40
Final extension	1 minute at 72°C	1

TABLE 15: PCR PROGRAMMES USED FOR GENERATION OF CDNA FRAGMENTS

2.2.1.3 Introduction of point mutations by PCR

All mutations described were introduced by inverse PCR using primers with mutated sequence and corresponding Bassoon fragments subcloned in pBluescriptII SK^{-} (Agilent Technologies) as a template (Ausubei et al., 2003). The final reaction mixture and the tempriture profile used are the same as described in 2.2.1.2 part of this thesis).

2.2.1.4 DNA agarose gel electrophoresis

DNA fragments obtained after PCR (2.2.1.2) or after restriction digestion (2.2.1.8) were separated according to their size by one-dimensional agarose gel electrophoresis. Agarose gels (0.75-1.5 % w/v) were prepared by melting the agarose (UltraPure, Gibco). To visualize the DNA under UV light, 5 -10 µl Ethidium bromide solution (10 mg/ml in H_2O) was added before gel polymerization. The DNA samples were prepared in 6x loading buffer and were loaded onto the gel. Gels were run at 80V in 1× TAE buffer. The DNA fragments were visualized under UV-light and photographed with an Eagle-Eye (Stratagene) using the gel documentation system Gel Doc (Biorad, München, Germany).

2.2.1.5 cDNA cloning into expression vectors

DNA fragments of interest were amplified by PCR (2.2.1.2). Following agarose gel electrophoresis in TAE buffer (2.2.1.4), the fragments were purified by the PCR cleanup gel extraction kit (Macherey-Nagel). The fragments were subjected to enzymatic digestion (2.2.1.8) and ligated with T4 DNA ligase to the pre-digested vector. The ligations were performed at 16 – 20°C for 2 – 8 hour. The used DNA fragment/vector ratio was 3:1. To select for positive clones, the ligated fragment-vectors were transformed into *E. coli* XL10 Gold competent cells for subsequent DNA mini-prep isolation.

2.2.1.6 Heat shock transformation of competent *E.coli* XL 10 Gold bacteria cells

The DNA ligation mixture (2.2.1.5) was incubated together with 100 µl of heat shock competent XL10 Gold bacteria for 10 minutes on ice. Heat shocking for 30 seconds at 42°C was followed by incubation on ice for 1 minute. Then 1 ml of prewarmed SOC medium was added and the tube incubated at 37°C for 1 h shaking at low speed. Bacterials were spined down at 1000×g for 1 min and the supernatant was decanted. The pellet was resuspented by vortexing in the remaining drops of liquid. The entire suspension was plated on LB agar plates containing the respective antibiotics. Plates were incubated over night at 37°C.

2.2.1.7 Plasmid isolation (Mini DNA preparation)

Buffer	Composition
P1 Buffer:	50 mM Tris/HCl pH 8.0, 10 mM EDTA, 100 µg/ml RNase A (4°C).
P2 Buffer:	200 mM NaOH, 1% (w/v) SDS
P3 Buffer:	3 M potassium acetate, pH 5.5

TABLE 16: BUFFERS FOR DNA PREPARATION (MINI SCALE)

DNA plasmids were purified from a 2 ml LB overnight culture by alkaline lysis. The cells were pelleted, resuspended in 300 µl of P1 buffer and lysed with 300 µl of P2 buffer. In this step proteins and DNA were denatured and RNA hydrolyzed. With 300 µl of P3 buffer the mixture was neutralized, which leads to the precipitation of denatured proteins and chromosomal DNA. The debris were removed by centrifugation of the lysate at 6000×g for 10 minutes. The supernatant was transferred to a new tube and 630 µl of isopropanol were added and mixed. The plasmid DNA was precipitated by centrifugation at 13000×g for 10 minutes at 4°C. The pelleted DNA was washed with ice-cold 500 µl of 70% (v/v) ethanol and centrifuged for 10 minutes at top speed. The pellet was dried, resuspended in 50 µl of dH_2O and stored at -20°C.

For mammalian cell transfection, DNA with high concentration and purity was prepared using the Plasmid Midi Kit (Qiagen) and/or the EndoFree Plasmid Maxi Kit (Qiagen500-EF). The

DNA concentration was determined by spectrophotometrical quantification at 260 nm by A_{260} * 50 = x µg/µl.

2.2.1.8 DNA restriction enzyme digestion

For analytical digestions 1 µg of DNA, harboring 1 restriction site, was incubated with 1 U of enzyme for 1 h (alternatively, 0.5 U for 2 h; 0.25 U per 4 h). For preparative digestions 5 to 10 fold overdigestion was made. Reaction mixture was incubated at 37°C, unless another temperature was recomended by manufacturer.

2.2.2 Yeast experiments

Twenty five ml of yeast culture medium (YPDA) were inoculated with one AH109 colony (from a plate kept at 4°C) and were cultured overnight at 30°C with shaking. 100 ml of fresh YPDA medium were inoculated with 10 ml of the overnight culture to a OD_{600} of 0.1 – 0.2 and grown for 5 hours at 30°C with shaking till the OD_{600} reached 0.9 - 1.0. Then, the yeast were centrifuged at 500×g for 2 minutes at room temperature. The pellet was washed for 2 minutes with 50 ml of 1× TE buffer and again centrifuged for 2 minutes at 500×g at room temperature. A following pellet-washing step with 1× TE/LiAc was performed for 10 minutes at room temperature and centrifuged at the same conditions as before. The washed pellet was resuspended in 1.5 ml 1× TE/LiAc to finally get the competent yeast. 10 µl of Carrier DNA, minimum 500 ng of BD and AD-plasmid and 50 µl of competent yeast cells were added to one reaction tube. The components were mixed by shaking and 300 µl of PEG/TE/LiAc was added and vortexed at medium speed for 10 seconds. The plasmid incorporation was achieved with heat shock for 40 minutes at 42°C. Cells were subsequently chilled on ice for 2 minutes. The yeast were collected by centrifugation at 500 x g for 1 minute at room temperature and then resuspended in 200 µl of water. 100 µl of the resupended pellet were plated on appropriate SD medium.

Cotransformed cells were selected by growth on –LW-medium. The interaction of coexpressed proteins activating expression of reporter genes was monitored as growth on –ALWH-medium after 4 and 7 days. Potential self-activation of constructs was always tested in parallel by cotransformation with empty prey or bait vectors.

2.2.3 Biochemical methods

2.2.3.1 Protein concentration determination: Micro amidoblack protein assay

Solution	Composition
Amidoblack solution	14.4 g amidoblack in 1 l methanol-acetic acid
Methanol-acetic acid	Methanol:acetic acid = 9:1
BSA stock solution	0.5 mg/ml

TABLE 17: SOLUTIONS FOR MICRO AMIDOBLACK PROTEIN ASSAY

Protein concentration was determined by the colorimetric amidoblack assay. To prepare the calibration curve, 0 – 20 µg BSA and 5 – 10 µl of sample were brought to a total volume of 100 µl with H_2O. 200 µl of amidoblack solution were added to both, the standard and sample solutions. All samples were incubated for 20 minutes at room temperature and centrifuged at maximum speed for 5 minutes. The supernatant was decanted and the pellet was washed tree times with methanol-acetic acid. Finally the pellet was resuspended in 500 µl of NaOH (0.1 N). The absorption was measured at 620 nm against NaOH.

2.2.3.2 SDS-PAGE using Laemmli system

Buffer	Composition
4x SDS-sample buffer	250 mM Tris/HCl, pH 6.8, 1% (w/v) SDS, 40% (v/v), glycerol, 4% β-mercaptoethanol, 0.02% bromophenol blue
Electrophoresis buffer	192 mM glycine, 0.1% (w/v) SDS, 25 mM Tris-base, pH 8.3
4x separating buffer	0.4% (w/v) SDS, 1.5 M Tris/HCl, pH 6.8
Separation gel (20%)	8.25 ml separation buffer, 7.5 ml 87% Glycerol, 16.5 ml 40% Acrylamyde, 330 µl EDTA (0.2 M), 22 µl TEMED, 120 µl 0.5% Bromophenol blue and 75 µl 10% APS
Separation gel (5%)	8.25 ml separation buffer, 17.94 ml dH2O, 1.89 ml 87% Glycerol, 4.12 ml 40% Acrylamide, 330 µl EDTA (0.2 M), 22 µl TEMED and 118 µl APS.
Stacking gel (5%)	6 ml stacking buffer, 7.95 ml dH2O, 5.52 ml 87% Glycerol, 3.90 ml 30 % Acrylamyde, 240 µl EDTA (0.2 M), 240 µl 10% SDS, 17.2 µl TEMED, 30 µl Phenol red and 137 µl 10% APS

TABLE 18: BUFFERS FOR TRIS-GLYCINE SDS-PAGE

Proteins were separated using one-dimensional sodium dodecyl sulphate polyacrylamide gel electrophoresis (SDS-PAGE) under fully denaturating conditions (Laemmli 1970). SDS-PAGE was performed in a gradient gel: a stacking gel was layered on top of a separating gel. The samples were first incubated with SDS-sample buffer at 95°C for 5 minutes and then loaded onto the gel. Gels were allowed to run at a constant current strength of 8 mA in an electrophoresis chamber (Hoefer Mighty Small System SE 250 from Amersham Biosciences) filled with 1x electrophoresis buffer. Subsequently the gels were either stained with

Coomassie blue or were used for immunoblotting.

2.2.3.3 Coommassie staining of SDS-PAGE

Solution	Composition
Coommassie blue staining solution	1 mg/1000 ml Coommassie brilliant blue R-250, 60% (v/v) methanol, 10% (v/v) acetic acid
Distaining solution	7% (v/v) acetic acid, 5% (v/v) methanol
Drying solution	5% (v/v) glycerin, 50% (v/v) methanol

TABLE 19: SOLUTIONS FOR COOMMASSIE STAINING OF SDS-PAGE

Polyacrylamide gels were stained with Coommassie solution for 30 minutes. Proteins were visualized by incubating the gel in distaining solution for 2 hours or overnight by shaking. Gels were visualized by Odyssey Infrared Imaging System (LI-COR Bioscience).

2.2.3.4 Western blotting

Proteins were electrotransfered from polyacrylamide gels to Millipore Immobilon-FL transfer membranes (polyvinylidene fluoride membrane (PVDF)). The transfer was performed in blotting buffer (192 mM Glycine, 0.2 % (w/v) SDS, 18 % (v/v) methanol, 25 mM Tris-Base, pH 8.3) at 4°C for 2 h with 200 mA.

2.2.3.5 Immunoblot detection

After transfer PVDF membranes were briefly pre-wet in 100% methanol, rinse with distilled water and dry at room temperature. Then membranes were wetted in PBS for several minutes. Blots were incubated at 4°C overnight with the primary antibody diluted in PBS-T containing 5 % of BSA and 0.025% of sodium azide. After three washing steps with PBS-T for 10 minutes each time, the membranes were submerged in peroxidise-coupled secondary antibodies (diluted in 1% of BSA) for 1 hour at room temperature. Membranes were rinsed again three times with PBS-T and immunodetection was carried out employing ECL films (GE Healthcare, Amersham HyperfilmTM ECL), which were developed automatically using Agfa Curix 60 developing machine.

2.2.3.6 Purification of fusion proteins

2.2.3.6.1 Induction of fusion protein synthesis (GST and His-Trx)

E.coli BL21 cells were transformed either with pGEX- or pET-vector. 100 ml of LB medium containing appropriate antibiotics were inoculated with one colony and cultured overnight at 37°C with shaking. 1000 ml of 2×YT culture medium including the appropriate antibiotics and 0,2% glucose was inoculated with 50 ml overnight culture. The dilution was incubated with shaking at 37°C until OD_{600} reached 0.5 - 0.7. Then the culture was induced with 0.3 mM IPTG and incubated at 20°C for 10 h (over night). Cells were harvested at 3000×g for 5 min at 4°C. Then bacteria were resuspended in 25 ml of icecold PBS; transfered in 50 ml Falcon tube and stored at -80°C.

2.2.3.6.2 Bacterial extract preparation

Frozen bacterial pellet was mixed with volume (25 ml) of 2× PBS buffer containing 1 tablet of EDTA-free Complete™ protease inhibitor (Roche), DNAse I (5 µg/ml) and RNAse A (10 µg/ml) and thawed on ice. Bacteria were lysed at 20000 psi using the french press. The lysate was diluted 1:1 with 2× PBS and 20% Triton X-100 was added to the final concentration 0.1%. The final dilution was stirred gently for 30 min at 4°C and then centrifuged for 10 min at 4°C. The supernatant was then transformed into a 50 ml centrifugation tube containing the affinity resin.

2.2.3.6.3 Affinity purification

Buffer	Composition
Elution buffer for GST-tagged proteins	10 mM Glutathione in 50 mM Tris/HCl, pH 8.0
Elution buffer for His-Trx-tagged proteins	150 mM imidazol in 2× PBS, pH 7.0

TABLE 20: BUFFERS FOR AFFINITY PURIFICATION OF FUSION PROTEINS FROM BACTERIA

The equilibration of 2 ml Talon Metal Affinity Resin (BD/Clontech) or glutathione Sepharose 4 Fast Flow (GE Healthcare) for purification of His-Trx- or GST-fusion proteins, respectively, was made in 50 ml centrifugation tube by washing two times with 2× PBS (pH 7.0). Then bacterial extract was transfered to the beads; mixed end-over-end for 1 h at 4°C and centrifuged for 3 min at 500×g. Supernatant was discarded. Talon beads were washed 3 times with 50 ml 2× PBS (pH 7.0) at 4°C for 3 min each and transfered to a disposible

column. 10 ml of 2× PBS was used for the last washing step. Fusion proteins were eluted by adding 2 ml elution buffer 3 times with 5 min incubation at room temperature. Three elution fractions were combined and elution buffer was exchanged by over night dialysis against 1× PBS. Dialysed protein fractions were stored at -80°C or, alternatively, were mixed with glycerol 1:1 and stored at -20°C.

2.2.3.7 EGFP-fusion proteins precipitation from transfected HEK293-T cells

HEK293-T cells grown in 75-cm^2 flasks were transfected using the Ca phosphate method (2.2.4.6.1). Cells were lysed in 50 mM Tris-HCl, pH 7.4, 0.5% TritonX-100, 100 mM NaCl, 10% glycerol, 1.5 mM $MgCl_2$, and Complete protease inhibitors for 15 min on ice 48 h after transfection. Cleared cell lysate was used for immunoprecipitation using MicroMACS anti-GFP Micro-Beads and MicroColumns (Miltenyi Biotec) according to the manufacturer's instructions, but using lysis buffer in all washing steps.

2.2.4 Cell culture techniques

Primary neurons, HEK293-T and COS-7 cells were cultured in 5% CO_2 at 37°C and a humidity of 95%. All supplemented cell culture media were filtrated using sterile filtration bottles with a pore size of 0.22 µm and kept at 4°C until usage. Media and reagents used for eucaryotic culture are listed in Table 23. All media were preincubated at 37°C before addition to cells.

Media and reagents for eukaryotes	Ingredients/Company
DMEM(mouse culture)	2% B27 (Gibco); 1 mM sodium pyruvate 100× (Gibco); 5 g/l AlbuMax II (Gibco); 2 mM L-glutamine 100X (Gibco) in DMEM (without: phenol red, L-glutamine, sodium pyruvate) (Gibco)
DMEM(10% FCS)	10% FCS (Gibco);1% Penicillin/Streptomycin 100× (Gibco); 2 mM L-Glutamine 100× (Gibco) in DMEM (Gibco)
NB (Neurobasal)	2% B27 (Gibco); 2 mM L-glutamine (Gibco); 1% Penicillin/Streptomycin 100× (Gibco) in Neurobasal
Distilled Water	Gibco /Millipore
HBSS+ (with Mg^{2+} and Ca^{2+})	Gibco
HBSS-	Gibco
Optimem	Gibco
AraC 1.5 mM	Calbiochem
10× Trypsin	Gibco
1× Trypsin	10% 10× Trypsin (Gibco); DMEM (10%FCS)
Paraffin	Paraplast embedding medium (Fischer)

TABLE 21: MEDIA AND REAGENTS FOR EUKARYOTIC CELL CULTURES

2.2.4.1 Splitting of cells into culture plates

HEK293-T and COS-7 cells were split by Heidi Wickborn, Sabine Opitz and Janina Juhle. Cells were washed twice with prewarmed HBSS- and subsequently incubated with 1 ml of 1× Trypsin per 75 cm^2 flask for 5 minutes at 37°C. After checking the dissociation of the cells from the plate, degradation of extracellular proteins by the protease trypsin was blocked by adding 9 ml of fresh, prewarmed DMEM (10% FCS). The cells then were transferred into plates with additional medium as indicated in each section.

2.2.4.2 Preparation of glass coverslips

Washing Glass coverslips for cell culture were placed into 50 ml tubes with 50% HNO_3 and incubated in an end-over-end shaker over night. On the next day, pH was neutralized by washing with cell culture or milipore water. Coverslips then were boiled in cell culture water using a microwave oven three times with exchanging the water in between. After washing one additional time they were separately dried on precision wipes and baked for 4 h at 200°C for sterilisation.

Coating Coverslips were transferred into a Ø 10 cm microbiological plastic dish and three paraffin dots were attached to each of them (paraffin heated to 150°C) (only for neuronal cell culture). They were coated with 100 µl of poly-D-lysine working solution (see Table 6) per coverslip and incubated over night in the cell culture incubator. On the next day cell culture water was added to each plate. Before usage of the coverslips they were washed three times with cell culture water and dried completely prior to plating of the cells.

2.2.4.3 Glial cells

Plating P1 to P3 pups (C57Bl6|J cre strain for mice culture and Wistar rat strain for rat culture) were decapitated and both brain hemispheres were removed, washed twice with HBSS- and incubated in 4.5 ml HBSS- with 0.5 ml 10× Trypsin for 20 minutes at 37°C. After washing once with HBSS+ medium was exchanged for 1 ml DMEM (10% FCS). Trituration of the hemispheres followed using a 1 ml pipette to obtain a nearly homogeneous cell solution. The material from two hemispheres filled up to a volume of 10 ml with DMEM (10% FCS) and was plated in one 75 cm^2 or it was filled up to a volume of 50 ml and plated into ten Ø 6 cm plates for direct usage.

Freezing Before freezing glial, glial cells were brought in solution using trypsin. The cell suspension of one bottle was transferred to 50 ml tubes and spinned down for 5 minutes at

1000×g. Resuspension in 1 ml ice cold DMEM (10% FCS) containing 10% DMSO followed. Slow freezing of the sample was performed by quick transfer into a bio safe freezing tube, initially on ice and then at -80°C. On the next day aliquots were transferred to -150°C and stored until usage.

Plating from Stocks 2-4 frozen glial cell aliquots were incubated at 37°C until melting started. Then 1 ml of prewarmed DMEM (10% FCS) was added. Cells were triturated and transferred to fresh DMEM (10% FCS) and plated on twenty Ø 6 cm plates with a final volume of 5 ml each.

2.2.4.4 Mouse hippocampal neurons

Mouse hippocampal neuron cultures were prepared by Cornelia Schoene. P0 mouse pups were genotyped (see 2.2.1.1) and decapitated and the heads were kept in HBSS+ on ice until dissection. Hippocampi were collected in fresh tubes on ice with HBSS+ and washed three times with cold HBSS-. After the last washing step, 4.5 ml HBSS- and 500 µl of 10× Trypsin were added and incubated for 20 min at 37°C. Hippocampi were washed once with HBSS+ and the medium was replaced by 1 ml DMEM (10% FCS). Trituration using a 1 ml pipette was performed by pipetting up and down 10 times. After counting the cells, the suspension was diluted to 250000 cells/ml. 100 µl of cell suspension were plated on the coated, washed and dried Ø 18 mm coverslips (see 2.3.4.2) and incubated for 1 h in the cell culture incubator. The media of the Ø 6 cm glial cell plates was exchanged by 5 ml DMEM (mouse culture) and five coverslips were turned into each plate with neurons and paraffin dots facing down. After two days 5 µl AraC (100×) were added to inhibit glial cell proliferation. The cells were fed every week by replacing 1 ml of old media with fresh one.

2.2.4.5 Rat hippocampal neurons

Rat hippocampal neuron cultures were prepared by Sabine Opitz and Heidi Wickborn from E16 to E17 rats. The general procedure for preparing rat hippocampal neurons is equivalent to the protocol for mouse hippocampal neurons 2.2.4.4. Neurons were cultivated in NB medium. 7.5 µl AraC was added to the cells at DIV3.

2.2.4.6 Transfections

2.2.4.6.1 Transfection of HEK293-T cells with Ca phosphate method

Solution	Composition
Solution A	0.5 M $CaCl_2$
Solution B	140 mM NaCl, 50 mM Hepes, 1.5 mM Na_2PO_4, pH 7.05

TABLE 22: SOLUTIONS FOR TRANSFECTION OF HEK293-T CELLS WITH CA PHOSPHATE METHOD

HEK293-T cells were grown in 75 cm^2 flasks in DMEM (10% FCS). 0,5 ml of Solution A was mixed with 25 µg DNA (for double transfection; 12.5 µg of each DNA). Then, 0.5 ml of Solution B, were added and, after 1 min, applied to cells in culture. The cells were incubated for 4 h at 37°C in 5% CO_2 atmosphere before exchange of growth media. Cells were grown for 24 hours before applied for further analyses.

2.2.4.6.2 Transfection of COS-7 cells on 24 well plates

The cells were grown on poly-D-lysine coated glass coverslips to 50–70% confluency. For a single construct transfection 1.5 µg DNA were used for 4 wells. For a double transfection 1 µg of each construct was used for the same number of wells. The DNA was resuspended in 200 µl DMEM without supplements, 8 µl of Polyfect (Qiagen, San Jose, CA, USA) was added and the transfection reaction was well mixed. After 5 minutes at room temperature 400 µl of COS-7 cells culture medium was added and 150 µl of this mixture was carefully dropped to each 4 wells and incubated for 48 hours.

2.2.4.6.3 Transfection of rat hippocampal neurons with EGFP-Bsn and EGFP-BsnRBM

Hippocampal neurons were transfected using the calcium phosphate method at 3 DIV. Prior transfection Ø 18 mm coverslips that showd have been transfected were transferred into a new 12-well plate containing 1 ml/well of prewarmed and equilibrated Optimem media (see Table 22) and kept in the incubator for 30 min. To prepare the precipitates 180 µl of transfection buffer (274 mM NaCl, 10 mM KCl, 1.4 mM Na_2HPO_4, 15 mM Glucose, 42 mM Hepes) was added dropwise to a solution containing 12 µg of DNA and 250 mM $CaCl_2$, under gentle stirring. The resulting mix was placed for 20 min at room temperature in the dark; 60 µl of the mix was then added per well, and neurons were placed in the incubator for 40 to 60 min. Medium was then exchanged for 1 ml 37°C prewarmed Neurobasal (see Table

22), followed by two 750-µl exchanges. Finally, the coverslips were transfered into the plate with original medium.

2.2.5 Immunocytochemistry, microscopy and image analysis

All primary antibodies for immunocytochemistry (ICC) were prediluted in 50% glycerol and stored at -20◦C (Table 10). Secondary antibodies were stored at 4◦C (Table 11).

2.2.5.1 Immunostaining of cell cultures

Cells were grown on Ø 18 mm (mouse and rat hippocampal neurons) and Ø 12 mm (COS-7 cells) coverslips and fixed for 3 to 5 minutes with 37°C prewarmed 4% PFA, 4% succrose in PBS. Blocking of PFA-reactivity and permeabilization of the cells was achieved by 15 minutes incubation in 10% FCS, 0.1% glycine, 0.3% Triton X-100 in PBS. The antibodies were diluted in 50 µl 3% FCS in PBS per Ø 18 mm coverslip and pipetted on a paraffin film in a wet chamber (For list of antibodies and corresponding dilutions see Table 10). The coverslips were turned with cells facing down on top of the antibody drop. Incubation with the primary antibody at 4°C over night was followed by three times washing with PBS. The secondary antibody was applied at RT for one hour. After washing three times for 15 min in PBS, coverslips were mounted in Mowiol (10 µl per Ø 18 mm coverslip). Mounted coverslips were stored at 4°C until usage.

2.2.5.2 Microscopy and image analysis

Hard- and software Images were taken using a Zeiss Axioplan 2 epifluorescence microscope (Metaview software, version 7.1.3) or a Leica SP5 confocal miroscope (LAS AF software, version 2.0.2) with a dynamice range of 12 bit. Image processing and analysis were performed using ImageJ (MacBiophotonics ImageJ Version 1.41a), Adobe Photoshop (Version 8.0) and Openview (Version 1.5 from Noam Ziv) software.

2.2.5.3 Analysis of synaptic immunofluorescence (IF)

To analyze IF at synapses as a relative measure for the synaptic amount of a protein mouse or rat hippocampal cultures were fixed and stained for a synaptic marker in the infrared channel (Cy5) and the protein of interest in the red channel (Cy3). Z-stacks were recorded using a confocal microscope (512x512 pixels, 12bit, 63x objective, 3x zoom, 3x frame averaging, z-step = 0.3 µm) and processed with ImageJ. Images then were opened with Photoshop and saved with a bite order for IBM PC. Analysis of synaptic IF was performed

using the Openview software. The software can detect synaptic puncta in one channel (Synaptic marker) and look for colocalization in a second (protein of interest). A third channel could be used to split synapses into two separate pools and to compare IF intensities.

2.2.6 Biosensor analysis

2.2.6.1 Biosensor analysis of RBPs interaction with Bassoon, Piccolo, Rim1 and $Ca_V2.2$ (direct amine coupling)

GST- and His-tagged fusion proteins were expressed and purified by affinity chromatography and dialyzed against PBS before biosensor analysis (2.2.3.6). All experiments were performed using a Biacore 2000 (Biacore) and a sensor chip (CM5; Biacore) at 25°C. His-Trx-fusion proteins were cupled to the chip surface the Amine Coupling kit (Biacore) according to the procedure recommended by the manufacturer. Soluble ligands (GST-tagged RBP fragments) were applied in HBS-EP (0.01 M Hepes buffer, pH 7.4, and 0.15 M NaCl with 0.005% surfactant P20) running buffer at a concentration of 20 µg/ml at a flow rate 20 µl/min for 6 min. The surface was regenerated using 15 mM NaOH, for 2 min at 20 µl/min. To standardize the results of measurements using ligands with different molecular masses, the molecular-binding activities (MBA) were calculated according to the equation:

$$\mathrm{MBA} = \frac{(\text{ligand response}) \times (\text{molecular mass of receptor})}{(\text{amount of receptor}) \times (\text{molecular mass of ligand})}$$

(Catimel et al., 1997).

2.2.6.2 Biosensor analysis of Bassoon interactions with DLCs (GST capturing)

GST- and His-tagged fusion proteins were expressed, purified and dyalyzed against PBS before biosensor analysis (2.2.3.6). Strep-His fusion proteins were purified by doublestep chromatography using HisPur matrix (Thermo Fisher Scientific) and Strep-Tactin Superflow (IBA). All experiments were performed using a Biacore 2000 (Biacore) and a sensor chip (CM5; Biacore) at 25°C. The active surface (with immobilized anti-GST antibody) was prepared using the Amine Coupling kit (Biacore) combined with the GST Capture kit (Biacore) according to the procedure recommended by the manufacturer. Binding GST-DLC1, GST-DLC2, and GST as control was performed in HBS-EP (0.01 M Hepes buffer, pH 7.4, and 0.15 M NaCl with 0.005% surfactant P20) running buffer at a concentration of 20 µg/ml and a flow rate of 20 µl/min for 6 min. Soluble ligands (Bassoon fragments) were

applied in HBS-EP running buffer containing 0.105% surfactant P20 at a concentration of 20 µg/ml at a flow rate 20 µl/min for 6 min. The parallel application of soluble ligand to the GST reference cell allowed controlling for nonspecific binding. The surface was regenerated using 10 mM Gly-HCl, pH 2.2, for 2 min at 20 µl/min. To standardize the results of measurements using ligands with different molecular masses, the molecular-binding activities (MBA) were calculated as described above (see 2.4.1).

2.2.7 Statistical data analysis

Statistical data analyses (t-test, ANOVA, curve fit, correlation analysis) was performed using GraphPad Prism 4.

3. Results

3.1 Characterization of Bassoon interaction with Dynein Light Chain[*]

3.1.1 Development of a new mito-targeting system

A majority of fusion proteins stays soluble and shows a relatively diffuse localization being over-expressed in heterologous cell system. This makes co-localization assays and accordingly visualization of protein interaction ineffective. To overcome these problems a co-recruitment assay utilizing the mitochondrial targeting sequence of Mas70p, fused to a protein of interest has been developed (Kessels & Qualmann, 2002; tom Dieck et al., 2005). As this initial mito-targeting system was not applicable in all instances, we have modified and improved it. The new system is based on the expression of one of the interaction partners fused to the mitochondrial targeting sequence of the rat mitochondrial transporter protein Tom20 and EGFP (enhanced green fluorescent protein) as a reporter. Tom20 is a major receptor of the mitochondrial preprotein translocation system and is bound to the outer membrane through the NH_2-terminal transmembrane domain (TMD) in a type I orientation, extruding the bulk of the COOH-terminal domain to the cytosol (Nin-Ccyt orientation). The mitochondria-targeting sequence of rat Tom20 (rTom20) was analyzed in COS-7 cells by Kanaji et al. (2000), who showed that moderate TMD hydrophobicity and a net positive charge within five residues of the COOH-terminal flanking region were both critical for efficient recruitment to mitochondria. Using specific primers we cloned rTom20 amino acid sequence 1-33 containing TMD and the essential flanking positive residues into an expression vector (Fig. 7A).

The new mito-targeting expression vector was generated on the backbone of vector pCMV-Tag3A (Invitrogen) (Fig. 7B). The nucleotide sequence 669 – 718 of pCMV-Tag3A vector was exchanged by Tom20 mito-targeting sequence leading to the creation of an intermediate vector pMito3-0. The EGFP sequence was inserted at position 779 of pMito3-0 and the obtained vector, called pMito3-EGFP, was used for further experiments.

[*] This part of the study was performed in close collaboration with Dr. Anna Fejtova (Fejtova et al., 2009)

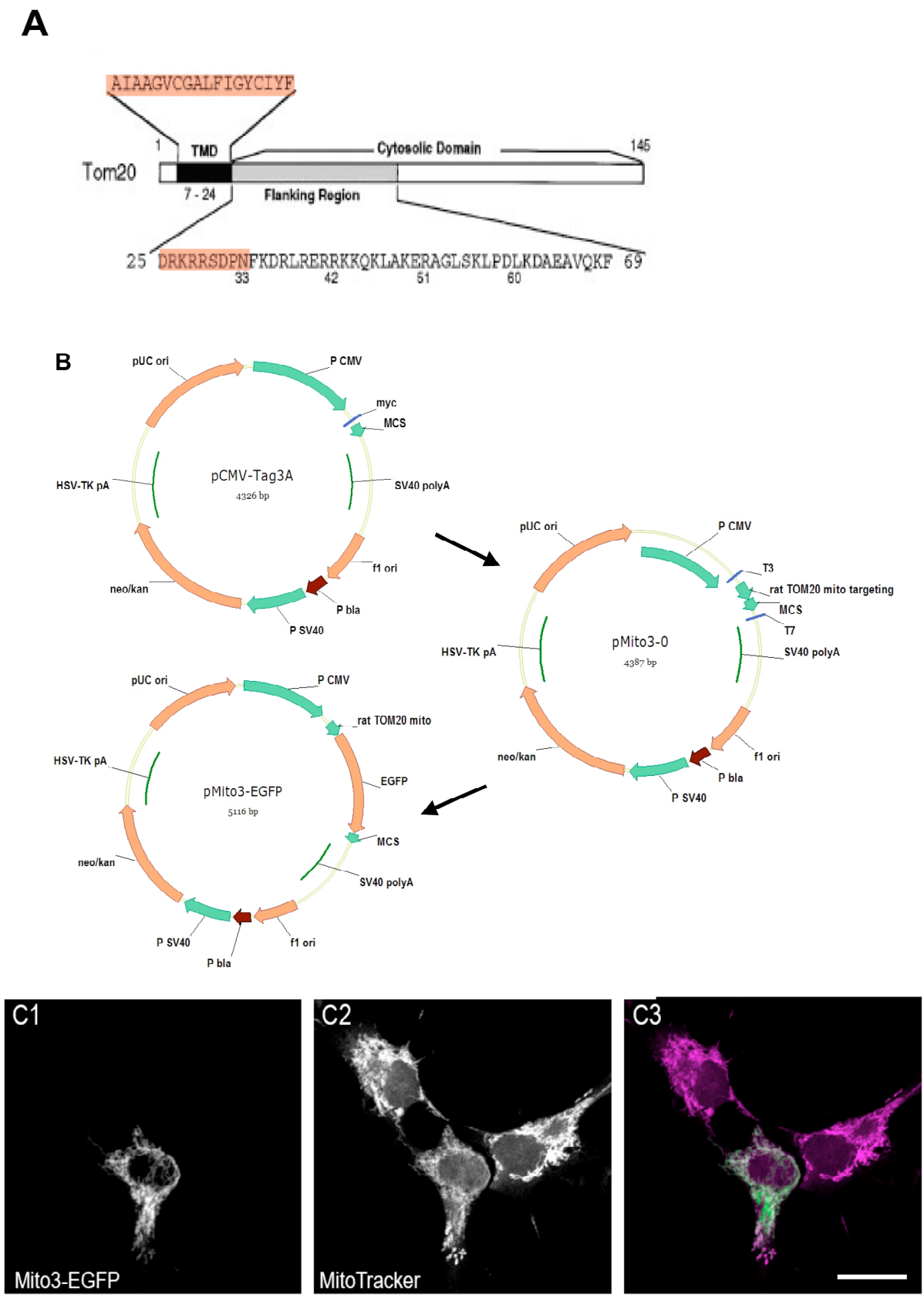

FIGURE 7. DEVELOPMENT OF A NEW MITO-TARGETING SYSTEM.
(A) Schematic structure of rTom20. Amino acid sequences of the trans-membrane domain (TMD) and the flanking region are shown (adapted from Kanaji et al., 2000). Amino acid sequence (Mito3) used to construct pMito3-EGFP expression vector is highlighted. **(B)** Schematic presentation of the cloning strategy for pMito3-EGFP. **(C)** COS-7 cells were transfected mito-targeting vector (Mito3-EGFP) (green) and stained with MitoTracker® (magenda) 18 h after transfection. Bar, 20 µm.

To control for proper subcellular targeting of Mito3-EGFP fusion protein, COS-7 cells were transfected with pMito3-EGFP vector. Approximately 80% of cells expressed EGFP 18 hours after transfection. Mitochondrial localization of EGFP was confirmed using MitoTracker®. Comparison transfected *vs.* nontranfected cells revealed neither difference in the cell shape nor in mitochondria localization (Fig. 7C).

3.1.2 Interaction of Bassoon with Dynein Light Chain (DLC) in living cells tested by mito-targeting assay

DLC1 was identified to interact with Bassoon when cDNA fragment Bsn2 covering amino acid residues (aa) 609 - 1692 of rat Bassoon was used as bait in a yeast two-hybrid (Y2H) screen (Fejtova et al., 2009). Seven independent positive clones carried the cDNA of DLC1. In subsequent experiments, the DLC-binding interface of Bassoon was narrowed down to fragment Bsn16 (aa1360 – 1441) and Bsn15 (aa1441 – 1692). DLC2 also interacted with those fragments in yeast (Fejtova et al., 2009).

To confirm the Y2H analyses, an interaction of Bassoon's DLC-binding region with DLC1 and DLC2 was examined using the newly established mito-targeting assay. COS-7 cells were transfected with pMito3-EGFP-DLC1 and pMito3-EGFP-DLC2 constructs. Staining of transfected cells with MitoTracker® demonstrated mitochondrial targeting of Mito-EGFP-DLC1, Mito-EGFP-DLC2 and the control fusion protein Mito-EGFP. Fragment Bsn14 (aa 1206 – 1692) fused to monomeric red fluorescent protein (mRFP) exhibited a rather uniform distribution in the cytoplasm, when co-expressed with Mito-EGFP (Fig. 8A2). In contrast, mRFP-Bsn14 was recruited to mitochondria when co-expressed with Mito-EGFP-DLC1 or Mito-EGFP-DLC2 (Fig. 8C2, 8E2). Recruitment of mRFP to mitochondria could not be detected when co-transfected with Mito-EGFP-DLC1 or Mito-EGFP-DLC2 (Fig. 8B2, 8D2).

3.1.3 DLC1 and DLC2 bind Bassoon with different strength

DLC1 and DLC2 are very similar proteins with 93% sequence identity. However, it has been proposed that they are sequestered to distinct protein complexes as shown for dynein or myosinV motor complexes (Naisbitt et al., 2000; Puthalakath et al., 2001). To assess a possible preference of the binding sites on Bassoon for the two DLC isoforms, we expressed and purified a set of His-thioredoxin fusion proteins covering first, second and third or all three binding motifs (Fig. 9B) and tested their relative binding affinities to purified GST-DLC1 or GST-DLC2 (Fig. 9A) using surface plasmon resonance technology. The results did not reveal any binding preference for single motifs, but we observed significantly higher binding

of fragments Bsn15 (motifs II and III) and Bsn13 (all 3 motifs) to GST-DLC2 as compared to GST-DLC1 (Fig. 9B, for numeric values see Fig. 9C).

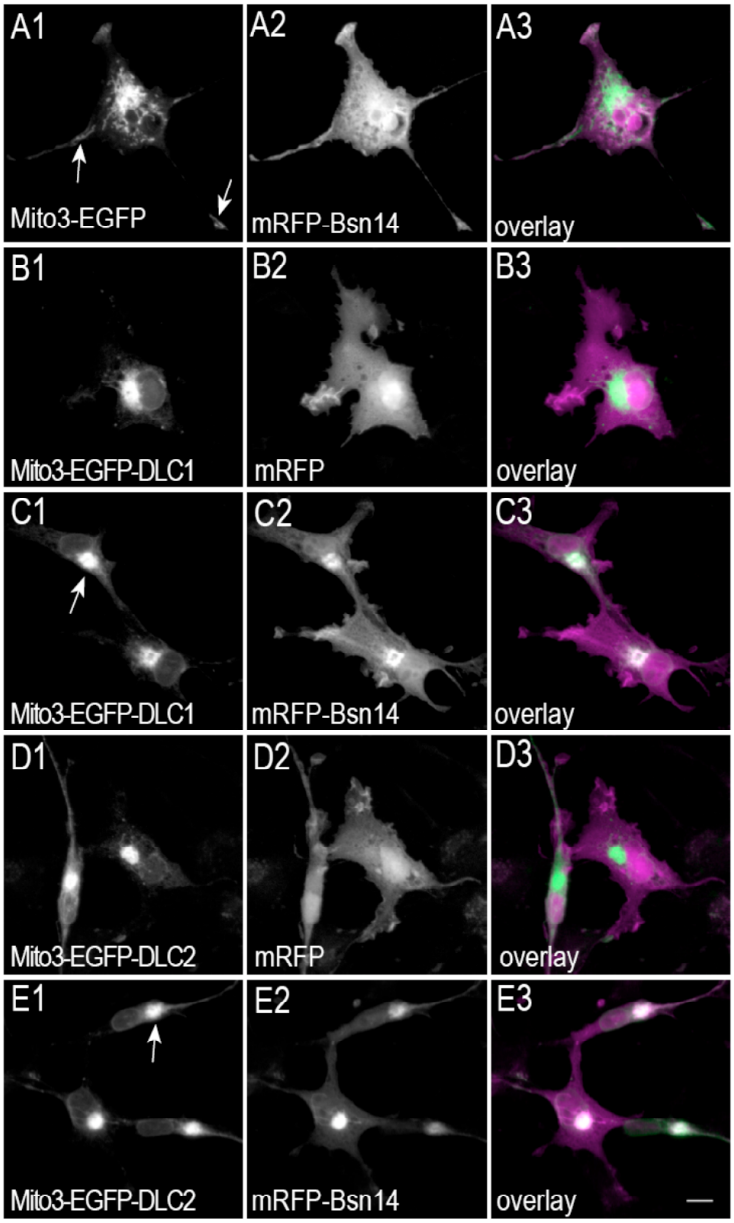

FIGURE 8. BASSOON INTERACTS WITH DLC1 AND DLC2 IN MITO-TARGETING ASSAY.
Mito-targeting assays in COS-7 cells. Cells were fixed 18 h after transfection. Mito-targeted EGFP (green) or EGFP-DLCs (green) are localized at mitochondria (compare A1–E1 with Fig. 1C). mRFP-Bsn14 (magenda) shows a uniform cytoplasmic distribution when coexpressed with Mito3-EGFP control construct (A2) but is co-recruited to mitochondria when mito-targeted DLC1 or DLC2 are coexpressed (C2 and E2). Targeting of DLC to mitochondria does not affect the localization of mRFP (magenda) (B2 and D2). The arrows in A1 indicate the normally distributed localization of mitochondria in cell protrusions. In contrast, mitochondria are clustered near the cell centers when Mito3-EGFP-DLC1 and Mito3-EGFP-DLC2 are expressed (C1 and E1, arrows). Bar, 10 µm.

The assay also confirms that the interaction of Bassoon and DLC is direct. Notably, we observed an increase of the relative binding affinities starting with fragments $Bsn15^{II}$ and $Bsn15^{III}$ (containing one DLC-binding site), to Bsn15 (containing two) and finally Bsn13 with three binding sites (Fig. 9C).

Thereby, site I seems to bind more tightly than sites II and III, and the relative binding affinities seem to be additive as DLC binding of Bsn13 represented roughly the sum of that of Bsn15 and Bsn16. These observations imply that the arrangement of three DLC-binding motifs in close proximity facilitates binding of Bassoon to DLC *in vivo.*

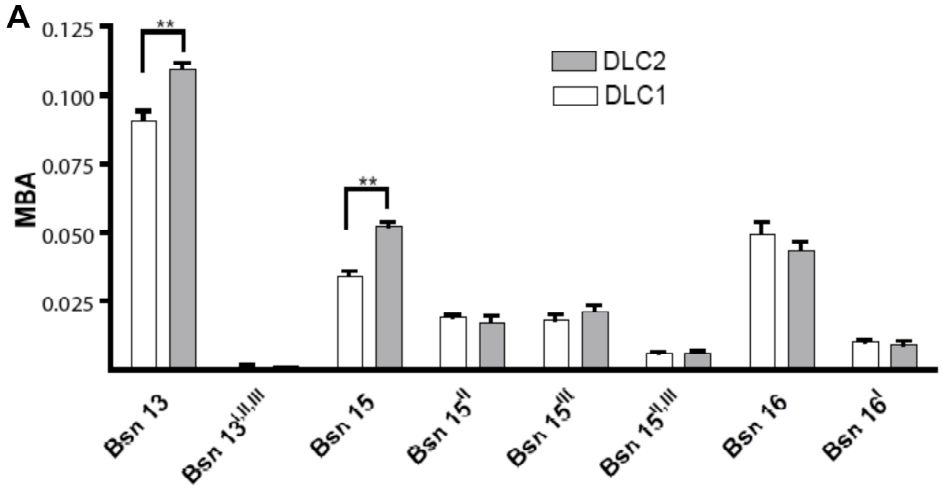

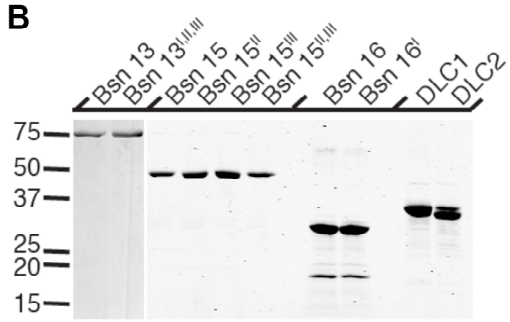

C

	DLC1 MBAx10^{-3} mean±SD	DLC2 MBAx10^{-3} mean±SD
Bsn 15	34,3±3,1	52,7±2,5
Bsn 15^{II}	19,3±1,2	17,7±3,5
Bsn 15^{III}	18,3±3,6	21,6±3,1
Bsn 15^{II,III}	6,3±0,6	6,7±1,2
Bsn 16	50±7	44±5,3
Bsn 16^{I}	10,3±1,2	9,3±2,1
Bsn 13	91,3±6,3	110,3±4
Bsn 13^{I,II,III}	1,7±0,6	2±0

FIGURE 9. DLC1 AND DLC2 BIND BASSOON WITH DIFFERENT AFFINITY IN SURFACE PLASMON RESONANCE ASSAY.
(A) Molecular-binding activities (MBA) of purified Bsn fragments to DLC1 and DLC2 in surface plasmon resonance assays. Error bars indicate SEM. **, P < 0.01. **(B)** Recombinant proteins used for the binding assays are shown on a Coomassie-stained SDS gel. Molecular mass is indicated in kilodaltons. **(C)** Quantitative results of surface plasmon resonance binding assays. The molecular binding activity (MBA) was calculated from 3-5 association-dissociation cycles performed for each interaction pair. The results shown were confirmed by a second measurement set, in which proteins coming from independent purifications were used.

3.1.4 Bassoon can function as a cargo adaptor in COS-7 cells

Two independent Bassoon regions, located on fragments Bsn15 and Bsn16, bind DLCs. To identify the exact DLC-binding site the aa sequence of both regions was screened for sequences similar to published DLC-binding consensus motifs (K/R)XTQT (Lo et al., 2001) and GIQVD (Fan et al., 2001; Liang et al., 1999). The sequence analysis revealed three TQT motifs (two in the fragment Bsn15 and one in the fragment Bsn16). A series of Y2H analysis using mutant constructs with TQT motif replaced by AAA (Fig. 10A) revealed that each of the

three identified TQT motifs could bind Bassoon independently and was sufficient for the binding. Those results were also confirmed in Mito-targeting assay in COS-7 cells and are tabulated in Fig. 10B (Fejtova et al., 2009).

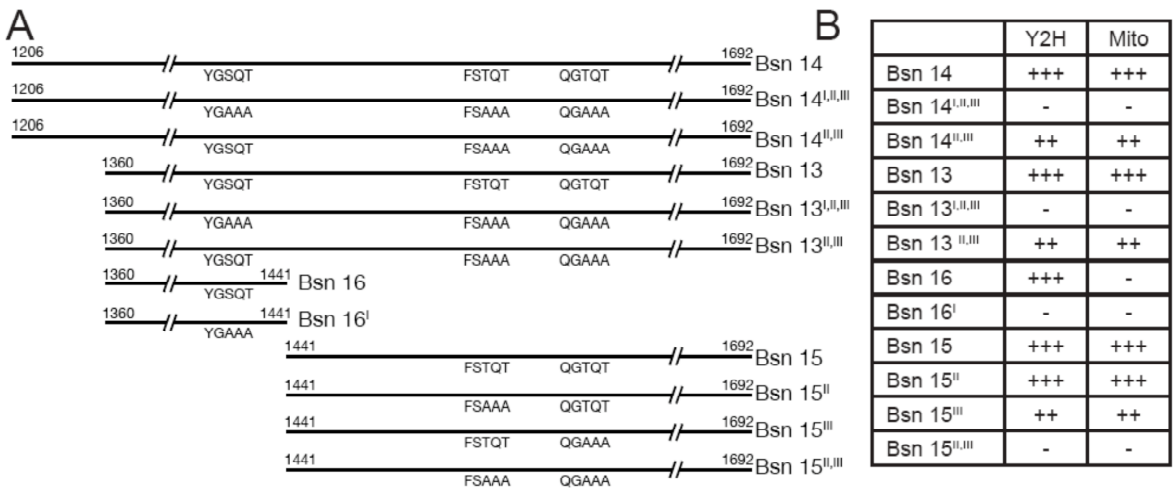

	Y2H	Mito
Bsn 14	+++	+++
Bsn 14I,II,III	-	-
Bsn 14II,III	++	++
Bsn 13	+++	+++
Bsn 13I,II,III	-	-
Bsn 13 II,III	++	++
Bsn 16	+++	-
Bsn 16I	-	-
Bsn 15	+++	+++
Bsn 15II	+++	+++
Bsn 15III	++	++
Bsn 15II,III	-	-

FIGURE 10. MAPPING OF THREE INDEPENDENTLY FUNCTIONAL DLC-BINDING SITES IN BASSOON.
(A) Bassoon constructs including the amino acid substitutions introduced at interaction sites I, II, and III and their relative lengths; bordering amino acid numbers refer to rat Bassoon. **(B)** Summary of binding assays in yeast (yeast two-hybrid [Y2H]) and in corecruitment assay by mito-targeting in COS-7 cells (Mito).

When DLC1 or DLC2 were targeted to the outer mitochondrial membrane in COS-7 cells the localization of mitochondria was remarkably distinct from that of mitochondria in cells expressing the control construct Mito3-EGFP (see Fig. 11A1, B1, D1). Normally, mitochondria are distributed throughout the cytoplasm of cells, sometimes even in their most distal regions (arrows in Fig. 8A1 and Fig. 11A1). In contrast, targeting of DLC to mitochondria results in their accumulation near the cell center, presumably due to DLC-mediated retrograde transport along microtubules via dynein. To test whether Bassoon can function as a cargo adaptor, we targeted the fragment Bsn15 to the outer mitochondrial membrane and observed the subcellular localization of mitochondria. After expression of Mito3-EGFP-Bsn15, mitochondria were clustered near the microtubule-organizing center (MTOC) of COS-7 cells visualized by co-staining of microtubules (Fig. 11B1,2). Targeting of the mutant fragment Bsn15^{II,III}, which can not bind DLC, to mitochondria did not alter their subcellular localization, confirming that an interaction with DLC was required for retrograde transport in COS-7 cells (Fig. 11C1). Treatment of COS-7 cells expressing Mito3-EGFP-Bsn15 with the microtubule depolymerizing drug nocodazole for 2 hrs prior to fixation and staining led to a disruption of clusters, whereas the treatment with the actin polymerization inhibitor cytochalasin D had no effect on cluster formation (Fig. 11D1, E1). These data suggest that fragment Bsn15 can operate as cargo adaptor via its binding to DLC and induces a microtubule-dependent retrograde transport of organelles in living cells. They also

suggest that Mito-targeting system can be used not only as a classical co-recruitment assay but also to shed light on a functional role of an examined protein interaction.

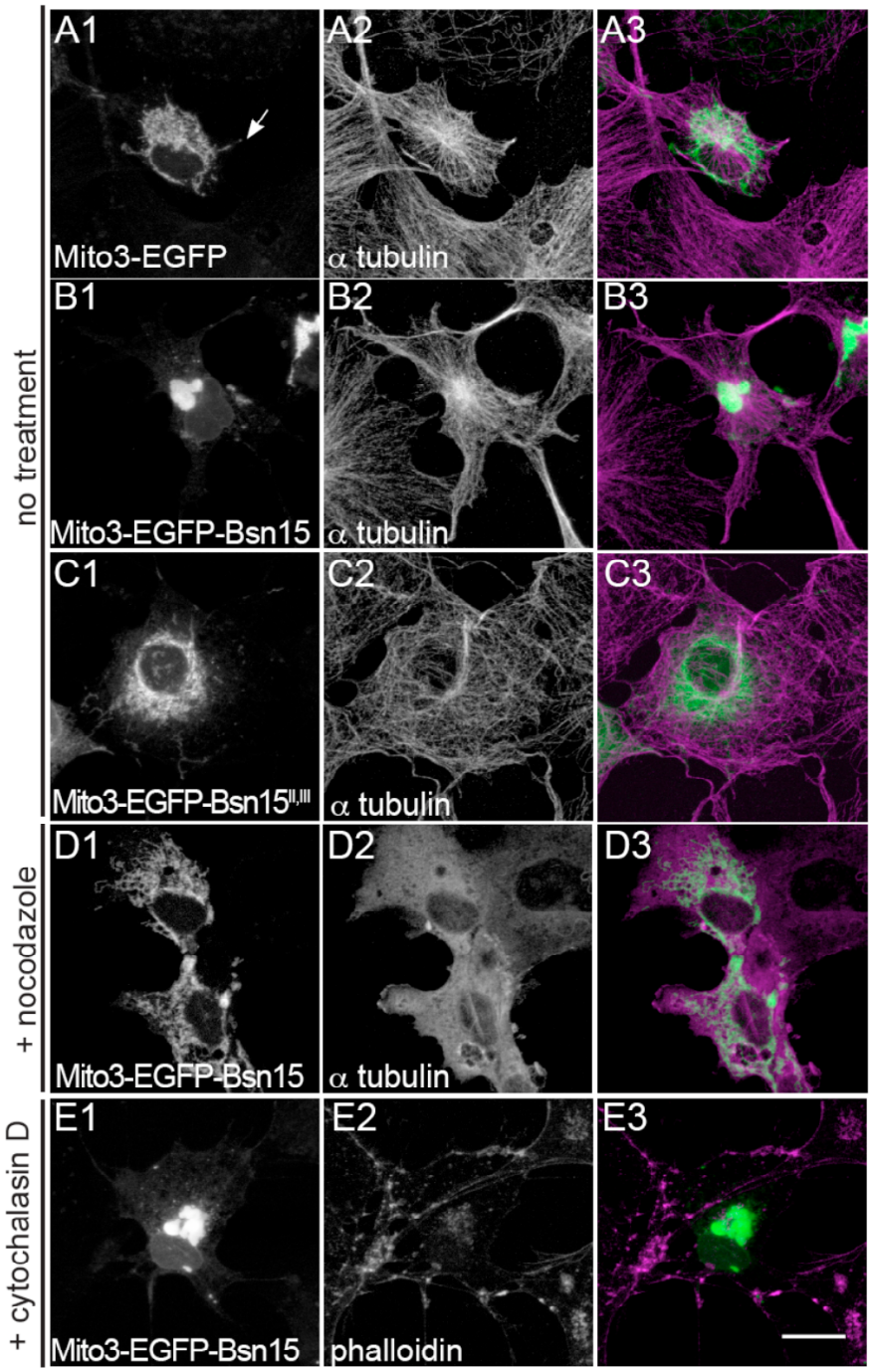

FIGURE 11. BASSOON CAN SERVE AS A CARGO ADAPTER FOR RETROGRADE TRANSPORT IN COS-7 CELLS. (A–E) Cells were transfected with mito-targeting constructs (green) and fixed 18 h later. The position of the MTOC is visualized by staining with anti–α-tubulin antibody (magenda) in A2–D2; actin is visualized with Alexa Fluor 568–coupled phalloidin (magenda) (E2). In cells expressing mito-targeted fragment Bsn15 containing the DLC-binding sites II and III, mitochondria accumulate at the MTOC. Mitochondria are distributed throughout the cytoplasm in cells expressing mito-targeted EGFP (row A), fragment Bsn15II,III with mutated DLC-binding sites (row C), or in cells expressing mito-targeted Bsn15 after treatment with nocodazole for 2 h before fixation (row D). Depolymerization of actin filaments with cytochalasin D (2 h before fixation) does not prevent the effect of Bsn15 (E1–E3). Bar, 20 µm.

3.2 Characterization of Bassoon and Piccolo interactions with Rim binding proteins

3.2.1 Bassoon can interact with Rim binding proteins

Rim binding protein 1 (RBP1) was originally identified by Wilko Altrock as a novel interaction partner of Bassoon in an Y2H screen using Bassoon fragment Bsn3 covering aa 1692 - 3263 of rat Bassoon as a bait (Fig.12).

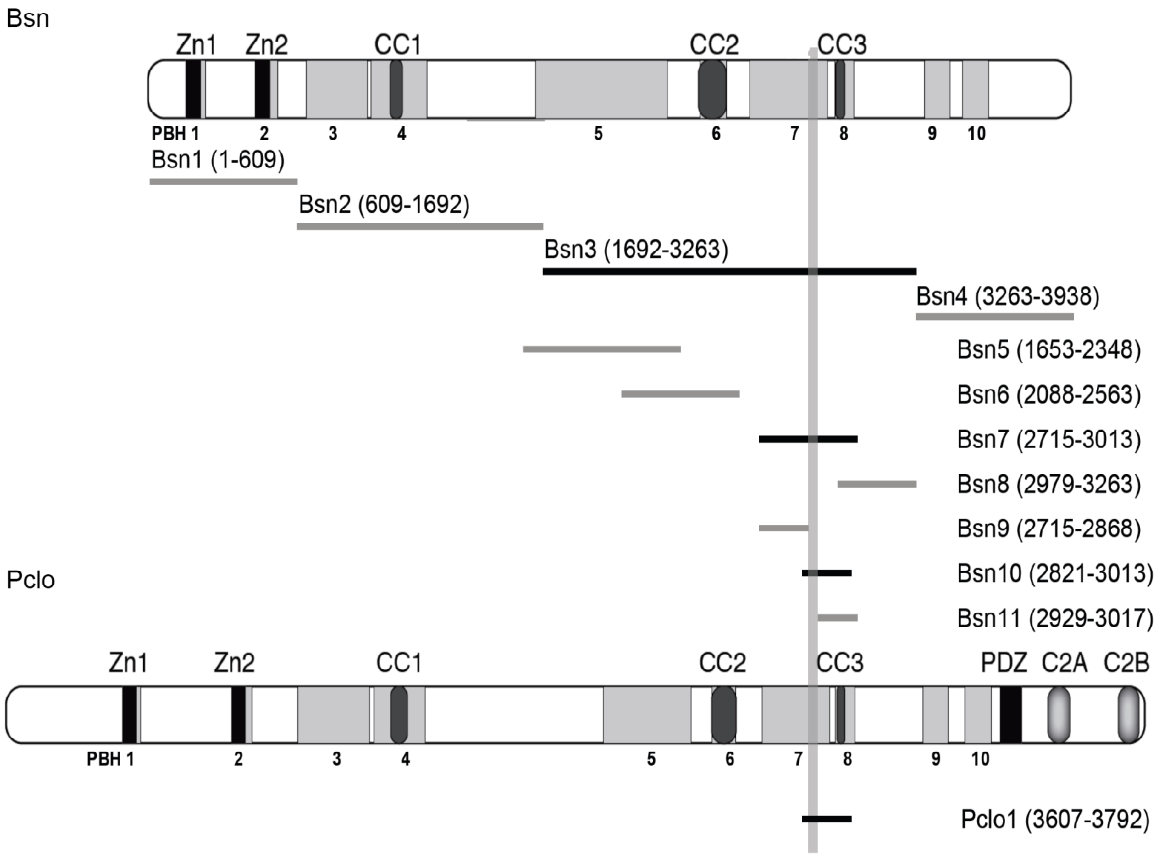

FIGURE 12. MAPPING OF RBP INTERACTION REGIONS ON BASSOON AND PICCOLO.
Overview of Bassoon and Piccolo fragments tested for binding to RBP1 and RBP2 in yeast-two hybrid assays. The extension of positive Bsn and Pclo clones is displayed in black and non-binding clones are indicated in grey. Number in brackets indicate amino acid num The corresponding region of Piccolo showed 54% of identity. In line with this, the Piccolo cDNA fragment Pclo1 (aa 3607 - 3792) interacted with RBPs in Y2H assays (Fig. 12) suggesting that functional RBP-binding interface is conserved between the two proteins.bers refering to rat Bassoon and Piccolo. Zn1/2, zinc fingers; CC1-3, coiled-coil regions; PDZ, PSD-95/Dlg/zonula occludence-1 homology domain; C2A/B, C2 domains; PBH1-10, regions of the Piccolo - Bassoon homology (depicted as grey boxes).

In subsequent experiments, which were done in close collaboration with Ferdinand Bischof, the RBP-binding interface of Bassoon was narrowed down to fragment Bsn10 (aa 2821 - 3013). Baits covering the other parts of Bassoon molecule did not show any binding. In Y2H assays Bsn10 was also able to interact with the other member of Rim binding proteins family

– RBP2. The binding region Bsn10 is situated within Piccolo-Bassoon homology (PBH) region 7.

To confirm the Y2H data in mammalian cells, an interaction of RBP-binding region of Bassoon with RBP1 and RBP2 was examined in the mito-targeting system after heterologous expression in COS-7 cells (Fig. 13). Staining of transfected cells with MitoTracker® demonstrated mitochondrial targeting of Mito3-EGFP-RBP1 and Mito3-EGFP-RBP2. mRFP-Bsn10 was recruited to mitochondria when co-expressed with Mito-EGFP-RBP2_SH3 II+III (Fig. 13B1). Recruitment of mRFP to mitochondria could not be detected when co-transfected with Mito-EGFP-RBP2_SH3 II+III (Fig. 13C1). Binding of RBP1 to Bassoon was also confirmed in mito-targeting system (Fig. 13A).

To further confirm the interaction in cells, co-immunoprecipitation experiments were done. These experiments were performed by Claudia Marini under my supervision during her practical training in the group of Prof. E. D. Gundelfinger. To this end c-myc-RBP2 was expressed together with EGFP-Bsn10 in HEK293-T cells and 24 hrs after transfection cell lysates were prepared and protein complexes were immunoprecipitated using anti-GFP antibody. Western blot analysis confirmed the successful co-precipitation of c-myc-RBP2 with over-expressed EGFP-Bsn10. In control experiments, we were unable to co-immunoprecipitate cmyc-tagged RBP2 when co-expressed with EGFP.

While c-myc-RBP2 was highly expressed in HEK293-T cells, neither c-myc-RBP1 nor EGFP-RBP1 was found in transfected cell lysates, probably due to low expression level and/ or fast degradation.

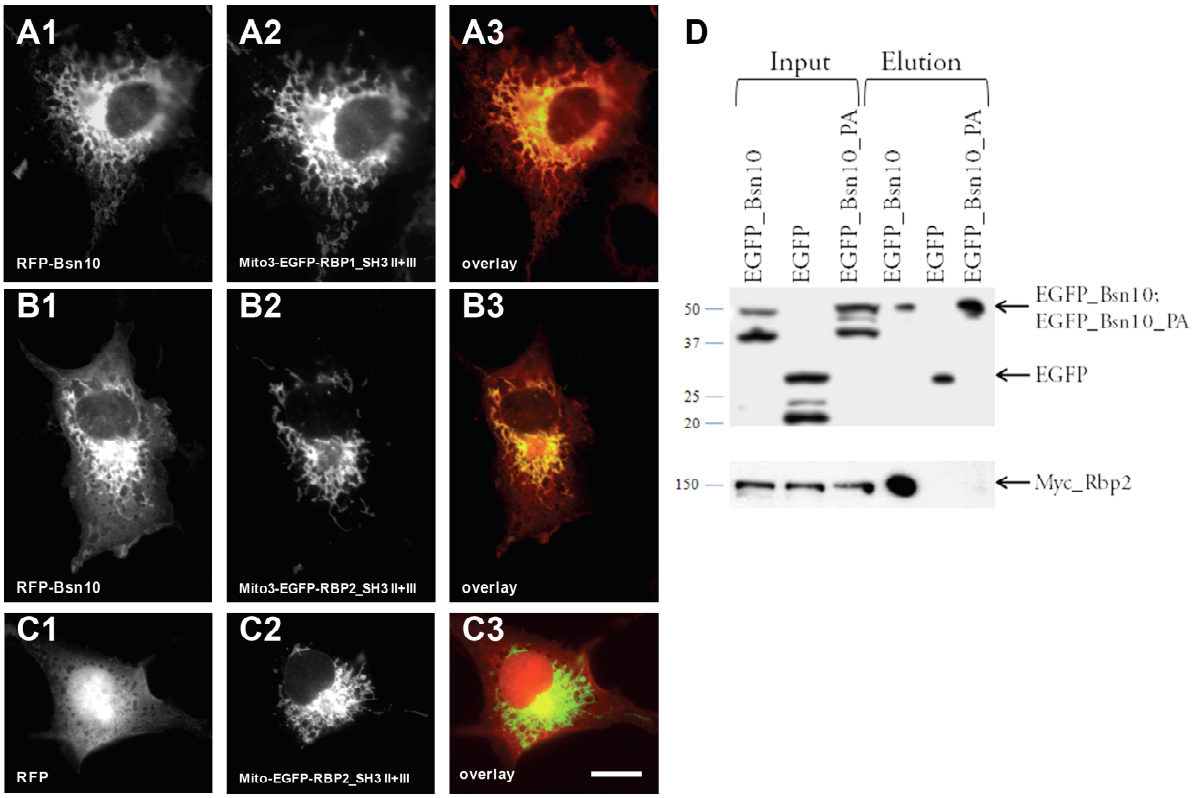

FIGURE 13. BASSOON INTERACTS WITH RIM BINDING PROTEINS IN MAMMALIAN CELLS.
(A – C) Cos-7 cells were fixed 18 h after transfection. Mito-targeted EGFP-RBP1/2_SH3 II+III (green) are localized at mitochondria (A2, B2, C2). RFP-Bsn10 (red) is co-recruited to mitochondria when co-expressed with mito-targeted EGFP-RBP1/2_SH3 II+III (A1, B1). Targeting of RBP2_SH3 II+III to mitochondria does not affect the localization of mRFP (red) (C1). Bar, 10 µm. **(D)** Overexpressed c-myc-RBP2 was precipitated with EGFP-Bsn10 but neither with EGFP alone nor with EGFP-Bsn10_PA. Molecular mass is indicated in kilodaltons. Figure 7D is provided by Claudia Marini.

3.2.2 Mapping of functional Bassoon and Piccolo binding motifs on RBP1 and RBP2

Sequence analysis of Bassoon fragment Bsn10, which bound RBPs in Y2H and Mito-targeting assays, revealed the existence of a proline-rich motif, which are known to bind to SH3 domains (reviewed in Mayer et al., 2001). Therefore we considered SH3 domains of RBPs as potential interaction regions for Bassoon and Piccolo. Using specific primers a number of cDNA fragments of the three SH3 domains of RBP1 and RBP2 was cloned from a rat cDNA library (Fig. 14A). This work was initiated by Ferdinand Bischof and taken over by me in initial phases of my doctoral thesis. The construct RBP1_0 (aa 1357 – 1556) does not contain any predictable structural features and is not conserved in RBP2. Bait constructs covering Bsn10 and the corresponding sequence of Piccolo (Pclo1) were shown to bind each of three SH3 domains of both RBP1 and RBP2 (constructs RBP1/2_SH3 I, RBP1/2_SH3 II and RBP1/2_SH3 III) in the Y2H assay (Fig. 14B). Constructs RBP1_SH3_II+III (aa 1557 – 1786) and RBP2_SH3_II+III (aa 873 – 1076) covering the second and the third SH3 domains simultaneously showed higher binding activity to Bassoon and Piccolo as was assessed by

colony number and size. In line with this observation, while single SH3 domains of RBPs were not able to co-recruit Bsn10 in Mito-targeting assay, Mito3-EGFP-RBP1/2_SH3 II+III showed clear co-recruitment (Fig. 13). RBP1_0 construct, which does not contain SH3 domains, bound neither Bassoon nor Piccolo in Y2H assays (Fig. 14B) and surface plasmon resonance assays (data not shown). Comparison of binding activities of distinct SH3 domains to Bassoon and Piccolo was performed using surface plasmon resonance technology (Fig. 15D-E) and discussed in chapter 3.2.4 of this thesis.

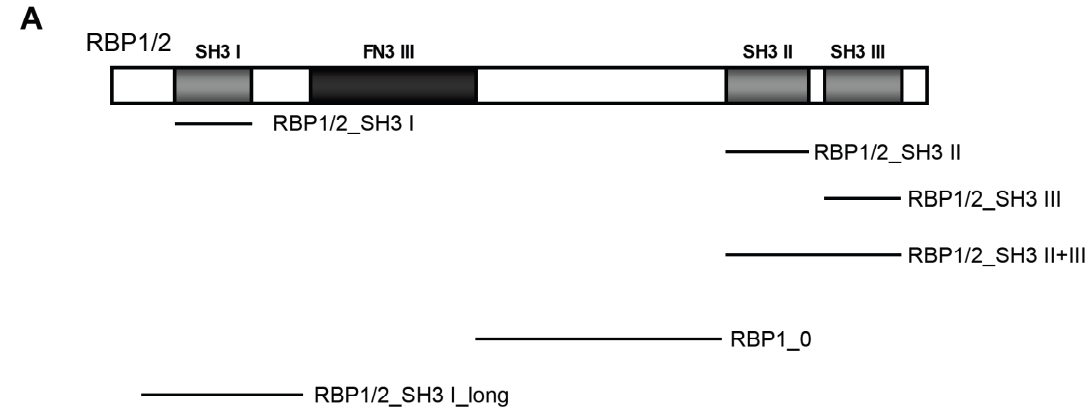

B

		Bsn10	Pclo1
RBP1_SH3 I	(652 - 712)	+++	++
RBP2_SH3 I	(191 - 251)	+++	++
RBP1_SH3 II	(1557 - 1622)	+	+
RBP2_SH3 II	(873 - 938)	+	+
RBP1_SH3 III	(1697 - 1758)	++	+
RBP2_SH3 III	(978 - 1039)	++	+
RBP1_SH3 II+III	(1557 - 1786)	+++	+++
RBP2_SH3 II+III	(873 - 1076)	+++	+++
RBP1_0	(1357 - 1556)	-	-

FIGURE 14. RIM BINDING PROTEINS CAN INTERACT WITH BASSOON AND PICCOLO THROUGH THEIR THREE SH3 DOMAINS.
(A) Overview of RBP1 and RBP2 fragments tested for binding to Bsn10 and Pclo1 in yeast two-hybrid assay. **(B)** Summary of results for Y2H assays. - = no interaction; +++ = interaction as strong as positive control for Y2H. Numbers in brackets indicate amino acid numbers corresponding to rat RBP1 and RBP2.

3.2.3 Identification of functional RBP-binding motifs on Bassoon and Piccolo

Mapping of RBP-interacting region on Bassoon in Y2H assays narrowed the interacting region to cDNA fragment Bsn10 (aa 2821 – 3013), which bound SH3 domains of RBPs. SH3 domains usually interact with proline-rich domains (reviewed in Mayer, 2001). Therefore we screened Bsn10 sequence for presence of PXXP motifs, two of which occur within this fragment. Two major classes of ligands for SH3 domains have been identified (Mayer, 2001).

Class I ligands have the general consensus +XφPXφP whereas class II ligands display the consensus sequence φPXφPX+, in which + is a basic residue, usually arginine, X is any amino acid, and φ is a hydrophobic residue. While the first identified PXXP motif (DPK**PLSP**TA) did fit neither class I nor class II ligands, the second one, RTLPSPP, fit the consensus sequences for class I and therefore was proposed as a binding motif for SH3 domains of RBPs. In line with this, a further shortened construct Bsn12 (aa 2869 – 2899) (Fig. 15A), which contains only the second PXXP motif interacted with SH3 domains of RBPs in the Y2H assay (Fig. 15B). The respective mutant construct where both proline residues (positions 4 and 7) and arginine residue (position 1) were exchanged to alanine (Bsn12_PA, Fig. 15A) did not bind RBPs in this assay (Fig. 15B). To verify that there were no additional RBP-interacting motifs in Bsn10 sequence the same point mutations were introduced into this construct (Bsn10_PA, Fig. 15A). Y2H analysis showed that the mutation of RTLPSPP was sufficient to disrupt the Bsn10 interaction with RBPs.

The corresponding sequence of Piccolo encoded in fragment Pclo1 showed the interaction with RBPs in Y2H assay (Fig. 12; Fig. 15B). Sequence analysis showed the presence of a corresponding PXXP motif – RTLPNPP. A further shortened fragment Pclo2 (aa 3653 – 3683) (Fig. 15A) also bound RBPs in this assay (Fig. 15B). Assessment of colony number and size suggested that Bassoon PXXP motif bound RBPs stronger in comparison to the homologous Piccolo sequence.

3.2.4 Distinct SH3 domains of RBPs bind Bassoon and Piccolo with relatively different strength

To further assess a possible preference of RBP-SH3 domains for Bassoon and Piccolo, we expressed and purified His-Thioredoxin (Trx)-Pclo2, His-Trx-Bsn12 and a respective mutant construct His-Trx-Bsn12_PA and tested their binding to purified GST fusion proteins covering distinct SH3 domains of RBPs using surface plasmon resonance technology. His-Trx-Bsn12_PA binding to RBP-SH3 domains did not show significant difference in comparison to His-Trx alone, which was used for normalization (Fig. 15C). This observation confirmed previously obtained Y2H data showing that mutation of both prolines (positions 4 an 7) and arginine residue at position 1 is sufficient to disrupt the PXXP motif of Bassoon and prevents its interaction with RBPs. MBAs of His-Trx-Bsn12 and His-Trx-Pclo2 to RBP-SH3 domains were measured and normalized to His-Trx alone (Fig. 15D). While both RBP1_SH3 I and RBP1_SH3 III showed detectable binding to both Bassoon and Piccolo, only RBP2_SH3 III could interact with these proteins in this assay. The MBA of RBP1_SH3 III was approximately 40% higher compared to the corresponding region of RBP2 (RBP2_SH3 III). Comparison of binding activities of distinct SH3 domains of RBP1 showed the significant

preference for RBP1_SH3 I to interact with both Bassoon and Piccolo (33% for Bassoon and 38% for Piccolo compared to RBP1_SH3 III and no significant binding to RBP1_SH3 II). In line with the Y2H data RBP1_SH3 III showed 20% higher binding activity to Bassoon than to Piccolo. The same tendency was observed for RBP1_SH3 I and RBP2_SH3 III. To verify that RBP2_SH3 bound neither Bassoon nor Piccolo not due to the wrong folding of this fusion protein we cloned longer fragment including the first SH3 domain of RBP2 (RBP2_SH3 I_long, aa 125 – 314 of rat RBP2). The corresponding longer version of SH3 I domain of RBP1 was also cloned (RBP1_SH3 I_long, aa 591 – 773 of rat RBP1) to control the construct length influence on affinity. MBAs of His-Trx-Bsn12 and His-Trx-Pclo2 to GST-RBP1_SH3 I_long and RBP2_SH3 I_long were measured and normalized to His-Trx alone (Fig. 15E). RBP1_SH3 I_long interacted with Bsn12 and Pclo2 with MBAs comparable with the shorter version – RBP1_SH3 I (for comparison see Fig. 15D). Both Bassoon and Piccolo bound RBP2_SH3 I_long slightly stronger than the corresponding RBP1 construct. In agreement with our Y2H data RBP2_SH3 I interaction with Bassoon was stronger compared to Piccolo.

3.2.5 Bassoon's but not Piccolo's interaction with RBPs might be regulated by phosphorylation

Sequence analysis of RBP-interacting PXXP motifs on Bassoon and Piccolo revealed that they differ in one aa residue at position 5, which is serine in Bassoon instead of asparagine in Piccolo (RTLPSPP *vs.* RTLPNPP). Furthermore, a proteomic study by Collins et al. (2005) showed that this particular serine residue in Bassoon (S2893 in rBsn) could be phosphorylated *in vivo* potentially by p38 MAPK. These findings raised the question if the affinity of Bassoon to RBPs can be influenced by phosphorylation. To assess this we generated Bassoon constructs, in which hyper- and hypophosphorylation mimicking mutations were introduced into the Bassoon construct Bsn12 by the mutation of serine to aspartate (hyper) or serine to alanine (hypo). The mutated fragments, Bsn12_SD and Bsn12_SA respectively, were assayed for binding to RBP1 constructs in the Y2H assay (Fig. 16A). Both Bsn12_SD and Bsn12_SA interacted with RBP1 constructs RBP1_SH3 I and RBP1_SH3 II+III in this assay. The construct Bsn12_PA containing nonfunctional PXXP motif was used as a negative control and did not show any interaction with any of the RBP1 constructs tested. The assessment of yeast colonies growth on a selection medium showed no difference for Bsn12_SD and Bsn12_SA in comparison to the wild type construct Bsn12.

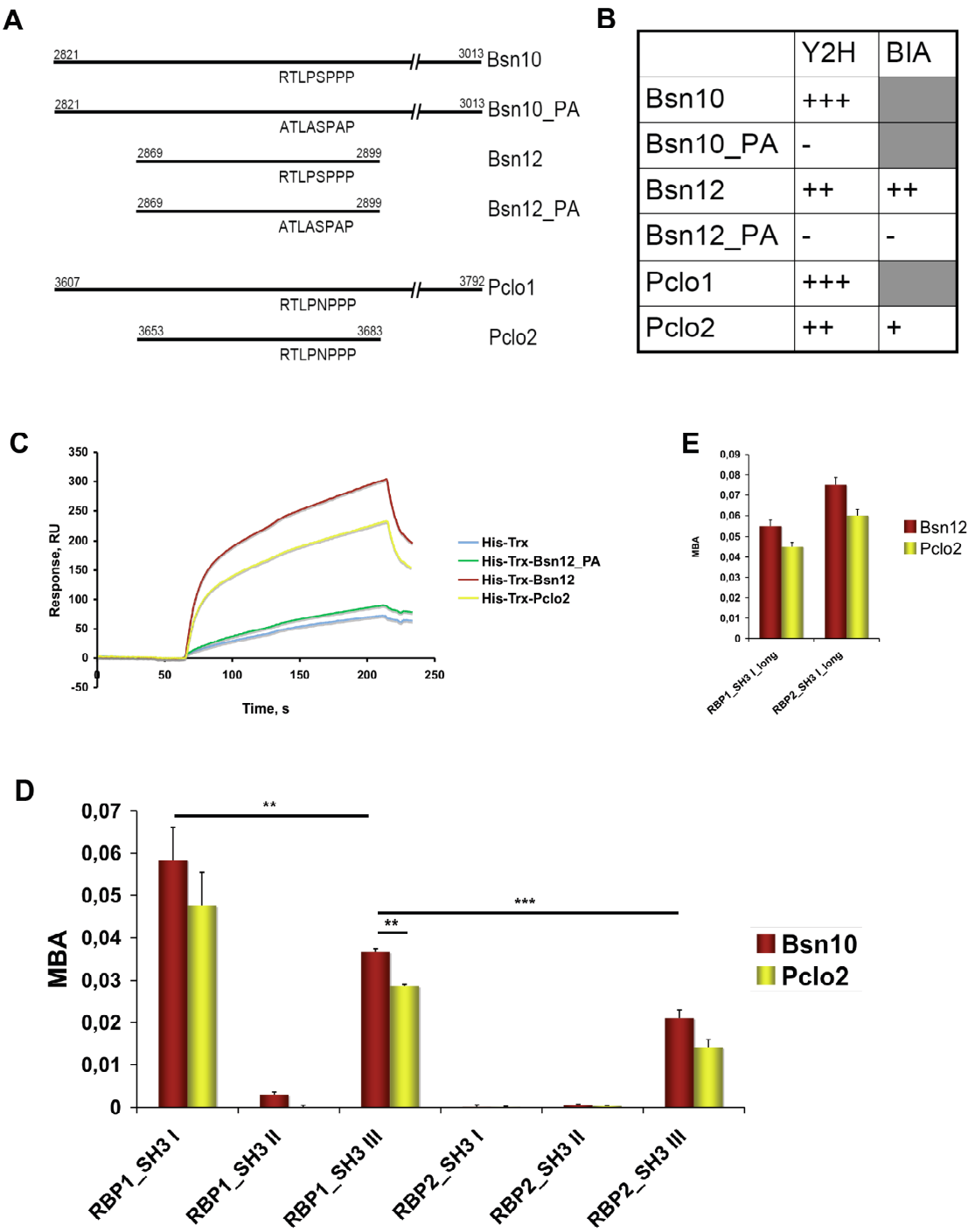

	Y2H	BIA
Bsn10	+++	
Bsn10_PA	-	
Bsn12	++	++
Bsn12_PA	-	-
Pclo1	+++	
Pclo2	++	+

FIGURE 15. BASSOON AND PICCOLO CAN INTERACT WITH RBPS THROUGH PXXP MOTIFS.
(A) Bassoon and Piccolo constructs including the amino acid substitutions introduced at RBP-interacting PXXP motifs; bordering amino acid numbers refer to rat Bassoon and Piccolo. **(B)** Summery of binding assays in yeasts (Y2H, yeast two-hybrid) and using surface plasmon resonance technology (BIA, Biacore). Whenever a construct was not used in a distinct assay the respective box is in gray. **(C)** The sensorgram shows the slope of response units (RU) over time after injection of GST-RBP1_SH3 I over immobilized His-Trx (blue), His-Trx-Bsn12_PA (green), His-Trx-Bsn12 (yellow), His-Trx-Pclo2 (dark red). **(D - E)** Molar-binding activities (MBA) of purified fragments of RBP1 and RBP2 to Bassoon and Piccolo constructs containing RBP-interacting PXXP motifs (Bsn12 and Pclo2 respectively) in surface plasmon resonance assay. Bar graphs show mean MBAs for each interaction, and error bars indicate SEM. **, $P < 0{,}01$; ***, $P < 0{,}001$.

Y2H assay provides positive results for interactions with broad range of binding affinities. While the phosphorylation of RBP-binding interface in Bassoon did not abolish its interaction with RBP, it could still affect their binding affinity. To test this possibility a competition assay was performed using surface plasmon resonance technology.

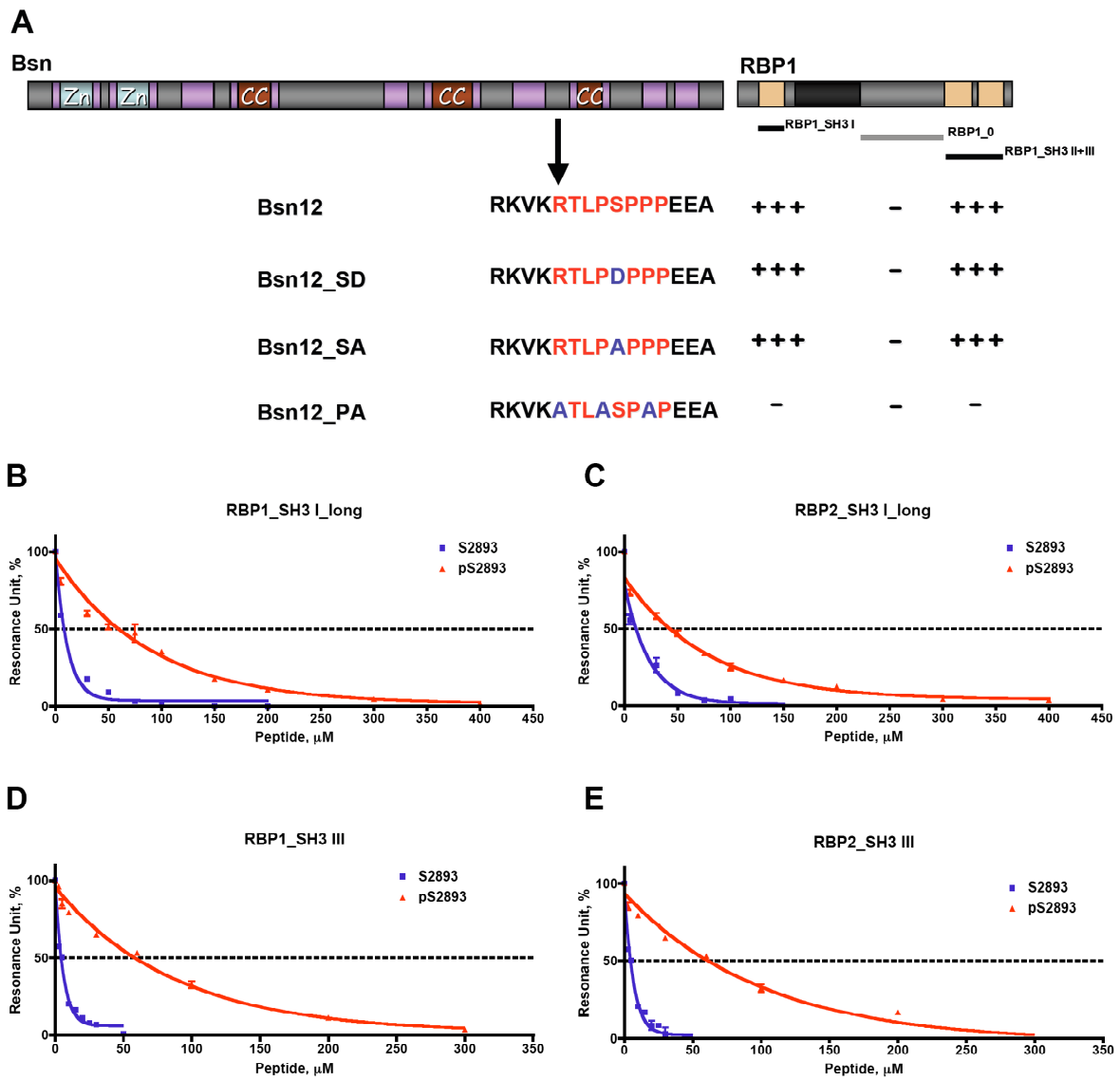

FIGURE 16. THE INTERACTION OF BASSOON, BUT NOT OF PICCOLO, WITH RBPS CAN BE MODULATED BY PHOSPHORYLATION.
(A) Yeast two-hybrid results of Bassoon phosphomimicking mutants with RBP1. Bsn12 – Bassoon fragment containing PXXP interaction motif for RBP1. Bsn12_SD – Bassoon mutant mimicking hyperphosphorylation state. Bsn12_SA – Bassoon mutant mimicking hypophosphorylation state. Bsn12_PA – Bassoon mutant with disrupted PXXP motif. The regions, which are encoded by RBP1_SH3 I, RBP1_SH3 II+III and RBP1_0, are indicated in the scheme for RBP1. - = no interaction; +++ = interaction as strong as positive control for Y2H. **(B - E)** Competitive inhibition of His-Trx-Bsn12 interaction with GST-RBP1_SH3 I_long (B), GST-RBP2_SH3 I_long (C), GST-RBP1_SH3 III (D) and GST-RBP2_SH3 III (E) by peptides encoding Bsn PXXP motif with non-phosphorylated serine residue at position 5 (S2893) and phosphorylated serine residue (pS2893) in a competition assay using surface plasmon resonance technology.

Bacterially expressed, thus non-phosphorylated, His-Trx-Bsn12, was used as a ligand immobilized on a chip surface. GST fusion proteins containing SH3 I and SH3 III of RBP1

and RBP2 were applied as soluble analytes and the binding was detected. Peptides corresponding to Bassoon's PPSP motif and its flanking sequences with phosphorylated (pS2893) or nonphosphorylated (S2893) serine residue was then used to inhibit RBP-constructs binding to His-Trx-Bsn12. For all RBP-constructs checked the inhibition was concentration dependent when S2893 or pS2893 was applied. In general the binding affinity of pS2893 peptide to all tested RBP-constructs was lower comparing to S2893 (Fig. 16B - E). Bsn12 interaction with RBP1_SH3 III (Fig. 16D) and RBP2_SH3 III (Fig. 16E) showed a similar inhibition pattern with approximately 15-fold excess of pS2893 comparing to S2893 needed to reach a 50% inhibition level (RBP1_SH3 III: 60 µM of pS2893 *vs.* 4 µM of S2893; RBP2_SH3 III: 70 µM of pS2893 *vs.* 4,5 µM of S2893). 50% inhibition of Bsn12 – RBP1_SH3 I_long interaction (Fig. 10B) was reached with 8-fold excess of pS2893 in comparison to S2893 (62,3 µM of pS2893 *vs.* 7,7 µM of S2893). For Bsn12 - RBP2_SH3 I_long interaction (Fig. 16C) 3,4-fold excess of pS2893 compared to S2893 peptide was necessary to reach a 50% inhibition level (54 µM of pS2893 *vs.* 16 µM of S2893). These observations imply that phosphorylation of a serine residue in RBP-interacting region of Bassoon decreases its binding capacity to RBP-SH3 domains.

3.3 Distinct SH3 domains of RBPs have different binding affinities to Rim1, Ca_V2.2, Bassoon, and Piccolo

RBP1 and RBP2 contain three structurally homologous SH3 domains, each interacting with more than one partner. RBP1 and a fragment of RBP2 were first identified by their capacity to interact with RIM1 (Wang et al., 2000). The authors of the original study suggested that the interaction between the RBPs and Rim1 resulted from binding of an SH3 domain of RBPs to a PXXP motif located between the two C2 domains of Rims (Fig. 17A). This suggestion was further confirmed by Hibino et al. (2002), who also showed that three SH3 domains of RBPs bound to PXXP motifs in α1 subunits of VDCCs (Fig. 17A). Our data postulates that SH3 domains of RBP1 and RBP2 can interact with specific PXXP motifs in Bassoon and Piccolo. So far, all known RBPs interaction partners, which are Rims, Ca_v2.1, Ca_v2.2, Bassoon and Piccolo, can interact with more than one SH3 domain *in vitro* (Fig. 17B). These observations raise the question – whether all these interactions take place simultaneously i.e. is there preference of SH3 domains for particular binding partners, or whether there is a competition between different partners for the same binding site. To tackle this question His-Trx fusion proteins covering PXXP motifs of Rim1, Ca_V2.2 (RIM1_1 and Ca_V2.2_1 respectively, Fig. 17C), Bassoon and Piccolo (Bsn12 and Pclo2, Fig. 14A) expressed in bacteria were tested for binding to GST-tagged SH3 domains of RBP1 and RBP2 using surface plasmon resonance technique. Molar binding activities for each distinct

SH3 domain of RBP1 and RBP2 to all known interaction partners were measured and normalized to the MBA of RBP1_SH3 I to Bsn12 (Fig. 17D).

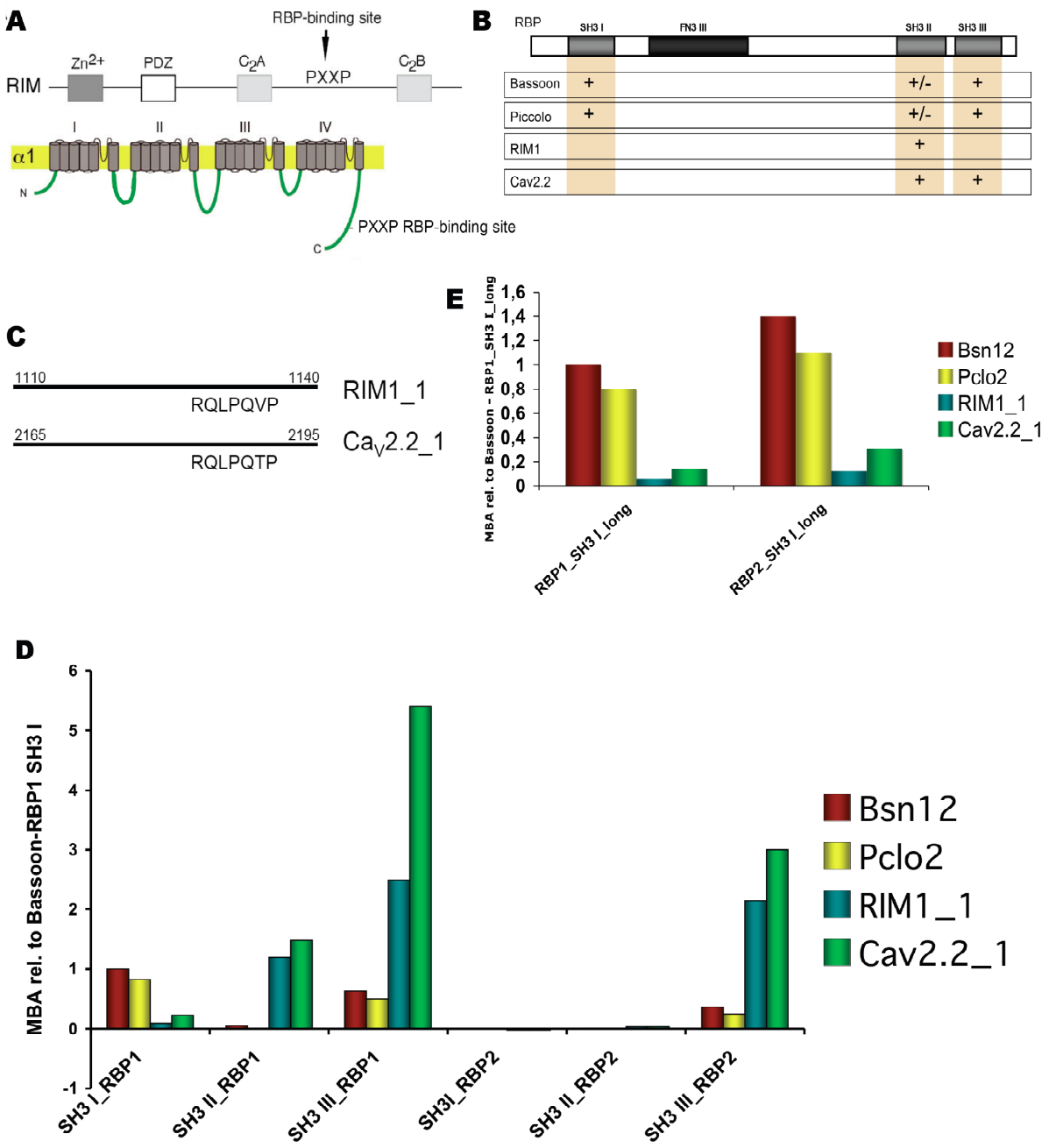

FIGURE 17. RIM BINDING PROTEINS CAN INTERACT SIMULTANEOUSLY WITH BASSOON OR PICCOLO, RIM1 AND CA_V2.2.
(A) A schematic diagram depicts the structure of Rab3-interacting molecules (Rims) and alpha 1 subunit of voltage dependent calcium channels (α1). RBP-interacting PXXP motifs are indicated. **(B)** Summary of known interaction partners for RBPs and their identified binding regions. SH3_I, II, III, SH3 domains; FN III, fibronectin III repeats. **(C)** RIM1 and Ca_V2.2 constructs covering RBP-interacting PXXP motifs used in surface plasmon resonance assay; bordering amino acid numbers refer to rat RIM1 and Ca_V2.2. **(D)** Molar binding activities (MBA) of purified RBP1 and RBP2 fragments to Bsn, Pclo, RIM1 and Ca_V2.2 fragments in surface plasmon resonance assays. MBAs are related to the MBA of RBP1_SH3 I to the Bsn fragment (=1). **(E)** MBAs of fragments covering SH3 I of RBP1 and RBP2 with prolonged flanking regions to Bsn, Pclo, RIM1 and Ca_V2.2 in surface plasmon resonance assay. MBAs are related to the MBA of RBP1_SH3 I_long to Bsn12 (=1).

For RBP1 clear differences in binding affinities were observed for distinct SH3 domains. RBP1_SH3 III showed approximately twice higher affinity to $Ca_V2.2$ PXXP ($Ca_V2.2$_1) than to the corresponding sequence of Rim1 (RIM1_1) and 11-times higher compared to Bassoon and Piccolo (Bsn12 and Pclo2, respectively). These observations make $Ca_V2.2$ the most prominent candidate to interact with RBP1 through its SH3 III domain *in vivo* assuming that molar abundance of all RBP-interacting proteins is similar. RBP1_SH3 II bound neither Bsn12 nor Pclo2, but showed clear interaction with both $Ca_V2.2$_1 and RIM1_1. Although its binding activities for RIM1_1 and $Ca_V2.2$_1 were comparable, taking into account a much higher probability for $Ca_V2.2$ to interact with RBP1 through its SH3 III domain, we suggest Rim1 as the most prominent candidate to bind RBP1_SH3 II *in vivo*. In contrast to SH3 II and SH3 III, the SH3 I domain of RBP1 showed significantly higher binding activity to Bassoon and Piccolo than to $Ca_V2.2$ or RIM1 and was suggested to bind one of these two proteins *in vivo*. SH3 III domain of RBP2 showed a binding pattern similar to the corresponding region of RBP1, although its overall binding activity to all investigated interaction partners was approximately 2-fold lower. RBP2_SH3 I and RBP2_SH3 II did not interact with any of the potential binding partners we checked in this assay probably due to misfolding of these constructs. RBP1_SH3 I_long and RBP2_SH3 I_long (Fig. 15A) were checked for their binding to all proteins of interest (Fig. 17E). RBP1_SH3 I_long showed the same interaction pattern as RBP1_SH3 I construct, interacting with Bassoon and Piccolo, while the binding of $Ca_V2.2$ and Rim1 was much weaker. The length of the fragment did not influence its binding activity, since the numerical MBAs for RBP1_SH3 I and RBP1_SH3 I_long did not show any difference. RBP2_SH3 I_long interacted with both Bsn12 and Pclo2 but not with RIM1_1 or $Ca_V2.2$_1. Comparison of relative binding activities for RBP1_SH3 I_long and RBP2_SH3 I_long revealed a slight preference for Bassoon and Piccolo to bind RBP2_SH3 I as compared to RBP1_SH3 I (postulating the same molar amounts of both proteins).

Next, we wanted to verify the localization of RBPs and their interaction partners in hippocampal neurons. Antibody raised against fragment RBP2_10 covering aa 589 – 869 of rat RBP2 CDS were provided for following experiments by Anna Fejtova. Rat hippocampal neurons were plated and cultured. Immunostainings with antibodies against Bassoon, $Ca_V2.1$, RBP2 and the presynaptic marker Synapsin, were performed at 14 DIV. In primary hippocampal neurons RBP2 immunoreactivity clearly overlapped Bassoon immunoreactivity at synaptic areas (Fig. 18A). The synaptic localization of puncta was confirmed by co-staining with anti-Synapsin antibodies. Anti-RBP2 antibody labeling was also observed in cell bodies of hippocampal neurons. Labeling for $Ca_V2.1$ (Fig. 18B) also partially co-localized with Bassoon immunoreactivity at synaptic puncta. To confirm that Bassoon, RBP2 and $Ca_V2.1$ can be present at the same synapses, counterstaining for those proteins was performed. The

significant amount of puncta showed the overlapped immunostaining for Bassoon, RBP2 and $Ca_V2.1$ (Fig. 18C).

Overall, our data imply that RBPs can interact simultaneously with Bassoon or Piccolo, RIM1 and VDCCs.

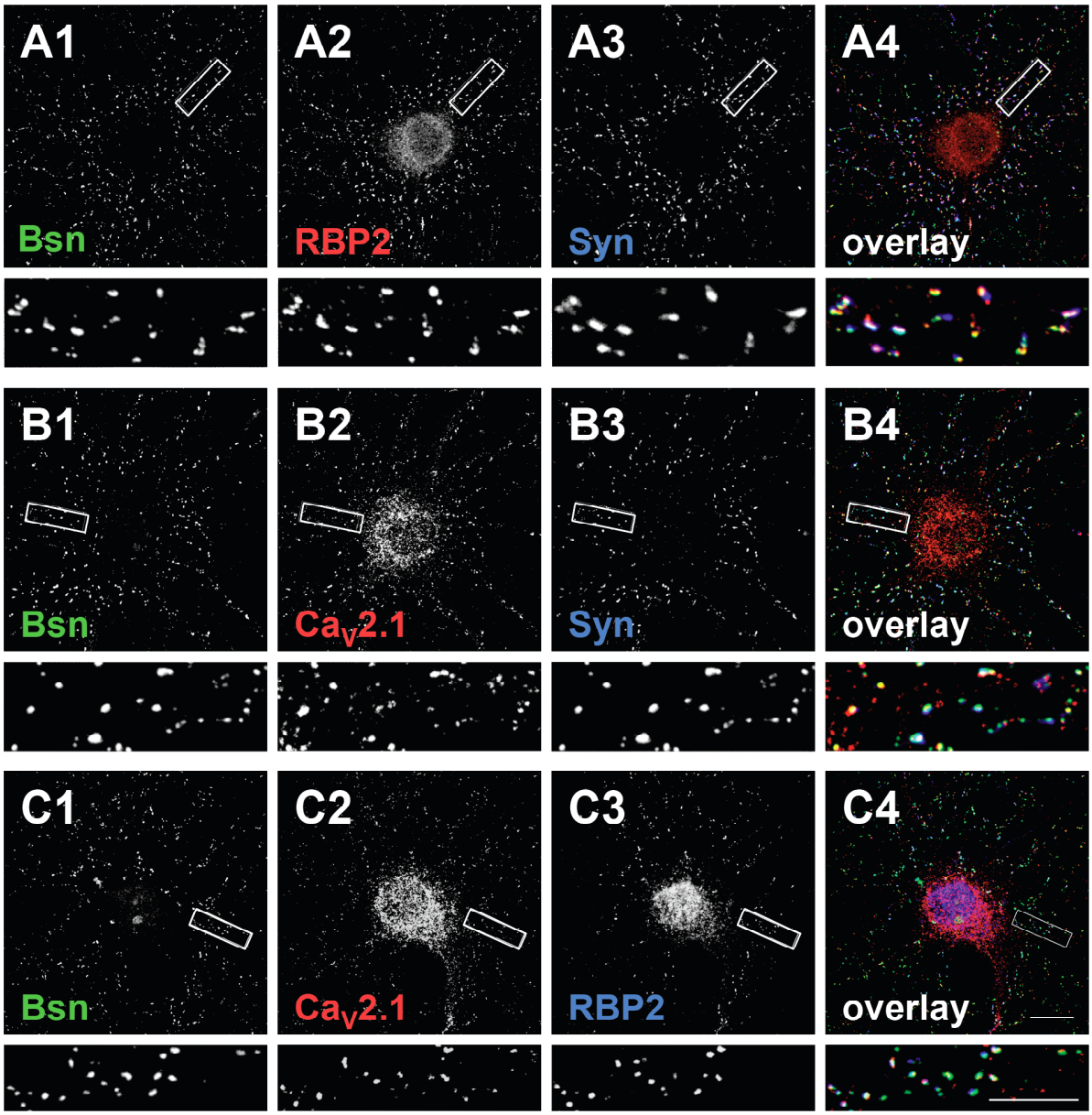

FIGURE 18. BASSOON CO-LOCALIZES WITH RBP2 AND $CA_V2.1$ AT SYNAPSES.
Rat hippocampal neurons were fixed at 14 DIV and immunostained to visualize the co-localization of Bassoon with RBP2 (A1-4) and $Ca_V2.1$ (B1-4) at synapses. The co-localization of Bassoon with RBP2 and $Ca_V2.1$ at the same puncta has been also demonstrated (C1-4). Higher magnifications of boxed regions are shown below the respective image. Bars: (A – C) 20 µm; (inserts) 10 µm.

3.4 Potential physiological functions of Bassoon interaction with Rim binding proteins

3.4.1 The lack of functional Bassoon reduces the amount of $Ca_V2.1$ at synapses

Mutant mice lacking the central region of the presynaptic active zone protein Bassoon were generated and characterized previously (Altrock et al., 2003). In the original study the authors showed that the lack of functional Bassoon causes a reduction in normal synaptic transmission. At the ribbon synapses of cochlear inner hair cells (IHCs) and photoreceptor cells Bassoon mutation leads to impaired ribbons anchoring at the presynaptic membrane (Khimich et al., 2005; Dick et al., 2003). Furthermore, calcium currents were significantly reduced in mutant IHCs, potentially due to insufficient recruitment and/or stabilization of VDCCs at the active zone (Khimich et al., 2005).

Based on these observations we sought to analyze the effect of lack of Bassoon on the levels of $Ca_V2.1$ at synaptic terminals. These experiments were done in close collaboration with Claudia Marini during her practical training (under my supervision) in the group of Prof. E. D. Gundelfinger. For our analysis we used a new mouse mutant, where the *bsn* gene is targeted by a retroviral insertion diminishing translation of Bassoon mRNA and transcription of Bassoon protein. Hippocampal neurons from BGT (*bsn* gene trap) mice and their wild type littermates were mixed in equal ratio, plated and co-cultured. Immunostainings with antibodies against synaptic marker Synapsin, SV protein Synaptophysin, $Ca_V2.1$ and Bassoon were performed at 16 and 23 DIV. This experimental setup allowed direct comparison of immunoreactivity for $Ca_V2.1$ and Synaptophysin between Bassoon negative (mutants) and Bassoon positive (WT) synapses, which were defined by staining for synapsin (Fig. 19A). The relative synaptic amounts of $Ca_V2.1$ were determined as the intensity of immunostaining normalized to mean $Ca_V2.1$ immunoreactivity of synapses formed by axons of wild type neurons in the same image. The relative synaptic amounts of Synaptophysin were used to control possible non-specific effects of the lack of Bassoon on the synapse molecular composition. The quantitative analysis revealed a significant decrease in mean amounts of $Ca_V2.1$ at 16 DIV (20%) and 23 DIV (30%) at Bassoon mutant synapses compared with synapses formed by axons of wild type neurons (Fig. 19B). Interestingly, while at 16 DIV the mean amounts of Synaptophysin were also significantly decreased (34%) comparing to the wild type synapses, they were not changed at 23 DIV, when there was no significant difference between Bassoon mutant synapses and the wild type ones (Fig 19C). These results suggest that Bassoon is involved in recruitment or retention of VDCC at the presynaptic terminals.

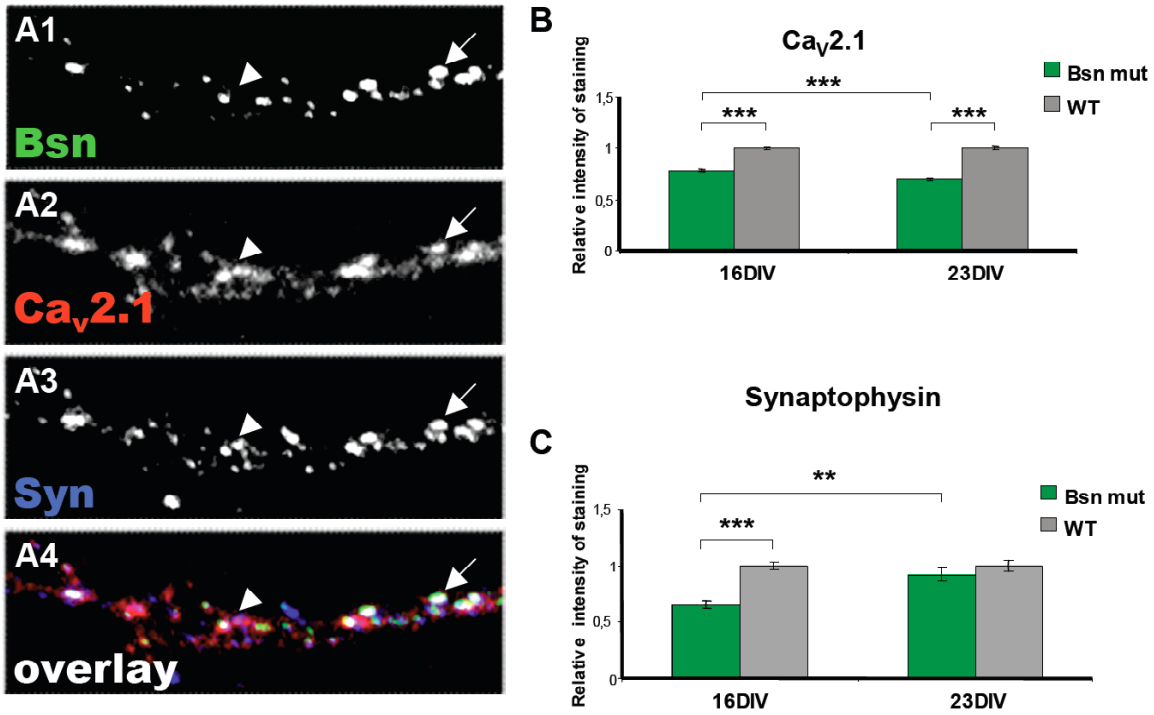

FIGURE 19. THE LACK OF FUNCTIONAL BASSOON REDUCES THE AMOUNT OF CA$_V$2.1 AT SYNAPSES.
(A) Co-staining of Ca$_V$2.1 (red) with Bassoon (green) and Synapsin (blue) in hippocampal neurons derived from Bassoon mutant and wild type mice at 16 DIV. Indicated are Bassoon mutant (arrowhead) and wild type (arrow) synapses. **(B - C)** Quantification of relative staining intensities for Ca$_V$2.1 (B) and Synaptophysin (C). Bar graphs show mean values of relative fluorescence intensity for each staining and error bars indicate SEM. Values are derived from three independent experiments. **, $P < 0{,}01$; ***, $P < 0{,}001$. Figures 13B and 13C are provided by Claudia Marini.

3.4.2 Bassoon recruits calcium channels through the interaction with Rim binding proteins

GFP-Bsn expressed in hippocampal neurons targets to synapses, but also forms aggregates within a cell body. Interestingly, these aggregates are positive for Ca$_V$2.1. To test the hypothesis that Bassoon is involved in calcium channels recruitment through the interaction with RBPs, an EGFP-tagged RBP-binding mutant (RBM) of Bassoon (EGFP-BsnRBM) unable to interact with RBPs was produced by introducing the aforementioned amino acid exchanges into RBP-binding PXXP motif of Bassoon. In this study, we compared the effects caused by EGFP-Bsn *vs.* EGFP-BsnRBM overexpression on localization of Ca$_V$2.1, RBP2 and synapsin. Rat hippocampal neurons were transfected with EGFP-Bsn or EGFP-BsnRBM at 3 DIV. Immunostainings with antibodies against synaptic marker Synapsin, Ca$_V$2.1 and RBP2 were performed at 14 DIV.

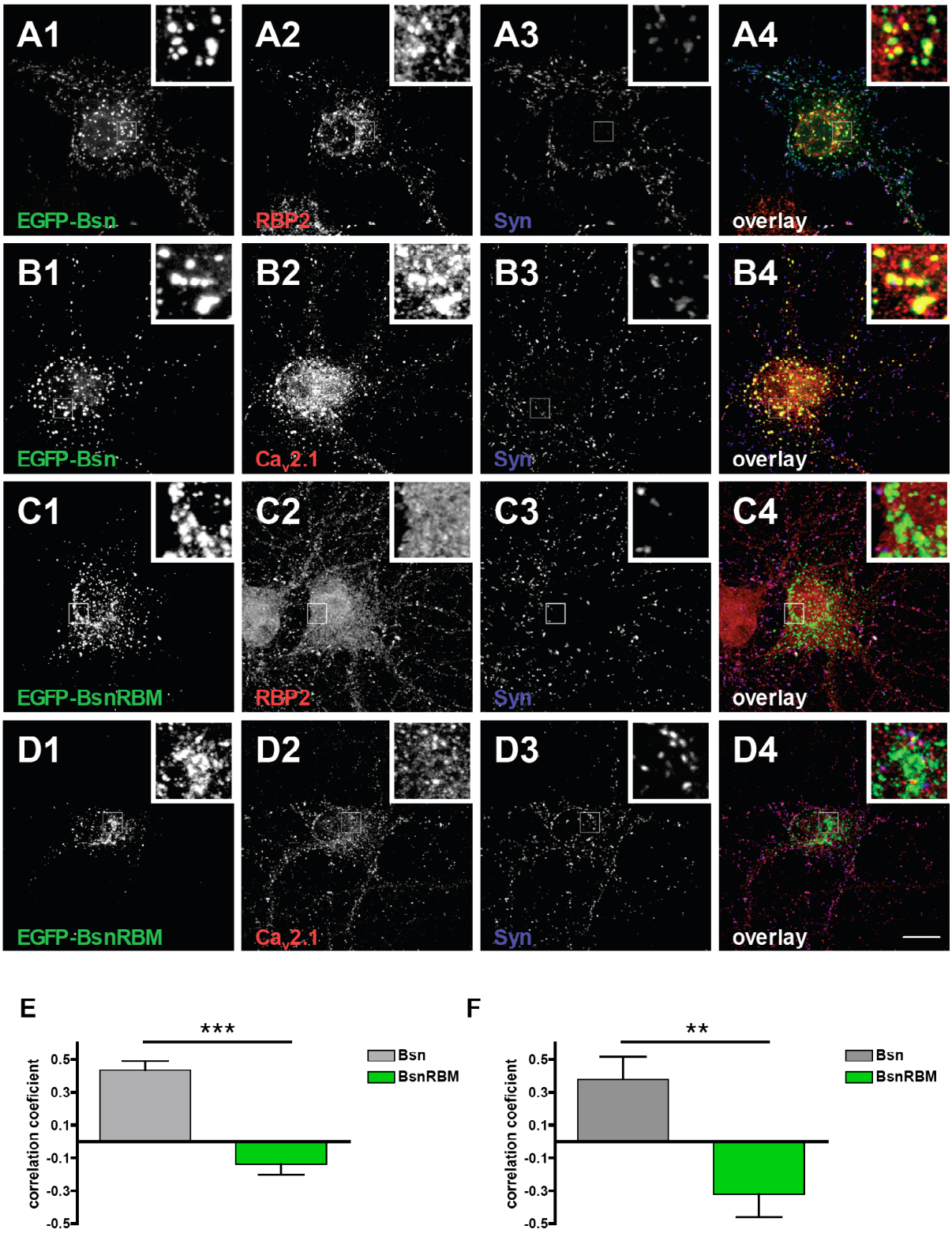

FIGURE 20. BASSOON BUT NOT BASSOON DEFICIENT FOR RBP BINDING RECRUITS CA$_V$2.1.
(A – D) Cells transfected at 3 DIV with EGFP-Bsn (A and B) and EGFP-BsnRBM (C and D) were fixed at 14 DIV and counterstained to visualize Synapsin, RBP2 (A and C) and Ca$_V$2.1 (B and D). Higher magnifications of the boxed regions are shown in the right up corner of the respective image. Bar, 20 µm **(E – F)** Quantification of correlation coefficients for synaptic RBP2 (E) and CaV2.1 (F) immunofluorescence intensities towards intensity of EGFP fluorescence caused by overexpressed EGFP-Bsn or EGFP-BsnRBM. Bar graphs show mean correlation coefficients for each staining, and error bars indicate SEM. **, $P < 0{,}01$; ***, $P < 0{,}001$.

As was expected, $Ca_V2.1$ were enriched at GFP-Bsn positive puncta (Fig. 20B2). The same effect was observed for RBP2 immunoreactivity (Fig. 20A2). On the contrary, we did not see any enrichment of synapsin (Fig. 20A3, 20B3) at Bsn-formed clusters; therefore the observed co-recruitment of RBP2 and $Ca_V2.1$ is rather specific than an over-expression artefact. When EGFP-BsnRBM was over-expressed it formed clusters similar to those formed by EGFP-Bsn (Fig. 20C1 and D1 compare to A1 and B1), but neither RBP2 (Fig. 20C2) nor $Ca_V2.1$ (Fig. 20D2) were co-recruited.

To verify whether Bassoon is involved in VDCC recruitment to synapses and whether this involvement is RBP-dependent the synaptic immunofluorescence (IF) intensities of $Ca_V2.1$ and RBP2 were correlated to the intensity of EGFP fluorescence caused by overexpressed EGFP-Bsn or EGFP-BsnRBM. Both $Ca_V2.1$ and RBP2 IF intensities showed positive correlation with EGFP intensity (r=0,38±0,14 and 0,43±0,05 for $Ca_V2.1$ and RBP2, respectively) at EGFP-Bsn transfected synapses (Fig. 20E, 20F). On the contrary, at synapses transfected with EGFP-BsnRBM the negative correlation between $Ca_V2.1$ and RBP2 IF intensities with EGFP fluorescence (r= [-0,32±0,14] and [-0,14±0,07] for $Ca_V2.1$ and RBP2, respectively) was observed (Fig. 20E, 20F).

Overall, the lack of $Ca_V2.1$ co-recruitment by Bassoon due to the mutation of RBP-interacting PXXP motif, confirms that Bassoon effects the localization of calcium channels interacting with them through RBPs.

4. Discussion

4.1 Bassoon – DLC interaction: three functional DLC-binding sites in Bassoon, role of Bassoon as a cargo adaptor protein for dynein motors

We have identified three independently functioning DLC-binding sites on Bassoon, all resembling, but not exactly matching, the DLC-binding consensus sequence (K/R)XTQT (Lo et al., 2001). This is in line with previously reported high diversity of binding sites identified among known DLC interacting partners (Lajoix et al., 2004). Notably, none of the three DLC-binding sites of Bassoon is conserved in its paralogue Piccolo. Mutated Bassoon fragments, where the essential (T/S)QT motifs were replaced by AAA did neither interact with DLCs in biochemical assays nor in yeast or mammalian cells. It is therefore likely that Bassoon binds DLCs via the target-interacting groove of DLCs, the interaction interface shared also by other known DLC interaction partners (Fan et al., 2001; Liang et al., 1999; Lo et al., 2001). Quantitative *in vitro* binding assays revealed that all three sites are active, that site I has a higher relative affinity for DLCs than sites II and III and that binding strengths seem to be additive. Thus the cluster of three DLC-binding motifs constitutes a multivalent interaction interface in Bassoon that is likely to facilitate DLC-Bassoon interaction.

In agreement with the high homology of DLC1 and DLC2, Bassoon was observed to bind both isoforms. However, quantitative binding assays with Bassoon fragments containing two or three DLC-binding interfaces showed significantly higher affinity for DLC2 than for DLC1.

One important cellular function of DLCs is to link their binding partners to dynein- or myosinV-dependent transport processes. In neurons, DLCs were shown to bind postsynaptic scaffold molecules like GKAP (Naisbitt et al., 2000) or gephyrin (Fuhrmann et al., 2002) and active retrograde transport was proposed as a mechanism contributing to activity-dependent remodeling of the postsynaptic receptor apparatus (Maas et al., 2006). However, the functional role of DLCs as cargo adaptors for dynein motors has become a subject of debate recently (Barbar, 2008; Vallee et al., 2004). The binding of DLC cargos occurs in the same binding groove as the binding to dynein motor complex via IC74 (Williams et al., 2007). In this configuration, the DLC-interaction partners would probably compete with the dynein motor complex for binding to DLC, rather than being linked to the dynein motor complex via DLC.

When DLC1 or DLC2 were targeted to the outer mitochondrial membrane in COS-7 cells, the localization of mitochondria was remarkably changed: normally, mitochondria are distributed throughout the cytoplasm of cells, in contrast, targeting of DLCs to mitochondria results in

their accumulation near the cell center. This finding could be explained by DLC-mediated retrograde transport of mitochondria along microtubules. To test whether Bassoon can function as a cargo adapter, the Bassoon fragment harboring DLC-binding sites was targeted to the outer mitochondrial membrane the subcellular localization of mitochondria was observed. After expression of DLC-interacting Bassoon sequence, mitochondria were clustered near the microtubule-organizing center (MTOC). This accumulation was dependent on both intact DLC-binding motifs and assembled microtubules and is best explained by assuming retrograde transport of Bassoon-tagged mitochondria. These findings support the view that Bassoon via its interaction with DLCs might function as a cargo adaptor for the retrograde motor dynein (Fig. 21). Methodologically, experiments done in frame of this project revealed the suitability of the novel mito-targeting assay developed here, to not only demonstrate existence of protein-protein interactions in living cells but also in some cases to tackle functional significance of these interactions.

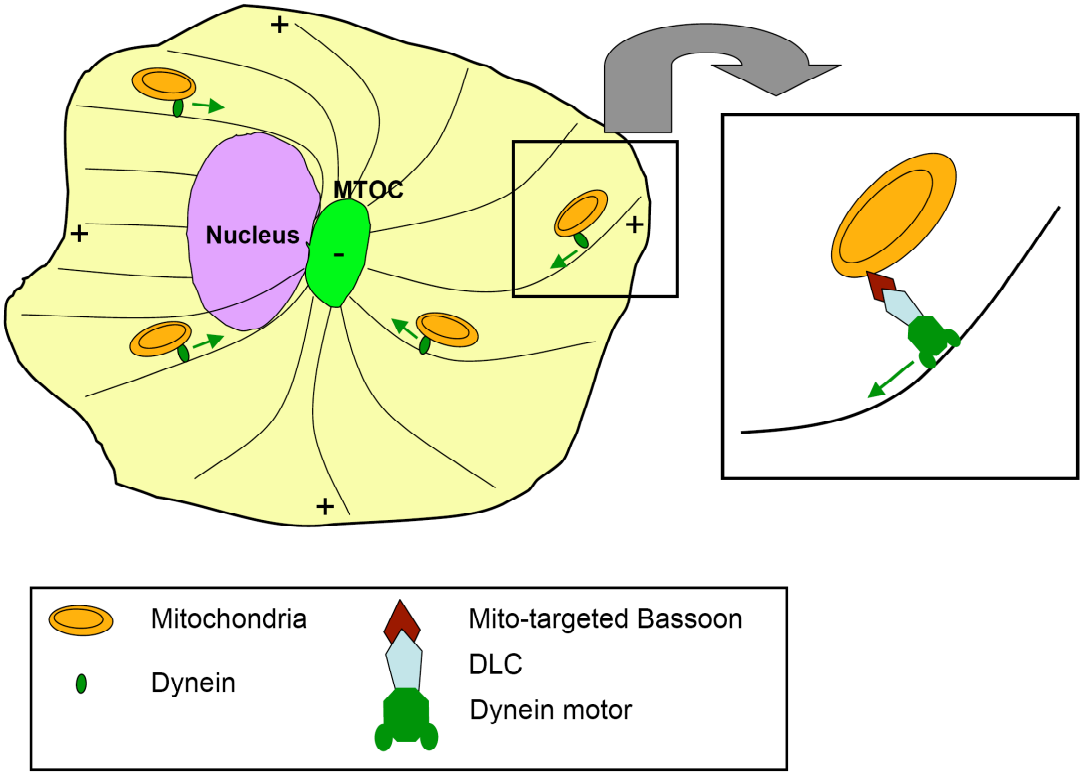

FIGURE 21. BASSOON VIA ITS INTERACTION WITH DLCS FUNCTIONS AS A CARGO ADAPTOR FOR THE RETROGRADE MOTOR DYNEIN IN COS-7 CELLS.

4.2 Piccolo and nonphosphorylated Bassoon bind preferentially to the first SH3 domain of RBPs

Here we report a novel interaction between the presynaptic active zone proteins Bassoon and Piccolo with RBP1 and RBP2. We identified specific PXXP motifs in Bassoon (RTLPSPP) and Piccolo (RTLPNPP), which can bind SH3 domains of RBPs. Mutated Bassoon fragments, in which the essential prolines at positions 4 and 7 and arginine at position 1 were replaced by alanine residues, did not interact with RBPs neither in biochemical assays nor in yeast cells. Initial Y2H analyses of Bassoon and Piccolo interactions with RBPs revealed that each of the three SH3 domains of both RBP1 and RBP2 were able to interact with both Bassoon and Piccolo. Y2H assays provide positive results for interactions within a broad range of binding affinities. Therefore to further assess a possible preference of RBP-SH3 domains for Bassoon and Piccolo, surface plasmon resonance technology was used to compare binding affinities of distinct RBP-SH3 domains for Bassoon and Piccolo PXXP motifs. These analyses revealed that both Bassoon and Piccolo interact preferentially with the SH3-I domain of RBPs. Sequence analysis showed a closer relationship between respective SH3 domains of RBP1 and RBP2 (for alignment of RBP1 and RBP2 see 6.1) compared to distinct SH3 domains within one protein sequence (e.g., RBP1_SH3 I is more homologous to RBP2_SH3 I [74% of identity] than to RBP1_SH3 II [56% of identity] or RBP1_SH3 III [62% of identity]). The target specificity of particular SH3 domains can be increased due to the interaction of ligand residues outside the core binding motif (PXXP) with surfaces on the SH3 domain outside the PPII binding groove (Feng et al., 1995). Given this, the relatively higher homology of RBP-SH3 I domains compared to the other SH3 domains of RBPs may provide a basis for the similar interaction patterns and, in turn, contribute to the higher affinities of RBP-SH3 I domains for Bassoon and Piccolo as compared to the other SH3 domains of RBPs.

Sequence analysis of RBP-interacting PXXP motifs in Bassoon and Piccolo revealed that they differ in one aa residue at position 5, which is a serine in Bassoon instead of an asparigine in Piccolo (RTLPSPP *vs.* RTLPNPP). Interestingly, a proteomic study by Collins et al. (2005) showed that this particular serine residue in Bassoon (S2893 in rBsn) can be phosphorylated *in vivo*. *In vitro* competition assays performed in this study revealed that phosphorylation of the serine residue in the RBP-interacting PPSP motif of Bassoon significantly hinders its interaction with RBP-SH3 I and RBP-SH3 III domains. Similarly, it has been reported that phosphorylation of Pak1 at S21, which is in the PXXP motif recognized by SH3 domain of Nck, leads to reduction in binding of Nck to Pak1 (Zhao et al., 2000); also the phosphorylation of several serine residues within or in close proximity to the PXXP motifs of tau inhibits its interactions with SH3 domain of several important signaling molecules, including Fyn, cSrc, Lck and 14-3-3 (Reynolds et al., 2008). Phosphorylation of two serine

residues located in close proximity to PXXP motif of the nonreceptor tyrosine kinase Abl, inhibits Abl interaction with SH3 domain of Abi2 up to 90% as compared to nonphosphorylated Abl (Jung et al., 2008). The authors of this paper suggested that negative charges introduced by phosphorylation disrupt electrostatic interactions with the arginine residue within the Abi2-interacting motif of Abl, resulting in dissociation of Abi2 from the Abl PXXP motif. A similar explanation for phosphorylation-dependent inhibition of interactions between SH3 domains and PXXP motifs would apply to the interaction of Bassoon and RBPs described in this study.

In quantitative *in vitro* assays, non-phosphorylated Bassoon had a slight preference for binding RBPs as compared to Piccolo. However, when Bassoon is phosphorylated Piccolo should bind more avidly to the SH3 I domains of RBPs. In this way phosphorylation may regulate which of two binding partners interacts with RBPs. Although due to their high structural similarity Bassoon and Piccolo are partially functionally redundant, several unique interaction partners suggest that these two proteins might be involved in distinct protein networks within presynaptic terminals. This is also indicated by the distinct phenotypes displayed by mouse mutants for Bassoon and Piccolo. Interestingly, the RBP1_SH3-I interaction with Bassoon was approximately twice more sensitive to phosphorylation of the serine residue within RBP-interacting PPSP motif of Bassoon compared to RBP2_SH3 I *in vitro*, suggesting a more dramatic effect of phosphorylation on Bassoon–RBP1 than on Bassoon–RBP2 interaction *in vivo.* This phenomenon may as well regulate the composition of RBP-containing protein complex *in vivo.*

The serine residue in RBP-interacting PSPP motif of Bassoon was predicted to be phosphorylated by p38 MAPK (Collins et al., 2005). In brain MAPKs can be activated by synaptic activity and are essential for some forms of synaptic plasticity (Imprey et al., 1999). In hippocampal neurons p38 MAPK is expressed both presynaptically (Maruyama et al., 2000) and postsynaptically (Bolshakov et al., 2000). P38 MAPK has also been implicated in presynaptic inhibition, because its activation is involved in the inhibition of $Ca_V2.2$ channels (Wilk-Blaszczak et al., 1998; Brust et al., 2006). Thus the reported effects of MAPK on Ca^{2+} currents might be mediated via modulation of the Bassoon/Piccolo–RBP–VDCC multiprotein complex.

4.3 RBPs can play an integrative role interacting simultaneously with Rim1, VDCCs and Bassoon or Piccolo

To date several presynaptic proteins have been shown to bind RBP-SH3 domains *via* specific PXXP motifs. Rim1 and VDCCs interact with both RBP1 and RBP2 (Wang et al., 2000; Hibino et al., 2002) and a model was suggested where RBPs can serve as linkers

between Rims and VDCCs (Hibino et al., 2002). Here we report that RBPs can also interact with specific PXXP motifs in Bassoon and Piccolo, preferentially *via* their SH3-I domains. The existence of three SH3 domains in RBPs and several potential binding partners raised the question whether these interactions take place simultaneously or whether there is a competition between distinct binding partners for the same binding site. To tackle this question the relative binding affinities for each SH3 domain of RBP1 and RBP2 for Rim1, $Ca_V2.2$, Bassoon and Piccolo were measured and, indeed, clear differences were observed: RBP-SH3-I domains bound preferentially Bassoon and Piccolo, while their ability to interact with Rim1 and $Ca_V2.2$ was very low. RBP-SH3-III domains could interact with all four analyzed partners but showed a clear preference for $Ca_V2.2$. RBP1-SH3-II had high binding strength for both – Rim1 and $Ca_V2.2$ (although the SH3-II binding strength towards $Ca_V2.2$ was approximately twice lower as compared to SH3-III), while its relative binding affinities for Bassoon and Piccolo were relatively low. The RBP2-SH3-II did not interact with any examined interaction partner, most likely due to the misfolding of the corresponding fusion protein in bacterial cells. A similar problem with RBP2-SH3-I was overcome by using longer fusion proteins containing SH3 domain with expanded flanking regions (RBP2_SH3-I_long). In our experiments, RBP2_SH3-I_long showed the same binding pattern as RBP1_SH3-I. Given this and taking into account the high homology between RBP-SH3-II domains (78% of identity) RBP2-SH3-II has probably the same interaction pattern as the corresponding region of RBP1, preferentially binding Rim1 and $Ca_V2.2$.

Assuming approximately equal molar ratios of these proteins *in vivo,* we here propose a model for RBP-based protein complex (Fig. 22). In this model RBPs might serve as structural modules for protein complex assembly, interacting simultaneously with Bassoon or Piccolo via RBP-SH3-I, Rim1 via RBP-SH3-II and VDCCs via RBP-SH3-III. The described complex might be involved in recruitment and/ or retention of VDCCs in presynaptic terminals and their co-clustering with docked SVs.

Experiments done in context of this project revealed the preferential interaction between the SH3-III domain of RBPs and the specific PXXP motif in $Ca_V2.2$ (RQLPQTP). The second type of VDCCs involved in neurotransmitter release, $Ca_V2.1$, contains the corresponding PXXP motif of exactly the same primary structure, suggesting that $Ca_V2.1$ channels also can interact with RBPs via their SH3-III *in vivo*. In this study, we show that RBP interaction with Bassoon might be regulated *via* phosphorylation of the S2893 residue in RBP-interacting PXXP motif of Bassoon. Sequence analysis of the corresponding PXXP motifs in $Ca_V2.2$ and $Ca_V2.1$ (RQL**PQTP**LTPR) revealed the presence of two threonine residues (positions 6 and 9) which potentially can be phosphorylated by p38 MAPK, cdk5 or GSK3β (according to NetPhosK 1.0). Whether phosphorylations of these residues take place *in vivo* and whether

these phosphorylations are implicated in regulation of VDCC interaction with RBPs is not known and will require further analyses.

The here reported interaction of core CAZ proteins Bassoon and Piccolo with VDCCs via RBPs might provide a physical link for Ca^{2+} channels to the scaffolding complex of the presynaptic cytomatrix. It might be essential for the functional organization of the AZ by linking Ca^{2+} channels of the presynaptic membrane to components of the exocytosis machinery for SVs. Moreover the observed modulation of interactions in the complex by phosphorylation inspires speculations about an activity-dependent regulation of the interactions and in turn a role in presynaptic plasticity processes.

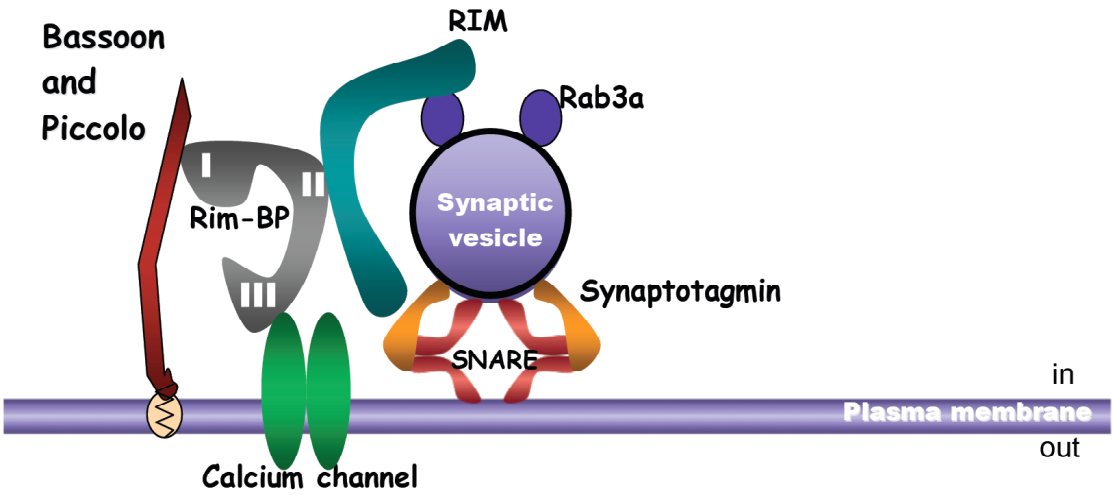

FIGURE 22. VIA THEIR MULTIPLE SH3 DOMAINS, RBPS INTERACTING WITH BASSOON AND PICCOLO MAY ACT AS LINKERS BETWEEN RIMS AND VOLTAGE-DEPENDENT CALCIUM CHANNELS, THUS ORGANIZING INDIVIDUAL STEPS OF THE SV CYCLE AND LOCALIZING THE PRIMING AND FUSION APPARATUS IN THE VICINITY OF THE VDCC.

4.4 Bassoon might be involved in retention of VDCCs at synapses

The first evidence that Bassoon might be involved in the retention or exact localization of VDCCs in presynaptic terminals came from studies on Bassoon mutant mice. In the original paper of Altrock et al. (2003), the authors showed that the lack of functional Bassoon causes a reduction in normal synaptic transmission. At the ribbon synapses of cochlear inner hair cells and photoreceptor cells, Bassoon mutation leads to impaired anchoring of ribbons at the presynaptic membrane (Khimich et al., 2005; Dick et al., 2003). Furthermore, calcium currents were significantly reduced in mutant inner hair cells, potentially due to insufficient recruitment and/or stabilization of VDCCs at the active zone (Khimich et al., 2005). Following this observations we investigated the effect of the absence of Bassoon on the amount of presynaptic $Ca_V2.1$ in mouse hippocampal neurons at 16 and 23 DIV. These analyses showed a significant reduction of synaptic $Ca_V2.1$ immunofluorescence intensity at both time

points in Bassoon knockout cultures as compared to wild-type ones. The intensity of the SV marker Synaptophysin immunofluorescence was also reduced in Bassoon knockout compared to the wild-type synapses at 16 DIV, but no significant difference was observed one week later, suggesting that in the absence of Bassoon maturation of synapses might be impaired or delayed. In contrast, the reduction of $Ca_V2.1$ immunofluorescence intensity in Bassoon knockout *vs.* wild type synapses followed an opposite trend; it was more pronounced at 23 DIV, than at 16 DIV (30% and 20%, respectively).

To assess whether Bassoon effects on VDCC localization require RBPs as linkers connecting these two proteins, the distribution of $Ca_V2.1$ in rat hippocampal neurons transfected either with EGFP-tagged wild type Bassoon or RBP-binding deficient Bassoon mutant was compared. Bassoon clustering in the cell body was observed in both cases, while endogenous RBP2 and $Ca_V2.1$ were co-recruited only to clusters formed by wild-type Bassoon. At synapses formed by axons of neurons transfected with EGFP-tagged wild-type Bassoon the immunofluorescence intensities of both RBP2 and $Ca_V2.1$ showed strong positive correlation with the intensity of EGFP fluorescence. On the contrary, the negative correlation was observed for the RBP2 and $Ca_V2.1$ immunofluorescence intensities and EGFP fluorescence intensity at synapses containing RBP binding-deficient Bassoon mutant. A plausible explanation might be that Bassoon contributes to definition of presynaptic slots for $Ca_V2.1$. Clues about the possible existence of presynaptic slots for VDCCs came from morphological studies of putative calcium channel organization at transmitter release sites (Heuser et al., 1979). Multiple studies showed that the precise localization of VDCCs in close proximity to synaptic vesicles requires their specific interactions with other proteins, such as plasma membrane SNARE proteins (Sheng et al., 1994; Mochida et al., 2003; Harkins et al., 2004) and the AZ scaffolding proteins Mint and CASK (Maximov and Bezprozvanny, 2002; Spafford et al., 2003; Spafford and Zamponi, 2003). Thus, the concept of slots may be broadened to include any sites of interaction that regulates the final localization of channels at the presynaptic AZ. Given this, the negative correlation observed for $Ca_V2.1$ at synapses transfected with RBP binding-deficient Bassoon mutant may indicate that this mutated protein fails to form slots for VDCCs when integrated into the presynaptic cytomatrix.

Interestingly, these slots may be specific for the calcium channel type (Cao et al., 2004). The mechanism for this discrimination needs further attention. RBP-interacting PXXP motif in $Ca_V2.2$ has the same primary structure as the corresponding region in $Ca_V2.1$, suggesting that Bassoon can be also involved in retention of $Ca_V2.2$ at presynaptic terminals. Overall, our data suggest that Bassoon might be involved in the retention and/or exact localization of VDCCs in presynaptic terminals. This mechanism requires RBPs, which interact simultaneously with Bassoon and VDCCs and therefore can serve as physical linkers for this protein complex assembly.

4.5 Perspectives

What might be the physiological significance of VDCC–RBP–Bassoon complex formation? Neurotransmitter release is proportional to the third or fourth power of Ca^{2+} entry (Augustine et al., 1987). Thus, regulation of presynaptic Ca^{2+} channels provides a sensitive and efficient tool to regulate neurotransmitter release, as a 2-fold change in the presynaptic Ca^{2+} current results in an 8- to 16-fold change in exocytosis. This, in turn, effects synaptic transmission and may contribute to short-term synaptic plasticity. In this regard the interesting direction for further analyses would be to directly assess the role of VDCC–RBP–Bassoon complex in synaptic transmission. To this end the dominant-negative approach to interfere with Bassoon binding to RBPs can be combined with paired patch-clamp recordings allowing estimation of possible changes in vesicular release probabilities. We expect that interference with Bassoon binding to RBPs will lead to impaired localization of VDCCs in presynaptic terminals, which, in turn, will cause the reduction of miniature EPSC frequencies or failures of evoked EPSPs. Notably, for this set of experiments, the previously arisen question, whether $Ca_V2.2$ are regulated by Bassoon in the same manner as $Ca_V2.1$, is of particular importance, due to their possible compensatory role in synaptic transmission (Cao et al., 2004).

5. References

- Altrock, W.D., S. tom Dieck, M. Sokolov, A.C. Meyer, A. Sigler, C. Brakebusch, R. Fässler, K. Richter, T.M. Boeckers, H. Potschka, C. Brandt, W. Löscher, D. Grimberg, T. Dresbach, A. Hempelmann, H. Hassan, D. Balschun, J.U. Frey, J.H. Brandstätter, C.C. Garner, C. Rosenmund, E.D. Gundelfinger. 2003. Functional inactivation of a function of excitatory synapses in mice deficient for the active zone protein Bassoon. *Neuron.* 37: 787-800.
- Augustine, G.J., M.P. Charlton, and S.J. Smith. 1987. Calcium action in synaptic transmitter release. *Annu. Rev. Neurosci.* 10:633–693.
- Barbar, E. 2008. Dynein light chain LC8 is a dimerization hub essential in diverse protein networks. *Biochemistry*. 47:503–508.
- Bennett, M.K., N. Calakos, and R.H. Scheller. 1992. Syntaxin: A synaptic protein implicated in docking of synaptic vesicles at presynaptic active zones. *Science* 257:255–259.
- Bolshakov, V.Y., L. Carboni, M.H. Cobb, S.A. Siegelbaum, F. Belardetti. 2000. Dual MAP kinase pathways mediate opposing forms of long-term plasticity at CA3-CA1 synapses. *Nat. Neurosci.* 3:1107–1112.
- Brust, T.B., F.S. Cayabyab, N. Zhou, and B.A. MacVicar. 2006. p38 mitogen-activated protein kinase contributes to adenosine A1 receptor-mediated synaptic depression in area CA1 of the rat hippocampus. *J Neurosci.* 26:12427-12438.
- Burton, P.R., and J.L. Paige. 1981. Polarity of axoplasmic microtubules in the directional transport in neurons. *Nat. Rev. Neurosci.* 6:201–214.
- Cai, Q., P.Y. Pan, and Z.H. Sheng. 2007. Syntabulin-kinesin-1 family member 5B-mediated axonal transport contributes to activity-dependent presynaptic assembly. *J. Neurosci.* 27:7284–7296.
- Cao, Y.Q., E.S. Piedras-Renteria, G.B. Smith, G. Chen, N.C. Harata, and R.W. Tsien. 2004. Presynaptic Ca2+ channels compete for channel type-preferring slots in altered neurotransmission arising from Ca2+ channelopathy. *Neuron* 43:387–400.
- Catimel, B., M. Nerrie, F.T. Lee, A.M. Scott, G. Ritter, S. Welt, L.J. Old, A.W. Burgess, and E.C. Nice. 1997. Kinetic analysis of the interaction between the monoclonal antibody A33 and its colonic epithelial antigen by the use of an optical biosensor. A comparison of immobilisation strategies. *J. Chromatogr. A.* 776:15–30.
- Catterall, W.A. 2000. Structure and regulation of voltage-gated calcium channels. *Annu. Rev. Cell Dev. Biol.* 16:521–555.

- Chardenot, P., C. Roubert, S. Galiègue, P. Casellas, G. Le Fur, and P. Soubrié, F. Oury-Donat. 2002. Expression profile and up-regulation of PRAX-1 mRNA by antidepressant treatment in the rat brain. *Mol Pharmacol.* 62:1314-1320.
- Chen, Y.A. and R.H. Scheller. 2001. SNARE-mediated membrane fusion. *Nat Rev Mol Cell Biol.* 2:98-106.
- Cohen, M.W., O.T. Jones, and K.J. Angelides. 1991. Distribution of Ca2+ channels on frog motor nerve terminals revealed by fluorescent omega-conotoxin. *J. Neurosci*. 11: 1032–1039.
- Davies, A., J. Hendrich, A.T. Van Minh, J. Wratten, L. Douglas, and A.C. Dolphin. 2007. Functional biology of the a2d subunits of voltage-gated calcium channels. *Trends Pharmacol. Sci.* 28:220–228.
- de Wit, H., A.M. Walter, I. Milosevic, A. Gulyás-Kovács, D. Riedel, J.B. Sørensen, M. Verhage. 2009. Synaptotagmin-1 docks secretory vesicles to syntaxin-1/SNAP-25 acceptor complexes. *Cell.* 138:935-946.
- de Wit, H., L.N. Cornelisse, R.F. Toonen, and M. Verhage. 2006. Docking of secretory vesicles is syntaxin dependent. *PLoS ONE*. 1:e126.
- Dick, O., S. tom Dieck, W.D. Altrock, J. Ammermüller, R. Weiler, C.C. Garner, E.D. Gundelfinger, Brandstätter J.H. 2003. The presynaptic active zone protein bassoon is essential for photoreceptor ribbon synapse formation in the retina. *Neuron*. 37:775-86.
- Dolphin, A.C. 2003. Beta subunits of voltage-gated calcium channels. *J. Bioenerg. Biomembr.* 35:599–620.
- Dunlap, K., J.I. Luebke, and T.J. Turner. 1995. Exocytotic Ca2+ channels in mammalian central neurons. *Trends Neurosci*. 18:89–98.
- Ertel, E.A., K.P. Campbell, M.M. Harpold, F. Hofmann, Y. Mori, E. Perez-Reyes, A. Schwartz, T.P. Snutch, T. Tanabe, L. Birnbaumer, et al. (2000). Nomenclature of voltage-gated calcium channels. *Neuron* 25, 533–535.
- Espindola, F.S., D.M. Suter, L.B. Partata, T. Cao, J.S. Wolenski, R.E. Cheney, S.M. King, and M.S. Mooseker. 2000. The light chain composition of chicken brain myosin-Va: calmodulin, myosin-II essential light chains, and 8-kDa dynein light chain/PIN. *Cell Motil. Cytoskeleton*. 47:269–281.
- Fan, J., Q. Zhang, H. Tochio, M. Li, and M. Zhang. 2001. Structural basis of diverse sequence-dependent target recognition by the 8 kDa dynein light chain. *J. Mol. Biol.* 306:97–108.
- Fasshauer, D., R.B. Sutton, A.T. Brünger, and R. Jahn. 1998. Conserved structural features of the synaptic fusion complex: SNARE proteins reclassified as Q- and R-SNAREs. *Proc. Natl Acad. Sci. USA* 95:15781–15786 (1998).

- Fejtova, A., D. Davydova, F. Bischof, V. Lazarevic, W.D. Altrock, S. Romorini, C. Schöne, W. Zuschratter, M.R. Kreutz, C.C. Garner, N.E. Ziv, and E.D. Gundelfinger. 2009. Dynein light chain regulates axonal trafficking and synaptic levels of Bassoon. *J Cell Biol.* 185:341-55.
- Feng, S., C. Kasahara, R.J. Rickles, and S.L. Schreiber. 1995. Specific interactions outside the proline-rich core of two classes of Src homology 3 ligands. *Proc. Natl. Acad. Sci. USA* 92:12408-12415.
- Fenster, S.D., M.M. Kessels, B. Qualmann, W.J. Chung, J. Nash, E.D. Gundelfinger, and C.C. Garner. 2003. Interactions between Piccolo and the actin/dynamin-binding protein Abp1 link vesicle endocytosis to presynaptic active zones. *J Biol Chem.* 278:20268-20277.
- Fenster, S.D., W.J. Chung, R. Zhai, C. Cases-Langhoff, B. Voss, A.M. Garner, U. Kaempf, S. Kindler, E.D. Gundelfinger, and C.C. Garner. 2000. Piccolo, a presynaptic zinc finger protein structurally related to bassoon. *Neuron* 25:203-14.
- Fuhrmann, J.C., S. Kins, P. Rostaing, O. El Far, J. Kirsch, M. Sheng, A. Triller, H. Betz, and M. Kneussel. 2002. Gephyrin interacts with Dynein light chains 1 and 2, components of motor protein complexes. *J. Neurosci.* 22:5393–5402.
- Fujimoto, K., T. Shibasaki, N. Yokoi, Y. Kashima, M. Matsumoto, T. Sasaki, N. Tajima, and T. Iwanaga, S. Seino. 2002. Piccolo, a Ca2+ sensor in pancreatic beta-cells. Involvement of cAMP-GEFII.Rim2.Piccolo complex in cAMP-dependent exocytosis. *J Biol Chem.* 277:50497-50502.
- Galiegue, S., O. Jbilo, T. Combes, E. Bribes, P. Carayon, G. Le Fur, and P. Casellas. 1999. Cloning and characterization of PRAX-1. A new protein that specifically interacts with the peripheral benzodiazepine receptor. *J. Biol. Chem.* 274: 2938–2952.
- Geppert, M., and T.C. Südhof. 1998. RAB3 and synaptotagmin: the yin and yang of synaptic membrane fusion. *Annu. Rev. Neurosci.* 21:75–95.
- Goldstein A.Y.N., X. Wang and T.L. Schwarz. 2008. Axonal transport and the delivery of pre-synaptic components. *Current Opinion in Neurobiology*. 18:495–503.
- Harkins, A.B., A.L. Cahill, J.F. Powers, A.S. Tischler, and A.P. Fox. 2004. Deletion of the synaptic protein interaction site of the N-type (CaV2.2) calcium channel inhibits secretion in mouse pheochromocytoma cells. *Proc. Natl. Acad. Sci. USA* 101:15219–15224.
- Harlow, M.L., D. Ress, A. Stoschek, R.M. Marshall, U.J. McMahan. 2001. The architecture of active zone material at the frog's neuromuscular junction. *Nature.* 409:479-484.

- Hayashi, T., McMahon H., Yamasaki S., Binz T., Hata Y., Südhof T.C., and Niemann H. 1994. Synaptic vesicle membrane fusion complex: action of clostridial neurotoxins on assembly. *EMBO J.* 13:5051-5061.
- Haynes, L.P., G.J. Evans, A. Morgan, and R.D. Burgoyne. 2001. A direct inhibitory role for the Rab3-specific effector, Noc2, in Ca^{2+}-regulated exocytosis in neuroendocrine cells. *J. Biol. Chem*. 276:9726–9732.
- Henkel, A.W., L.L. Simpson, R.M. Ridge, and W.J. Betz. 1996. Synaptic vesicle movements monitored by fluorescence recovery after photobleaching in nerve terminals stained with FM1-43. *J. Neurosci*. 16:3960–3967.
- Hibino, H., R. Pironkova, O. Onwumere, M. Vologodskaia, A.J. Hudspeth, and F. Lesage, 2002. RIM binding proteins (RBPs) couple Rab3-interacting molecules (RIMs) to voltage-gated Ca(2+) channels. *Neuron* 34:411–423.
- Hirokawa, N., and R. Takemura. 2005. Molecular motors and mechanisms of olfactory nerve of the frog. *Proc. Natl. Acad. Sci. USA*. 78:3269–3273.
- Hofmann, F., L. Lacinova, and N. Klugbauer. 1999. Voltage-dependent calcium channels: from structure to function. *Rev. Physiol. Biochem. Pharmacol*.139:33–87.
- Impey, S., K. Obrietan, and D.R. Storm. 1999. Making new connections: role of ERK/MAP kinase signaling in neuronal plasticity. *Neuron* 23:11–14.
- Jaffrey, S.R., and S.H. Snyder. 1996. PIN: an associated protein inhibitor of neuronal nitric oxide synthase. *Science*. 274:774–777.
- Jahn, R. and T.C. Südhof. 1999. Membrane fusion and exocytosis. *Annu Rev Biochem.* 68:863-911.
- Jung, J.H, A.M. Pendergast, P.A. Zipfel, and J.A. Traugh. 2008. Phosphorylation of c-Abl by protein kinase Pak2 regulates differential binding of ABI2 and CRK. *Biochemistry* 47:1094-1104.
- Khimich, D., R. Nouvian, R. Pujol, S. tom Dieck, A. Egner, E.D. Gundelfinger, and T. Moser. 2005. Hair cell synaptic ribbons are essential for synchronous auditory signaling. *Nature.* 434:889-894.
- Kim, D.K., and W.A. Catterall. 1997. Ca2+-dependent and –independent interactions of the isoforms of the a1A subunit of brain Ca2+ channels with presynaptic SNARE proteins. *Proc. Natl. Acad. Sci. USA* 94:14782–14786.
- Kim, S., J. Ko, H. Shin, J.R. Lee, C. Lim, J.H. Han, W.D. Altrock, C.C. Garner, E.D. Gundelfinger, R.T. Premont, B.K. Kaang, and E. Kim. 2003. The GIT family of proteins forms multimers and associates with the presynaptic cytomatrix protein Piccolo. J *Biol Chem.* 278:6291-6300.

- Kittel, R.J., C. Wichmann, T.M. Rasse, W. Fouquet, M. Schmidt, A. Schmid, D.A. Wagh, C. Pawlu, R.R. Kellner, K.I. Willig, et al. 2006. Bruchpilot promotes active zone assembly, Ca2+ channel clustering, and vesicle release. *Science* 312:1051–1054.
- Kraszewski, K., L. Daniell, O. Mundigl, and P. De Camilli. 1996. Mobility of synaptic vesicles in nerve endings monitored by recovery from photobleaching of synaptic vesicle-associated fluorescence. *J. Neurosci.* 16:5905–5913.
- Lajoix, A.D., R. Gross, C. Aknin, S. Dietz, C. Granier, and D. Laune. 2004. Cellulose membrane supported peptide arrays for deciphering proteinprotein interaction sites: the case of PIN, a protein with multiple natural partners. *Mol. Divers.* 8:281–290.
- Landis, D.M. 1988. Membrane and cytoplasmic structure at synaptic junctions in the mammalian central nervous system. *J. Electron Microsc Tech.*10(2):129-51.
- Leal-Ortiz, S., C.L. Waites, R. Terry-Lorenzo, P. Zamorano, E.D. Gundelfinger, and C.C. Garner. 2008. Piccolo modulation of Synapsin1a dynamics regulates synaptic vesicle exocytosis. *J Cell Biol.* 181:831-46.
- Lee, K.H., S. Lee, B. Kim, S. Chang, S.W. Kim, J.S. Paick, and K. Rhee. 2006. Dazl can bind to dynein motor complex and may play a role in transport of specific mRNAs. *EMBO J.* 25:4263–4270.
- Leveque, C., O. El Far, N. Martin-Moutot, K. Sato, R. Kato, M. Takahashi, and M.J. Seagar. 1994. Purification of the N-type calcium channel associated with syntaxin and synaptotagmin: a complex implicated in synaptic vesicle exocytosis. *J. Biol. Chem.* 269, 6306–6312.
- Li, L., L.S. Chin, O. Shupliakov, L. Brodin, T.S. Sihra, O. Hvalby, V. Jensen, D. Zheng, J.O. McNamara, P. Greengard. 1995. Impairment of synaptic vesicle clustering and of synaptic transmission, and increased seizure propensity, in synapsin I-deficient mice. *Proc. Natl Acad. Sci. USA.* 92:9235–9239.
- Li, Q., A. Lau, T.J. Morris, L. Guo, C.B. Fordyce, and E.F. Stanley. 2004. A syntaxin 1, Galpha(o), and N-type calcium channel complex at a presynaptic nerve terminal: analysis by quantitative immunocolocalization. *J. Neurosci.* 24:4070–4081.
- Liang, J., S.R. Jaffrey, W. Guo, S.H. Snyder, and J. Clardy. 1999. Structure of the PIN/LC8 dimer with a bound peptide. *Nat. Struct. Biol.* 6:735–740.
- Lo, K.W., S. Naisbitt, J.S. Fan, M. Sheng, and M. Zhang. 2001. The 8-kDa dynein light chain binds to its targets via a conserved (K/R)XTQT motif. *J. Biol. Chem.* 276:14059–14066.
- Maas, C., N. Tagnaouti, S. Loebrich, B. Behrend, C. Lappe-Siefke, and M. Kneussel. 2006. Neuronal cotransport of glycine receptor and the scaffold protein gephyrin. *J. Cell Biol.* 172:441–451.

- Maruyama, M., T. Sudo, Y. Kasuya, T. Shiga, B. Hu, and H. Osada. 2000. Immunolocalization of p38 MAP kinase in mouse brain. *Brain. Res.* 887:350–358.
- Maximov A., T. Südhof, I. Bezprozvanny. 1999. Association of neuronal calcium channels with modular adaptor proteins. *J. Biol. Chem.* 274:24453-24456.
- Maximov, A., and I. Bezprozvanny. 2002. Synaptic targeting of N-type calcium channels in hippocampal neurons. *J. Neurosci.* 22:6939–6952.
- Mayer, B.J. 2001. SH3 domains: complexity in moderation. *J. Cell Sci.* 114:1253–1263.
- Miljanich, G.P., and J. Ramachandran. 1995. Antagonists of neuronal calcium channels: structure, function, and therapeutic implications. *Annu. Rev. Pharmacol. Toxicol.* 35: 707–734.
- Miller, K.E., J. DeProto, N. Kaufmann, B.N. Patel, A. Duckworth, and D. Van Vactor. 2005. Direct observation demonstrates that Liprin-alpha is required for trafficking of synaptic vesicles. *Curr. Biol.* 15:684–689.
- Missler, M., W. Zhang, A. Rohlmann, G. Kattenstroth, R.E. Hammer, K. Gottmann, and T.C. Sudhof. 2003. Alpha-neurexins couple Ca2+ channels to synaptic vesicle exocytosis. *Nature* 423:939–948.
- Mittelstaedt, T., and S. Schoch. 2007. Structure and evolution of RIM-BP genes: Identification of a novel family member. *Gene* 403:70–79.
- Mochida, S., Z.H. Sheng, C. Baker, H. Kobayashi, and W.A. Catterall. 1996. Inhibition of neurotransmission by peptides containing the synaptic protein interaction site of N-type Ca2+ channels. *Neuron* 17:781–788.
- Mochida, S., R.E. Westenbroek, C.T. Yokoyama, K. Itoh, and W.A. Catterall. 2003. Subtype-selective reconstitution of synaptic transmission in sympathetic ganglion neurons by expression of exogenous calcium channels. *Proc. Natl. Acad. Sci. USA* 100: 2813–2818.
- Naisbitt, S., J. Valtschanoff, D.W. Allison, C. Sala, E. Kim, A.M. Craig, R.J. Weinberg, and M. Sheng. 2000. Interaction of the postsynaptic density-95/guanylate kinase domain-associated protein complex with a light chain of myosin-V and dynein. *J. Neurosci.* 20:4524–4534.
- Navarro, C., H. Puthalakath, J.M. Adams, A. Strasser, and R. Lehmann. 2004. Egalitarian binds dynein light chain to establish oocyte polarity and maintain oocyte fate. *Nat. Cell Biol.* 6:427–435.
- Okada, Y., H. Yamazaki, Y. Sekine-Aizawa, and N. Hirokawa. 1995. The neuron-specific kinesin superfamily protein KIF1A is a unique monomeric motor for anterograde axonal transport of synaptic vesicle precursors. *Cell*. 81:769–780.

- Olivera, B.M., G.P. Miljanich, J. Ramachandran, and M.E. Adams, M.E. 1994. Calcium channel diversity and neurotransmitter release: The omega-conotoxins and omega-agatoxins. *Annu. Rev. Biochem.* 63:823–867.
- Patel M.R., E.K. Lehrman, V.Y. Poon, J.G. Crump, M. Zhen, C.I. Bargmann, K. Shen. 2006. Hierarchical assembly of presynaptic components in defined C. elegans synapses. *Nat Neurosci.* 9:1488-1498.
- Pfister, K.K., E.M. Fisher, I.R. Gibbons, T.S. Hays, E.L. Holzbaur, J.R. McIntosh, M.E. Porter, T.A. Schroer, K.T. Vaughan, G.B. Witman, et al. 2005. Cytoplasmic dynein nomenclature. *J. Cell Biol.* 171:411–413.
- Pieribone V.A., O. Shupliakov, L. Brodin, S. Hilfiker-Rothenfluh, A.J. Czernik, P. Greengard. 1995. Distinct pools of synaptic vesicles in neurotransmitter release. *Nature.* 375:493–497.
- Poirier M.A., J.C. Hao, P.N. Malkus, C. Chan, M.F. Moore, D.S. King, M.K. Bennett. 1998. Protease resistance of syntaxin–SNAP-25–VAMP complexes. Implications for assembly and structure. *J. Biol. Chem*. 273:11370–11377.
- Poncer, J.C., R.A. McKinney, B.H. Gähwiler, and S.M. Thompson. 1997. Either N- or P-type calcium channels mediate GABA release at distinct hippocampal inhibitory synapses. *Neuron* 18, 463–472.
- Pravettoni, E., A. Bacci, S. Coco, P. Forbicini, M. Matteoli, and C. Verderio. 2000. Different localizations and functions of L-type and N-type calcium channels during development of hippocampal neurons. *Dev Biol.* 227:581-94.
- Premont, R.T., A. Claing, N. Vitale, J.L. Freeman, J.A. Pitcher, W.A. Patton, J. Moss, M. Vaughan, and R.J. Lefkowitz. 1998 *Proc. Natl. Acad. Sci. USA.* 95:14082–14087.
- Puthalakath, H., A. Villunger, L.A. O'Reilly, J.G. Beaumont, L. Coultas, R.E. Cheney, D.C. Huang, and A. Strasser. 2001. Bmf: a proapoptotic BH3 – only protein regulated by interaction with the myosin V actin motor complex, activated by anoikis. *Science*. 293:1829–1832.
- Regehr, W.G., K.R. Delaney, and D.W. Tank. 1994. The role of presynaptic calcium in short-term enhancement at the hippocampal mossy fiber synapse. *J. Neurosci.* 14:523–537.
- Rettig, J., Z.H. Sheng, D.K. Kim, C.D. Hodson, T.P. Snutch, and W.A. Catterall. 1996. Isoform-specific interaction of the a1A subunits of brain Ca2+ channels with the presynaptic proteins syntaxin and SNAP-25. *Proc. Natl.Acad. Sci. USA* 93:7363–7368.

- Reynolds, C.H., C.J. Garwood, S. Wray, C. Price, S. Kellie, T. Perera, M. Zvelebil, A. Yang, P.W. Sheppard, I.M. Varndell, D.P. Hanger, and B.H. Anderton. 2008. Phosphorylation regulates tau interactions with Src homology 3 domains of phosphatidylinositol 3-kinase, phospholipase Cgamma1, Grb2, and Src family kinases. *J Biol Chem.* 283:18177-18186.
- Rizzoli S.O. and W.J. Betz. 2005. Synaptic vesicle pools. *Nat Rev Neurosci.* 6(1):57-69.
- Rosenmund C., A. Sigler, I. Augustin, K. Reim, B. Brose, J.-S. Rhee. 2002. Differential control of vesicle priming and short-term plasticity by Munc13 isoforms. *Neuron.* 33:411-425.
- Rosenmund C., J. Rettigy and N. Brose. 2003. Molecular mechanisms of active zone function. *Current Opinion in Neurobiology*. 13:509-519.
- Schnorrer, F., K. Bohmann, and C. Nusslein-Volhard. 2000. The molecular motor dynein is involved in targeting swallow and bicoid RNA to the anterior pole of *Drosophila* oocytes. *Nat. Cell Biol.* 2:185–190.
- Schoch, S., and E.D. Gundelfinger. Molecular organization of the presynaptic active zone. 2006. *Cell Tissue Res.* 326:379-391.
- Schroer, T.A., S.T. Brady, and R.B. Kelly. 1985. Fast axonal transport of foreign synaptic vesicles in squid axoplasm. *J. Cell Biol.* 101:568–572.
- Shapira, M., R.G. Zhai, T. Dresbach, T. Bresler, V.I. Torres, E.D. Gundelfinger, N.E. Ziv, and C.C. Garner. 2003. Unitary assembly of presynaptic active zones from Piccolo-Bassoon transport vesicles. *Neuron*. 38:237–252.
- Sheng, Z.H., J. Rettig, M. Takahashi, and W.A. Catterall. 1994. Identification of a syntaxin-binding site on N-type calcium channels. *Neuron* 13:1303–1313.
- Sheng, Z.H., J. Rettig, T. Cook, and W.A. Catterall. 1996. Calcium-dependent interaction of N-type calcium channels with the synaptic core-complex. *Nature* 379:451–454.
- Shibasaki, T., Y. Sunaga, K. Fujimoto, Y. Kashima, and S. Seino. 2004. Interaction of ATP sensor, cAMP sensor, Ca2+ sensor, and voltage-dependent Ca2+ channel in insulin granule exocytosis. *J Biol Chem*. 279:7956-7961.
- Shirataki, H., K. Kaibuchi, T. Sakoda, S. Kishida, T. Yamaguchi, K. Wada, M. Miyazaki, and Y. Takai. 1993. Rabphilin-3A, a putative target protein for smg p25A/rab3A p25 small GTP-binding protein related to synaptotagmin. *Mol. Cell. Biol.* 13:2061–2068.
- Siksou L., Rostaing P., Lechaire J.P., Boudier T., Ohtsuka T., Fejtova A., Kao H.T., Greengard P., Gundelfinger E.D., Triller A., Marty S. 2007. Three-dimensional architecture of presynapti terminal cytomatrix. *J. Neurosci*. 27:6868–6877.

- Snutch, T.P., and P.B. Reiner. 1992. Ca2+ channels: diversity of form and function. *Curr. Opin. Neurobiol.* 2:247–253.
- Spafford, J.D., and G.W. Zamponi. 2003. Functional interactions between presynaptic calcium channels and the neurotransmitter release machinery. *Curr. Opin. Neurobiol.* 13: 308–314.
- Spafford, J.D., D.W. Munno, P. Van Nierop, Z.P. Feng, S.E. Jarvis, W.J. Gallin, A.B. Smit, G.W. Zamponi, and N.I. Syed. 2003. Calcium channel structural determinants of synaptic transmission between identified invertebrate neurons. *J. Biol. Chem.* 278:4258–4267.
- Stanley, E.F. 1993. Single calcium channels and acetylcholine release at a presynaptic nerve terminal. *Neuron* 11:1007–1011.
- Stryker, E. and K.G. Johnson. 2007. LAR, liprin alpha and the regulation of active zone morphogenesis. *J Cell Sci.* 120:3723-3728.
- Südhof, T.C. 2004. The Synaptic Vesicle Cycle. *Annu. Rev. Neurosci.* 27:509–547.
- Szabo, Z., G.J. Obermair, C.B. Cooper, G.W. Zamponi, and B.E. Flucher. 2006. Role of the synprint site in presynaptic targeting of the calcium channel CaV2.2 in hippocampal neurons. *Eur. J. Neurosci*. 24:709–718.
- Takahashi, M., M.J. Seagar, J.F. Jones, B.F. Reber, and W.A. Catterall. 1987. Subunit structure of dihydropyridine-sensitive calcium channels from skeletal muscle. *Proc. Natl. Acad. Sci. USA.* 84:5478–5482.
- Takao-Rikitsu, E., S. Mochida, E. Inoue, M. Deguchi-Tawarada, M. Inoue, T. Ohtsuka, Y. Takai. 2004. Physical and functional interaction of the active zone proteins, CAST, RIM1, and Bassoon, in neurotransmitter release. *J Cell Biol.* 164:301-11.
- Takei Y., A. Harada, S. Takeda, K. Kobayashi, S. Terada, T. Noda, T. Takahashi, and N. Hirokawa. 1995. Synapsin I deficiency results in the structural change in the presynaptic terminals in the murine nervous system. *J. Cell Biol.* 131:1789–1800.
- tom Dieck, S., L. Sanmartí-Vila, K. Langnaese, K. Richter, S. Kindler, A. Soyke, H. Wex, K.H. Smalla, U. Kämpf, J.T. Fränzer, M. Stumm, C.C. Garner, and E.D. Gundelfinger. 1998. Bassoon, a novel zinc-finger CAG/glutamine-repeat protein selectively localized at the active zone of presynaptic nerve terminals. *J Cell Biol.* 142:499-509.
- tom Dieck, S., W.D. Altrock, M.M. Kessels, B. Qualmann, H. Regus, D. Brauner, A. Fejtova, O. Bracko, E.D. Gundelfinger, and J.H. Brandstatter. 2005. Molecular dissection of the photoreceptor ribbon synapse: physical interaction of Bassoon and RIBEYE is essential for the assembly of the ribbon complex. *J. Cell Biol.* 168:825–836.

- Tsien, R.W., D. Lipscombe, D.V. Madison, K.R. Bley, and A.P. Fox.1988. Multiple types of neuronal calcium channels and their selective modulation. *Trends Neurosci.* 11:431–438.
- Tsien, R.W., P.T. Elinor, and W.A. Horne. 1991. Molecular diversity of voltage-dependent calcium channels. *Trends Neurosci.* 12:349–354.
- Tucker, W.C., A. Schwarz, T. Levine, Z. Du, Z. Gromet-Elhanan, M.L. Richter, G. Haran. 2004. Observation of calcium-dependent unidirectional rotational motion in recombinant photosynthetic F1-ATPase molecules. *J Biol Chem.* 279:47415-47418.
- Vadlamudi, R.K., R. Bagheri-Yarmand, Z. Yang, S. Balasenthil, D. Nguyen, A.A. Sahin, P. den Hollander, and R. Kumar. 2004. Dynein light chain 1, a p21-activated kinase 1-interacting substrate, promotes cancerous phenotypes. *Cancer Cell*. 5:575–585.
- Vale, R.D. 2003. The molecular motor toolbox for intracellular transport. *Cell*. 112:467 480.
- Vallee, R.B., J.C. Williams, D. Varma, and L.E. Barnhart. 2004. Dynein: An ancient motor protein involved in multiple modes of transport. *J. Neurobiol.* 58:189–200.
- Varoqueaux F., A. Sigler, J.S. Rhee, N. Brose, C. Enk, K. Reim, C. Rosenmund. 2002. Total arrest of spontaneous and evoked synaptic transmission but normal synaptogenesis in the absence of Munc13-mediated vesicle priming. *Proc Natl Acad Sci USA*. 99:9037-9042.
- Voets, T. 2001. Dissection of three Ca2R-dependent steps leading to secretion in chromaffin cells from mouse adrenalin slices. *Neuron*. 28:537-545.
- Wang, Y., M. Okamoto, F. Schmitz, K. Hofmann, and T.C. Südhof. 1997. Rim is a putative Rab3 effector in regulating synaptic-vesicle fusion. *Nature* 388:593–598.
- Wang, Y., S. Sugita, and T.C. Südhof. 2000. The RIM/NIM family of neuronal C2 domain proteins. Interactions with Rab3 and a new class of Src homology 3 domain proteins. *J. Biol. Chem.* 275, 20033–20044.
- Westenbroek, R.E., J.W. Hell, C. Warner, S.J. Dubel, T.P. Snutch, and W.A. Catterall. 1992. Biochemical properties and subcellular distribution of an N-type calcium channel a1 subunit. *Neuron* 9:1099–1115.
- Westenbroek, R.E., T. Sakurai, E.M. Elliott, J.W. Hell, T.V.B. Starr, T.P. Snutch, and W.A. Catterall (1995). Immunochemical identification and subcellular distribution of the a1A subunits of brain calcium channels. *J. Neurosci.* 15:6403–6418.
- Williams, J.C., P.L. Roulhac, A.G. Roy, R.B. Vallee, M.C. Fitzgerald, and W.A. Hendrickson. 2007. Structural and thermodynamic characterization of a cytoplasmic dynein light chain-intermediate chain complex. *Proc. Natl. Acad. Sci. USA*. 104:10028–10033.

- Yokoyama, C.T., S.J. Myers J. Fu, S.M. Mockus, T. Scheuer, and W.A. Catterall. 2005. Mechanism of SNARE protein binding and regulation of Cav2 channels by phosphorylation of the synaptic protein interaction site. *Mol. Cell. Neurosci*. 28:1–17.
- Yokoyama, C.T., Z.H. Sheng, and W.A. Catterall. 1997. Phosphorylation of the synaptic protein interaction site on N-type calcium channels inhibits interactions with SNARE proteins. *J. Neurosci*. 17:6929–6938.
- Yoshida, A., C. Oho, A. Omori, R. Kawahara, T. Ito, and M. Takahashi. 1992. HPC-1 is associated with synaptotagmin and w-conotoxin receptor. *J. Biol. Chem.* 267:24925–24928.
- Zerial M. and H. McBride. 2001. Rab proteins as membrane organizers. *Nat Rev Mol Cell Biol.* 2:107-117.
- Zhai, R.G. and H.J. Bellen. 2004. Hauling t-SNAREs on the microtubule highway. *Nat Cell Biol.* 6:918-919.
- Zhai, R.G., H. Vardinon-Friedman, C. Cases-Langhoff, B. Becker, E.D. Gundelfinger, N.E. Ziv, and C.C. Garner. 2001. Assembling the presynaptic active zone: a characterization of an active one precursor vesicle. *Neuron*. 29:131–143.
- Zhang W., A. Rohlmann, V. Sargsyan, G. Aramuni, R.E. Hammer, T.C. Südhof, and M. Missler. 2005. Extracellular domains of alpha-neurexins participate in regulating synaptic transmission by selectively affecting N- and P/Q-type Ca2+ channels. *J Neurosci*. 25:4330-4342.
- Zhao, Z.S., E. Manser, T.H. Loo, and L. Lim. 2000. Interaction between PAK and nck: a template for Nck targets and role of PAK autophosphorylation. *Mol. Cell. Biol.* 20: 3906-17.

6. Appendix

6.1 RBP1 and RBP2 sequence alignment

```
RBP1_rn      MEQLTTLPRLGDPGAMEPWALPAWQHWTQGQGCKPGDASASIAATPTALQVKGLRSEESS  60
RBP2_rn      ------------------------------------------------------------
Homology

RBP1_rn      EPAGAHSPGPIRNTDPEGTETVLPKLGQQAESPGYSCSRLEGEDAQAYKAKFNIGFGDRP  120
RBP2_rn      ------------------------------------------------------------
Homology

RBP1_rn      NLELLRALGELQQRCTILKEENQMLRKSSFPETEEKVRRLKRKNAELAVIAKRLEERAQK  180
RBP2_rn      ------------------------------------------------------------
Homology

RBP1_rn      LQETNMRVVSAPVPRPGSSLELCRKALARQRARDLSETATALLAKDKQIAALQRECRELQ  240
RBP2_rn      ------------------------------------------------------------
Homology

RBP1_rn      ARLSLVGKEGPQWLHMRDFDRLLRESQREVLRLQRQIALRNQREPLRPARSQGSTAPSSV  300
RBP2_rn      ------------------------------------------------------------
Homology

RBP1_rn      GAPAPGAPGETVLEDDVESPQVVLGEPEKQLRVQQLESELCKKRKKCESLEQEARKKQRR  360
RBP2_rn      ------------------------------------------------------------
Homology

RBP1_rn      CEELELQLRAAQNENARLVEENSRLSGKATEKEQVEWENAELKGQLLGVTQERDSALRKS  420
RBP2_rn      ------------------------------------------------------------
Homology

RBP1_rn      QGLQSKLESLEQVLKHMREVAQRRQQLEEEHEQARLSLQEKQEEVRRLQQAQAEAKREHE  480
RBP2_rn      ----------------MREAAERRQQLELEHEQALAILNAKQQEIQLLQQS---------
Homology                      ***.*:****** *****   *: **:*:: ***:

RBP1_rn      GAVQLLESTLDSMQARVRELEGQCRSQTERFSLLAQELQAFRLHPGPLDLLTSALGCNAL  540
RBP2_rn      ---------------KVRELEEKCRVQSEQFNLLSRDLEKFRQHAGSIDLLGSNS--VAL
Homology                   :***** :** *:*:*.**:::*: ** *.*.:*** *     **

RBP1_rn      GDHPPPHCCCSSPQPCQGSGPKDLDLPPGSPGRCTPKSSEPALATLTGVPRRTAKKAESL  600
RBP2_rn      LDVP---------------------LAPGKP--FSQYMNGLATSIHKGHEGPTGHYSVIG
Homology      * *                     *.**.*   :    .  * :  .*    *.: :

RBP1_rn      SNSSRSESIHNSPKSCPTPEVDTASEVEELEVDSVSLLPAAPEGHSGGARIQVFLARYSY  660
RBP2_rn      DYIPLSGDKLESPCVKPSFLLRSSSPRCRFESEMDDDRSSNKSKHSSSGKVHLCVARYSY
Homology     .  . * .  :**   *:  : ::*   .:* :  .  .:  . **...:::: :*****

RBP1_rn      NPFEGPNENPEAELPLTAGEYIYIYGNMDEDGFFEGELMDGRRGLVPSNFVERVSDDDLL  720
RBP2_rn      NPFDGPNENPEAELPLTAGKYLYVYGDMDEDGFYEGELLDGQRGLVPSNFVDFIQDNE--
Homology     ***:***************:*:*:**:******:****:**:*********: :.*::

RBP1_rn      STLPRELADSSHSSGPELSFLSGGGGGCSSGGQSSGGRSQPRPEEEATGDELS--LSPPP  780
RBP2_rn      SRFAGTLG----SE-QDQNFLNHSG--ISLERDSILHLHSPTQVDSGITDNGGGTLDVNI
Homology     * :.  *.    *.  : .**. .*   *   :*     .*   :..  *: .  *.

RBP1_rn      EGLGEPLAVPYPRHITVLKQLAHSVVLAWE---LPPERVDLRGFHIFVNGELRQALGPGV  840
RBP2_rn      DDIGEDI-VPYPRKITLIKQLAKSVIVGWEPPAVPPGWGTVSSYNVLVDKETRMSLALGR
Homology     :.:** : *****:**::****:**::.**   :**    : .::::*: * * :*. *

RBP1_rn      PPKAVLENMDLRAGPLHVSVQALTSKGSSDPLRCCLAMGAGAGVVPSQLRIHRLTATSAE  900
RBP2_rn      RTKALIEKLNTAACTYRISVQCVTSRGNSDELQCTLLVGKDVVVAPSQLRVDNITQISAQ
Homology      .**::*:::  * . ::***.:**:*.** *:* * :* .. *.*****:..:*  **:
```

```
RBP1_rn      ITWVPGNSNLAHAVYLNGEECPPARPSTYWATFCNLRPGTLYQARVEAQIPSQGPWEPGW  960
RBP2_rn      LSWLPTNSNYSHIIFLNEEELDIVKAARYKYQFFNLRPNMAYKVKVLAQ-PHQMPWQLPL
Homology     ::*:* *** :* ::** **   .:.: *   * ****.  *:.:* ** * * **:

RBP1_rn      ERPELRAATLQFTTLPAGLPDAPLDVQAEPGPSPGIVMISWLPVTIDAAGTSNGVRVTGY  1020
RBP2_rn      EQREKKEACVEFSTLPAGPPAPPQDVTVQAGATTASVQVSWKPPALTPTGLSNGANVTGY
Homology     *: * : * ::*:***** * .* ** .:.*.:.. * :** * :: .:* ***..****

RBP1_rn      AVYADGQKIMEVASPTAGSVLVEVSQLQLLQACHEVTVRTMSPHGESTDSIPAPVAPALA  1080
RBP2_rn      GVYAKGQRVAEVIAPTADGAAVELVRLRSLEA-KAVSVRTLSAQGESMDSALAAIPPDLL
Homology     .***.**:: ** :***... **: :*: *:* : *:***:*.:*** **  *.:.* *

RBP1_rn      SACQPARMSCLSPRPSPEVRTPLASVSPGLGYTSLPLRHPVPHGTQDSPASLSTEMSKGP  1140
RBP2_rn      VPPAPHPRTAPPPKP-LASDMDTKDLGPHVKVDESWEQSRPPGPAHGHMLEPPDMHSTGP
Homology      .  *   :. .*:*         .:.* :   .   :   *  ::.   . .   *.**

RBP1_rn      QEEPPVPCSQEEAGSAVHRTSEEKRAMEPTLGQEGPDPVAPFLAKQAVECTSGDAGPTPC  1200
RBP2_rn      GRRSPSPSRILPQPQGAPVSTTVAKAMAREAAQRVAE--SNRLEKRSLFLEQSSAGPYAN
Homology      ...* *.      ...  ::   :**    .*. .:  :  * *:::   ...*** .

RBP1_rn      STQEELTQKEPSTEVCHRGDLDSELKLRSEKEGMSELGVHLVNSLVDHSRNSDLSDIQEE  1260
RBP2_rn      SDEEDG---YASPEVKRRGTSVDDFLKGSE-LGQQPHCCHGDEYHTESSRGSDLSDIMEE
Homology     * :*:     .*.** :**   .::   **  * .    *  :  .: **.****** **

RBP1_rn      EEEEEEEEELGSRPCSFQKQVAGNSIGENGAKPQPDPSCETDSDEEILEQILELPLQRLC  1320
RBP2_rn      DEEE-------------------------------------------LYSEMQL------
Homology     :***                                           * . ::*

RBP1_rn      SKKLFSIPEEEEEEDEEEGLGKPGPSSSSQDPSQPERALLGLDCESSQPQGPGLCPLSPE  1380
RBP2_rn      -------------EDG----GRRRPSGTSHN----------------------------
Homology                  **     *:  **.:*::

RBP1_rn      LSGAREHLEDVLGVVGGNSRRRGGCSPEKLPNRKRPQDPREHCSRLLGNGGPQTSARPVP  1440
RBP2_rn      ----------ALKILG-NSALMG--------RG----DRMEHVSRRYSHSGGG------P
Homology               .* ::* **   *        .     *  ** **  .:.*        *

RBP1_rn      PRDRGSLPVIEGTRVGQEPGGRGRPGLSRRCPRGPAPESSLVSCLSPKCLEISIEYDSED  1500
RBP2_rn      QRHRPMAPSID------EYTGR--------------------DHLSP---------DFYD
Homology      *.*   * *:      *  **                    . ***         *  *

RBP1_rn      EQEVGSGGVSISSSCYPTDGEAWGTAAVGRPRGPVKVNSGSNTYLRLPAWEKGEPERRGH  1560
RBP2_rn      ESETDPG-----------------------------------------------------
Homology     *.*...*

RBP1_rn      SAIGRTKEPPSRATETGESRGQDNSGRRGPQRRGARVLRTGTTELAPPRSPQEAPSHQDL  1620
RBP2_rn      -------------------------------------------------------AEEL
Homology                                                              ::*

RBP1_rn      PLRVFVALFDYDPISMSPNPDAGEEELPFREGQILKVFGDKDADGFYRGESGGRTGYIPC  1680
RBP2_rn      PARIFVALFDYDPLTMSPNPDAAEEELPFKEGQIIKVYGDKDADGFYRGETCARLGLIPC
Homology     * *:*********::*******.******:****:**:************: .* * ***

RBP1_rn      NMVAEVAVDTPIGRQQLLQRGFLPPNVLTQGSGNGPSVYPSAHTPGPPPKPRRSKKVELE  1740
RBP2_rn      NMVSEIHADDEEMMDQLLRQGFLPLNTPVEKIE---------RS-------RRS------
Homology     ***:*: .*     :***::**** *. .:            ::       ***

RBP1_rn      DPAQLCPGPPKLIHSAALKTSRPMVAAFDYNPRENSPNMDVEAELPFRAGDVITVFGNMD  1800
RBP2_rn      ---GRGHSVP----------TRRMVALYDYDPRESSPNVDVEAELLFCTGDIITVFGEID
Homology            . *          :* *** :**:***.***:****** * :**:*****::*

RBP1_rn      DDGFYYGELNGQRGLVPSNFLEGPGPEAGGLDSGTSQAESQDSRVIIQGPPVPPGWHYAL  1860
RBP2_rn      EDGFYYGELNGQKGLVPSNFLE----------------EVPDD-VEVHLSDAPP--HYSH
Homology     :***********:********                *  *. * :: . .**  **:

RBP1_rn      SSGSSSKTKLGESQGIAEKKQGLLAKGKELLKRLGSRKD                       1890
RBP2_rn      DPPMRTKAKR-----VSQPP-------------------
Homology     ..   :*:*      :::
```

FIGURE 23. PRIMARY STRUCTURE OF RIM BINDING PROTEINS: COMPARISON OF RBP1 AND RBP2.

The sequences of rat RBP1 (NCBI Reference Sequence: XP_213427.4) and RBP2 (NCBI Reference Sequence: XP-341072.3) are aligned in single letter amino acid code. RBPs are composed of three dispersed SH3 domains (highlighted in yellow) and three consecutive fibronectin III repeat domains (undelined in green). The amino acid numbering corresponds to RBP1_rn sequence.

6.2 Constructs used in this project

Construct name (Gene)	Amino acids (rat cDNA)	vector	tag	done by
Bsn	95-3938	pCSM-EGFP	EGFP	T. Dresbach
BsnRBM	95-3938; R2888A; P2891A; P2894A	pCSM-EGFP	EGFP	D. Davydova
Bsn1	1-609	pGBKT7		W. Altrock
Bsn2	609-1692	pGBKT7		W. Altrock
Bsn3	1692-3263	pGBKT7		W. Altrock
Bsn4	3263-3938	pGBKT7		W. Altrock
Bsn5	1653-2348	pGBKT7		W. Altrock
Bsn6	2088-2563	pGBKT7		W. Altrock
Bsn7	2715-3013	pGBKT7		W. Altrock
Bsn8	2979-3263	pGBKT7		W. Altrock
Bsn9	2715-2868	pGBKT7		W. Altrock
Bsn10	2821-3013	pGBKT7		W. Altrock
Bsn10	2821-3013	pEGFP-C2	EGFP	D. Davydova
Bsn10	2821-3013	pRFP-C2	mRFP	F. Bischof
Bsn10_PA	2821-3013; R2888A; P2891A; P2894A	pGBKT7		D. Davydova
Bsn10_PA	2821-3013; R2888A; P2891A; P2894A	pEGFP-C2	EGFP	D.Davydova
Bsn11	2929-3017	pGBKT7		W. Altrock
Bsn12	2869-2899	pGBKT7		F. Bischof
Bsn12	2869-2899	pET-32a(+)	His-Trx	F. Bischof
Bsn12_PA	2869-2899; R2888A; P2891A; P2894A	pGBKT7		D. Davydova
Bsn12_PA	2869-2899; R2888A; P2891A; P2894A	pET-32a(+)	His-Trx	D. Davydova
Bsn12_SD	2869-2899; S2893D	pGBKT7		D. Davydova
Bsn12_SD	2869-2899; S2893D	pET-32a(+)	His-Trx	D. Davydova
Bsn12_SA	2869-2899; S2893A	pGBKT7		D. Davydova
Bsn12_SA	2869-2899; S2893A	pET-32a(+)	His-Trx	D. Davydova
Bsn13	1360-1692	pET-32a(+)	His-Trx	A. Fejtova
$Bsn13^{I,II,III}$	1360-1692; SQT1424AAA; TQT1500AAA; TQT1526AAA	pET-32a(a)	His-Trx	A. Fejtova
Bsn14	1206-1692	pRFP-C2	mRFP	A. Fejtova
Bsn15	1441-1692	pET-32a(+)	His-Trx	A. Fejtova
Bsn15	1441-1692	pMito3-EGFP	Mito-EGFP	A. Fejtova
$Bsn15^{II}$	1441-1692; TQT1500AAA	pET-32a(+)	His-Trx	A. Fejtova
$Bsn15^{III}$	1441-1692; TQT1526AAA	pET-32a(+)	His-Trx	A. Fejtova
$Bsn15^{II,III}$	1441-1692; TQT1500AAA; TQT1526AAA	pET-32a(+)	His-Trx	A. Fejtova
Bsn16	1360-1441	pET-32a(+)	His-Trx	A. Fejtova

Bsn16[I]	1360-1441; SQT1424AAA	pET-32a(+)	His-Trx	A. Fejtova
$Ca_V2.2_1$	2165-2195	pET-32a(+)	His-Trx	D. Davydova
DLC1	1-89	pGEX-5X-1	GST	A. Fejtova
DLC1	1-89	pMito3-EGFP	Mito-EGFP	A. Fejtova
DLC2	1-89	pGEX-5X-1	GST	A. Fejtova
DLC2	1-89	pMito3-EGFP	Mito-EGFP	A. Fejtova
Pclo1	3607-3792	pGBKT7		D. Davydova
Pclo2	3653-3683	pGBKT7		D. Davydova
Pclo2	3653-3683	pET-32a(+)	His-Trx	D. Davydova
RBP1	1-1786	pEGFP-C2	EGFP	D. Davydova
RBP1	1-1786	pCMV-Tag3B	myc	D. Davydova
RBP1_SH3 I	652-712	pGADT7		D. Davydova
RBP1_SH3 I	652-712	pGEX-5X-1	GST	D. Davydova
RBP1_SH3 I_long	591-773	pGADT7		D. Davydova
RBP1_SH3 I_long	591-773	pGEX-5X-1	GST	D. Davydova
RBP1_SH3 II	1557-1622	pGADT7		F. Bischof
RBP1_SH3 II	1557-1622	pGEX-5X-1	GST	F. Bischof
RBP1_SH3 III	1697-1758	pGADT7		F. Bischof
RBP1_SH3 III	1697-1758	pGEX-5X-1	GST	F. Bischof
RBP1_SH3 II+III	1557-1786	pGADT7		F. Bischof
RBP1_SH3 II+III	1557-1786	pMito3-EGFP	EGFP	F. Bischof
RBP1_0	1357-1556	pGADT7		F. Bischof
RBP1_0	1357-1556	pGEX-5X-1	GST	F. Bischof
RBP2	1-1076	pCMV-Tag3B	myc	D. Davydova
RBP2_SH3 I	191-251	pGADT7		D. Davydova
RBP2_SH3 I	191-251	pGEX-5X-1	GST	D. Davydova
RBP2_SH3 I_long	125-314	pGADT7		D. Davydova
RBP2_SH3 I_long	125-314	pGEX-5X-1	GST	D. Davydova
RBP2_SH3 II	873-938	pGADT7		D. Davydova
RBP2_SH3 II	873-938	pGEX-5X-1	GST	D. Davydova
RBP2_SH3 III	978-1039	pGADT7		D. Davydova
RBP2_SH3 III	978-1039	pGEX-5X-1	GST	D. Davydova
RBP2_SH3 II+III	873-1076	pGADT7		D. Davydova
RBP2_SH3 II+III	873-1076	pMito3-EGFP	Mito-EGFP	D. Davydova
RIM1_1	1110-1140	pET-32a(+)	His-Trx	D. Davydova
Tom20_TMD	1-35	pMito3-EGFP	Mito-EGFP	D. Davydova

6.3 Abbreviations

% (v/v) – percent by volume
% (w/v) – percent by mass
aa – amino acid
Abp1 – amiloride binding protein 1
AMP – adenosine monophosphate
ATP – adenosin triphosphate
AZ – active zone
BGT Mice – Bassoon gene trap mice
BRP – Bruchpilot
BSA – bovine serum albumin
Bsn – Bassoon
BsnRBM – Bassoon Rim binding protein mutant

cAMP – cyclic adenosine monophosphate
cAMP-GEFII – cAMP-guanidine nucleotide exchange factor II
CASK – calcium/calmodulin-dependent serine protein kinase
CAST – CAZ-associated structural protein
CAZ – cytomatrix at the active zone
Cdk – Cyclin-dependent kinase
cDNA – complementary DNA
CDS – coding sequence
COS-7 – african green monkey cell line
CtBP – C-terminal binding protein
COOH-terminal – carboxy-terminal
DIV – Days *in vitro*
DLC – dynein light chain
DMEM – Dulbecco´s Modified Eagle Medium
DMSO – dimethyl sulfoxide
DNA – deoxyribonucleic acid
DTT – dithiothreitol
E.coli – *Escherichia coli*
EDTA – ethylenediamine-N,N,N´,N´-tetraacetic acid
EGFP – Enhanced green fluorescent protein
ERC protein – expressed in renal carcinoma
F-actin – filamentous actin
FCS – fetal calf serum
Fig. – figure
GDP – guanosine diphosphate
GIT1 – G protein-coupled receptor kinase interacting ArfGAP 1
Gp – Guinea pig
GSK3β – Glykogen Synthase Kinase 3β
GST – glutathion-S-transferase
GTP – guanosine triphosphate
GTPase – guanosine triphosphatase
HBSS – Hank´s Balanced salts
HEK cells – human embryonic kidney cells
HEPES – 4-(2-hydroxyethyl)-1-piperazineethanesulfonic acid
IF – immunofluorescence
IgG – immunoglobulin G
IHC – inner hair cell
IP – immunoprecipitation
IPSC – inhibitory postsynaptic currents
IPTG – isopropyl-f-D-l-thiogalactopyranoside
kDa – kilo Dalton
m – Mouse
MAPK – Mitogen-activated protein kinase
MBA – molar binding activity
Mint – Munc-18 interacting protein
mRFP – monomeric red fluorescence protein
mRNA – messenger ribonucleic acid
MTOC – mitochondria organizing centre
NH_2-terminal – amino-terminal
P – postnatal day
PAGE – polyacrylamide gel electrophoresis
PBH domain – Piccolo-Bassoon homology domain
PBS – phosphate buffered saline
Pclo – Piccolo
PCR – polymerase chain reaction
PEG – polyethylene glycol

PFA – Paraformaldehyde
PTV – Piccolo-Bassoon transport vesicle
PVDF – Polyvinyliden fluiride
Rab protein – Ras-related in brain protein
Rb – rabbit
RBP – Rim binding protein
Rim – Rab3 interacting molecule
RNA – ribonucleic acid
rpm – revolutions per minute
RRP – ready releasable pool
RT – Room temperature
SDS – sodium dodecyl sulfate
SDS-PAGE – sodium dodecyl sulfate polyacrylamide gel electrophoresis
SH3 domain – Src-homology 3 domain
SNAP-25 – synaptosome-associated protein 25 kDa
SNARE – soluble N-ethyl-maleimide-sensitive fusion protein attachment protein receptors
SV – synaptic vesicle
SVP – synaptic vesicle precursor
TEMED – N,N,N´,N´-Tetramethylethylenediamine
TMD – transmembrane domain
Tris – Tris(hydorxymethyl)-aminomethane
Tris/HCl – Tris(hydorxymethyl)-aminomethanhydrochloride
Trx – theoredoxin
TX-100 – triton X-100
U – unit
VDCC – voltage-dependent calcium channel
Y2H – yeast two hybrid
Δ – deletion

Curriculum vitae

Name:	**Daria**
Family name:	**Davydova**
Date of birth:	**October 21st 1982**
Place of birth:	**Saint-Petersburg, Russia**
Nationality:	**Russian Federation**
Parents:	**Sergey Davydov**
	Tamara Davydova

Education

1989-1999:	**Primary and secondary school. Municipal school Nr. 197**
1999-2003:	**Saint-Petersburg State University, Saint-Petersburg, Russia**
2003:	**The Bachelor Degree of Biology in the major of „Biology“**
2003-2005:	**Saint-Petersburg Stait University, Saint-Petersburg, Russia**
2005:	**The Master's Degree of Biology in the major of „Biology“**
08.2005-12.2005 :	**Practical training at the Leibniz Institute for Neurobiology, Magdeburg, Germany.**
2006-2009:	**Doctoral Thesis. Otto von Guericke Universität -Leibniz Institute for Neurobiology, Magdeburg, Germany**

October, 15th 2009, Magdeburg

Scientific publications:

- ⇨ Fejtova, A., **D. Davydova**, F. Bischof, V. Lazarevic, W.D. Altrock, S. Romorini, C. Schöne, W. Zuschratter, M.R. Kreutz, C.C. Garner, N.E. Ziv, and E.D. Gundelfinger. 2009. Dynein light chain regulates axonal trafficking and synaptic levels of Bassoon. *J Cell Biol.* 185:341-55.